Metal Chalcogenide Nanostructures: Characteristics and Synthesis

Ho Soon Min | Yarub Al-Douri

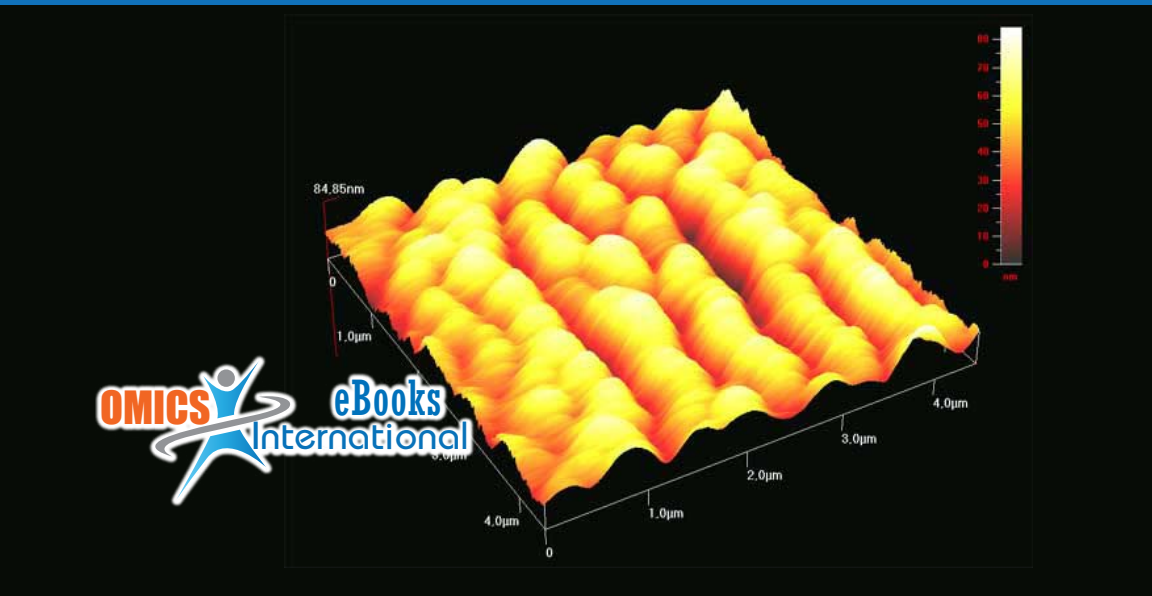

OMICS eBooks International

Metal Chalcogenide Nanostructures: Characteristics and Synthesis

Edited by

Ho Soon Min
Associate Professor, Centre for Green Chemistry and Applied Chemistry,
INTI International University, Putra Nilai, 71800, Negeri Sembilan, Malaysia

Yarub Al-Douri
Professor, Nanotechnology and Catalysis Research Centre (NANOCAT),
University of Malaya, 50603, Kuala Lumpur, Malaysia

ISBN: 978-1-63278-029-4
DOI: 10.4172/978-1-63278-029-4-030

Published: January 2019
Printed: January 2019

Published by OMICS International
Heathrow Stockley Park, Lakeside House,1 Furzeground Way,
Heathrow UB11 1BD, UK

CONTENTS

PREFACE

Currently, metal chalcogenides have attracted great attention from researcher. There are several deposition techniques have been used to prepare binary, ternary, quaternary and penternary thin films. Metal chalcogenides have multi-application like energy storage, optoelectronic, sensor, laser device, catalysts, and solar cells to thermoelectric. Because of they have unqiue peoperties (optical, electrical, physical properties). Nanostructured metal chalcogenides possess better performance than bulk due to ultra-high specific area, unique quantum effect and high reactivity. However, wide application of nanostructured metal chalcogenides is strongly hindered by lacking of effective-cost, high yield with excellent control over morphology, size and compositions of material. This environmentally friendly approach is capable of producing metal chalcogenide nanostructures in one-pot reaction on large scale, which were investigated for their thermoelectric properties towards conversion of waste heat into electricity. The results have demonstrated that physical properties of metal chalcogenide nanostructures are strongly dependent on metal chalcogenides types, deposition technique, and their figures of merits are comparable with previously bulk or nanostructured counterparts.

Dr. Ho Soon Min

Dr. Yarub Al-Douri

ACKNOWLEDGEMENTS

I am thankful to all the persons/ colleagues/ university staff who supported me on this book. Also, I am grateful to the OMICS International eBooks Team in the publishing of this book.

Chapter 1

Spin-coating Technique to Synthesize Cu_2cdsns_4 Quaternary Alloy Nanostructures and Investigate the Optical and Structural Properties

Y. Al-Douri[1,2,3]*, Ali Abu Odeh[4]
[1]Nanotechnology and Catalysis Research Centre (NANOCAT), University of Malaya, 50603 Kuala Lumpur, Malaysia
[2]Physics Department, Faculty of Science, University of Sidi-Bel-Abbes, 22000-Algeria
[3]Department of Mechatronics Engineering, Faculty of Engineering and Natural Sciences, Bahcesehir University, 34349 Besiktas, Istanbul, Turkey
[4]Khawarizmi International College, 68297 Al Ain, UAE

***Corresponding author:** Y. Al-Douri, Nanotechnology and Catalysis Research Centre (NANOCAT), University of Malaya, 50603 Kuala Lumpur, Malaysia, E-mail: yaldouri@yahoo.com

Abstract

Photovoltaics were successfully synthesized using Cu_2CdSnS_4 quaternary alloy nanostructures on p-type silicon substrate via sol-gel method at different annealing temperatures up to 500 °C. UV-vis and photoluminescence (PL) spectrofluorometers have been utilized to investigate the optical properties of refractive index and optical dielectric constant. It is found that direct energy gap, 1.29-1.31 eV. Also, X-ray diffraction (XRD) has been used to investigate the structural properties. Applied ultrasonic effect to explore crystallite size that has a proportional relationship with annealing temperature. Our results have agreement with other experimental and theoretical data.

Keywords

Cu_2CdSnS_4; Quaternary alloy; Nanostructures; Optical; Band gap

Introduction

I_2-II-IV-VI_4 (I=Cu,Ag; II=Zn,Cd; I =Si,Ge,Sn; VI=S,Se) quaternary alloys have drawn intense interest for their suitable energy band gaps (E_g);1.1-1.5 eV, high optical absorption coefficient;10^4-10^5 $cm^{-1}$and high abundant elements for potential

Metal Chalcogenide Nanostructures: Characteristics and Synthesis, Edited by Ho Soon Min and Yarub Al-Douri

application in photovoltaics. There is a need to expand the range of materials that can be incorporated into effective-cost solar cells. Hence, expensive and scarce elements such as indium and gallium are replaced by other materials such as zinc and tin to have photovoltaics (PVs) that satisfy our needs [1-3]. PVs technology has been divided into three generations, the overall efficiency and performance vary greatly due to different types of semiconductor materials [4]. High efficiency affects price/Watt and power/m^2. Thus, reaching an effective efficiency is the most important step for any PV technology [5]. $CuInGaSe_2$ quaternary alloy gains much interest, it has been synthesized by [6] sintering technology and precursor nanoparticle-ink, which showed an efficiency of 2.392%. The performance of dye synthesized solar cells could be improved by enhancing the light absorption by local surface plasmon (LSP) effect from Ag@4-choloroaniline core shell nanoparticles [7]. $CuInS_2$ (CIS) nanoparticles were synthesized and coated on FTO at room temperature; the coated FTO was sintered so that a compact and dense $CuInS_2$ layer was measured for photovoltaic characteristics such as V_{oc}, J_{sc} and FF [8]. As well, ultrasonic method is used to prepare $CuInS_2$ microspheres in solvent like propylene glycol and precursors as indium chloride, copper oxalate and thioacetamde. It is estimated the energy gap of $CuInS_2$ microsphere to be 2.28 eV [9]. $CuInS_2$ nanocrystals were synthesized by a new precursor complex, [bis (2-hyroxyacetophenato) copper (II)], [Cu $(HAP)_2$], via a microwave method, the nanoparticles of $CuInS_2$ were used to prepare $CuInS_2$ film by doctor's blade technique [10]. CdS quantum dots, gold nanoparticles (GNPs) and gold nanorods (GNRs) are incorporated into the active layer for enhancing light absorption in comparison with single nanoparticles, where found conversion efficiency equals 147% that belongs to synthesized solar cells [11].

Another quaternary alloy that drawn increasing interest in the past few years is Cu_2ZnSnS_4 where synthesized with high quality, phase purity and the energy band gap was around 1.44-1.48 eV [12]. A few works on Cu_2CdSnS_4 (CCTS) quaternary alloys have been reported, many kinds of methods have been used to synthesize Cu_2CdSnS_4 quaternary alloy, through solvothermal approach under controlled temperatures [13], a combination of successive ionic layer absorption, reaction method and the chemical bath deposition method [14], microwave irradiation method [15], facile synthesis [16], simple solvothermal method [17], spray pyrolysis deposition [18] and co-sputtering deposition [19]. First-principles calculations have been employed to study the optical and electronic properties of Cu_2ZnSiS_4 and $Cu_2ZnSiSe_4$ in wurtzite-kesterite and wurtzite-stannite structures [20]. They have discussed and presented optical transitions at high symmetry points between valence bands, conduction bands and band structures to analyze different properties. In addition, they have obtained optical constants and dielectric function spectra as well. While, Wang and Lou [21] have developed analytical absorption model for 0.53 eV GaInAsSb alloy for both p-n and n-p configurations. The spectrum-insensitive optimal doping, $N_{a(d)} = 3 \times 10^{17}$ cm^{-3} is noticed in diode light-doped layer for all configurations. By improving the doping in the light-doped layer, thickness compensation between emitter and base has been noticed for normal structures and, for each considered structure can be employed by consuming less material to achieve comparable output as that for optimal one. Comparing to GaSb diode, 2-3-fold efficiency enhancement can be expected for low-temperature spectrum illumination, making the concerned device an efficient

candidate for low-temperature applications. Moreover, Adegoke et al. [22] have used organometallic hot-injection synthetic route to synthesis highly luminescent and photo stable alloyed quaternary CdSeTeS core QDs of two different sizes. Characterization of the nanocrystals were performed using TEM, XRD, UV/vis and fluorescence spectrophotometric techniques. They have demonstrated alloyed quaternary CdSeTeS core QDs possess unique optical properties that are advantageous over conventional core/shell systems.

Herein, Cu_2CdSnS_4 quaternary alloy nanostructures deposited via spin coating technique on p-type silicon substrate under a wide range of annealing temperature from room temperature to 500 ◦C. Meanwhile, optical and structural properties were investigated in details. This paper is organized as follows; section 2 details the experimental procedure whereas, section 3 details the results and discussions. Finally, conclusion is summarized in section 4.

Experimental

Sigma-Aldrich Company has supplied with chemicals and solvents that were necessary for experiment. The cadmium chloride ($CdCl_2$) (0.8 mol/L), copper chloride ($CuCl_2$) (0.8 mol/L), thiourea (CH_4N_2S) (0.8 mol/L), tin chloride ($SnCl_2$) (0.8 mol/L), monoethanolamine (MEA) and 2-methoxyethanol (2-metho) were prepared for solution of Cu_2CdSnS_4 quaternary precursors. The solvent and stabilizer were the 2-metho and MEA, respectively.

$$Molarity(M) = \frac{M_s}{V} \tag{1}$$

$$M_s = \frac{W(gm)}{M_{wt}(grams/moles)} \tag{2}$$

where M_s is number of moles, V is liquid volume, W is weight (gm) and M_{wt} is molecular weight (gm/mol).

After preparing the precursors individually, they were mixed together in a beaker at a molar ratio of 2:1:1:4, in order to be consistent with the stoichiometric composition of Cu_2CdSnS_4. Three hours including stirring speed 1500 revolution per minute (RPM) under applied temperature 50 °C via magnetic stirrer (WiseStirMSH 30D, Germany) have been utilized to dissolve metals within stirring. It is necessary to use extra thiourea during deposition to compensate losing of sulfur, the resulted solution is yellow and transparent. It has been divided into two, the first is deposition procedure and second is covered by laboratory film inside ultrasonic cleaner (DELTA DC200H, Taiwan) with deionized water for 30 min under 50 °C. therefore, two solutions are got, with and without ultrasonic effect. The substrate used in this process is p-type Si wafer, 525 µm thickness, one side polished, 100 mm diameter and 100 orientations. It is cleaved into 2 cm x 2 cm for each piece. Thus, every piece is considered to be an independent substrate. These substrates have been cleaned by using a standard that explained by [23] for cleaning silicon wafers which need to be performed before high-temperature processing steps such as oxidation and annealing of silicon wafers.

As usual, with and without ultrasonic, few drops of solutions on p-type Si wafer. A rotation speed, 500 rpm for 30 sec of spin coater (Laurell WS-400B, USA)

for deposited solution to get more homogenous one. After that, hot plate of 80 °C has been used to dry the substrate. This process has been repeated 15 times to get proper thickness and uniform nanostructures. Finally, 5 samples with ultrasonic and same without ultrasonic are obtained.

Diffusion furnace (MODU-LAB, USA) has been employed to apply annealing temperature for eight of ten samples for up to 1300 °C in controlled atmosphere. For both with and without ultrasonic and annealing temperatures, 200, 300, 400 and 500 °C for 1 hour under Nitrogen gas N_2 flow to save the deposited nanostructures coherent, the samples were cooled to room temperature. UV-vis spectrometer (Perkin Elmer Lambda 35, USA) has been used to test the optical properties of reflection Spectra of Cu_2CdSnS_4 quaternary alloy nanostructures of range 200-1000 nm. Also, photoluminescence (PL) (Flourolog-3, USA) of range between 200 nm to 1100 nm has been brought to investigate the band gap.

The structural properties of Cu_2CdSnS_4 quaternary alloy nanostructures have been investigated by using X-ray diffractometer (Philips PW 1710, USA), which record the intensity as a function of Bragg's angle in 2θ range from 10^o - 60° degree at a rate of 5^o/min using Cu kα (λ = 1.5406 Å). The major diffraction peaks have been recorded and attributed to the corresponding planes.

Results and Discussion

Optical properties

UV-vis spectroscopy within range 200-1000 nm has been used to investigate reflection spectra under different annealing temperature effect, room temperature, 200, 300, 400 and 500 °C. **Figure 1** shows the effective wavelength ranges between 820 and 960 nm. With ultrasonic, lowest reflectance at 500 °C is 25%, while, highest reflectance at 300 °C is 63%. Meanwhile, without ultrasonic, lowest reflectance at 400 °C is 57%, while highest reflectance at 500 °C is 70%. It can explore from **Figure 1** with ultrasonic, the reflection levels are lower than without ultrasonic and there is a clear effect of ultrasonic on reflection at different temperatures therefore, these levels at 400 and 500 °C away from others that is meaning there is a distinction between varied reflections unlike without ultrasonic.

Using Tauc formula for band gap calculation, the E_g of nanostructured Cu_2CdSnS_4 quaternary alloy can be calculated using:

$$(ahv)^2 = A(hv-E_g) \quad (3)$$

Where A is a constant, a is the absorption coefficient, h is the Planck's constant, v is incident photon frequency and E_g is the energy band gap. To calculate E_g of absorption spectra $(ahv)^2$ versus hv of nanostructured Cu_2CdSnS_4 quaternary alloy at different annealing temperatures via extending a straight-line of curve to zero absorption coefficients as illustrated in **Figure 2**. For ultrasonic, E_g is 1.29 eV at room temperature, it is dropped to 1.28 eV and 1.275 eV with increasing the annealing temperature to 200 and 300°C respectively, then increased to 1.33 eV at 400 °C, but it is dropped again slightly to 1.31 eV at 500 °C. Whereas, a closer look at without ultrasonic effect revealed that E_g starts with 1.285 eV and dropped to 1.26 eV with increasing the annealing temperature to 200 °C, followed

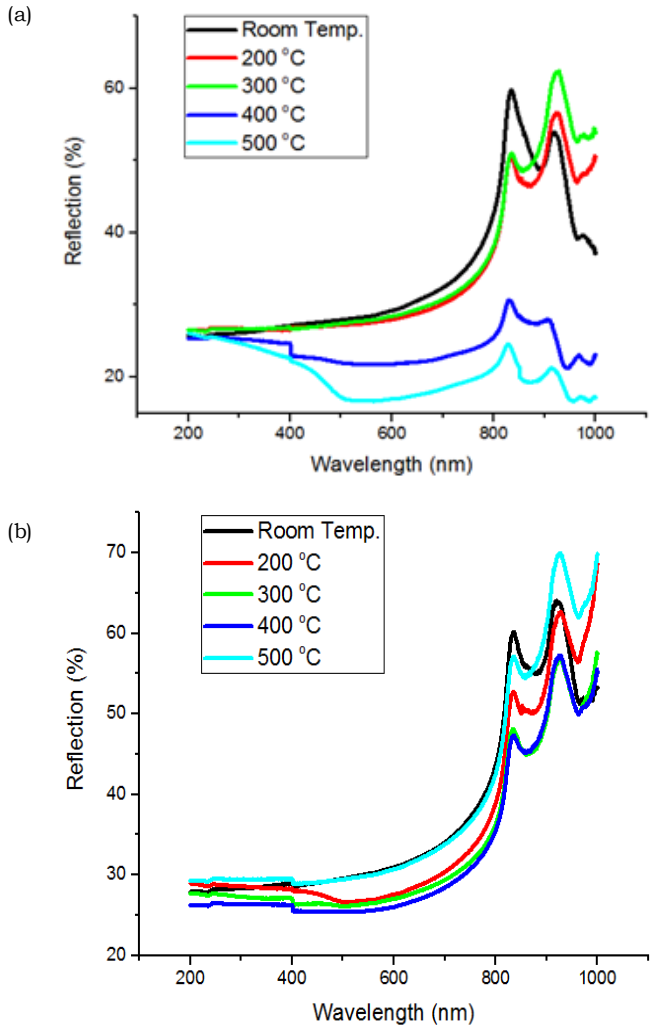

Figure 1: Reflection (%) a with ultrasonic and b without ultrasonic spectra of Cu_2CdSnS_4 nanostructures deposited on p-Si substrates at different annealing temperature effect, room temperature, 200, 300, 400 and 500 °C [38].

by slight increase to 1.265 eV at 300 °C, then increased to 1.27 eV with increasing the annealing temperature to 400 °C. It is dropped again to 1.26 eV at 500 °C. It is noticed that the variations between different levels of energy band gap for without ultrasonic are half approximately than with ultrasonic, that is attributed to ultrasonic effect, which leads to reduction of electron velocity as displayed in **Figure 3**. The PL of nanostructured Cu_2CdSnS_4 quaternary alloy is shown in **Figure 4**. With ultrasonic, E_g at room temperature is 1.59 eV, dropped to 1.57 eV, 1.56 eV, 1.55 eV and 1.54 eV as annealing temperature increases to 200 °C, 300 °C, 400 °C and 500 °C. respectively. While, without ultrasonic, the E_g starts with 1.59 eV, 1.57 eV and 1.54 eV as annealing temperature increases to 200 °C and 300 °C and 400 °C, respectively, but it is increased to 1.53 eV as annealing temperature

increases to 500 °C. Briefly, the resulted E_g is in good accordance with other Cu_2CdSnS_4 values [13-19]. The band gaps are quite close to the optimum band gap, which indicate that Cu_2CdSnS_4 quaternary alloy nanostructures are promising

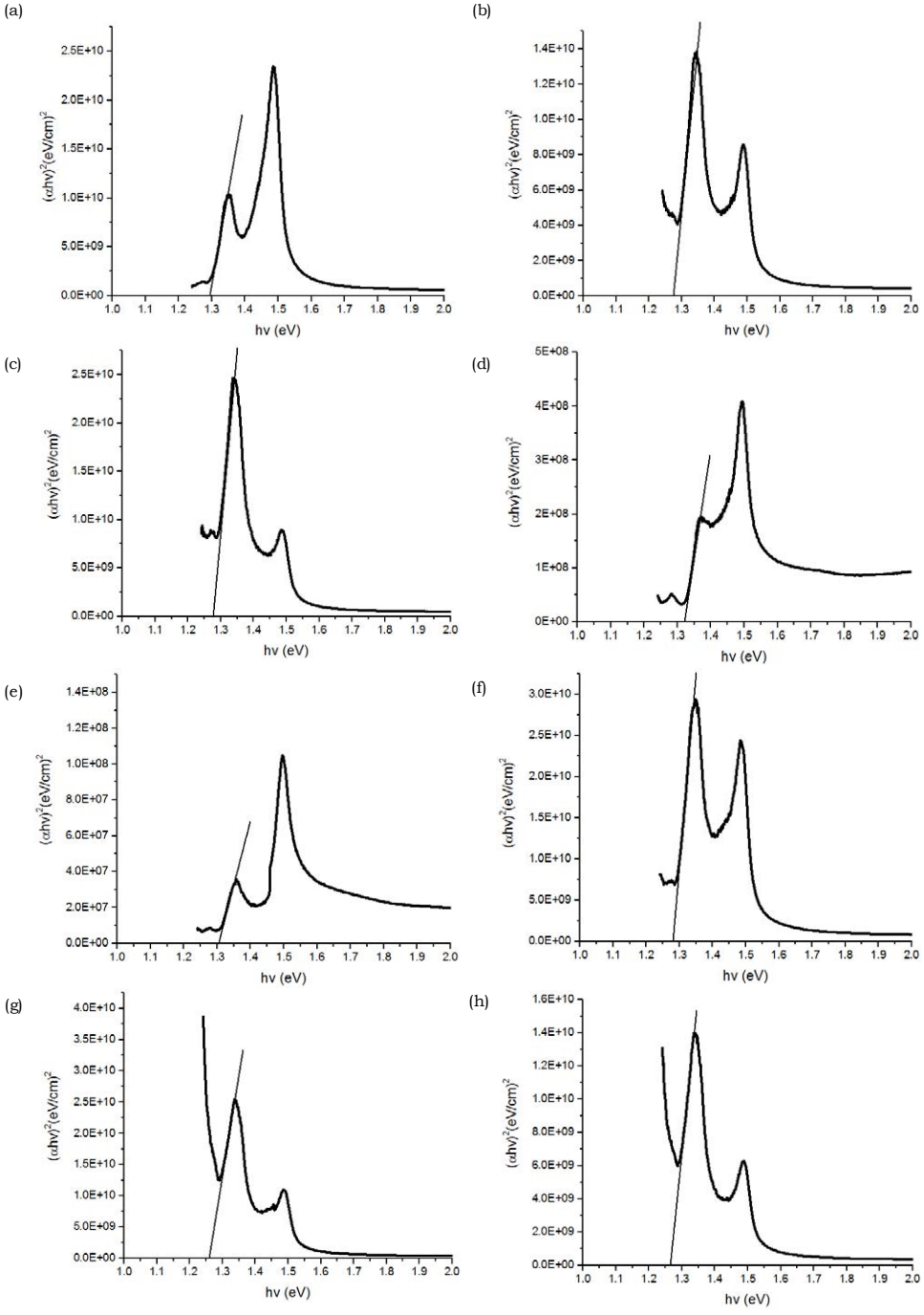

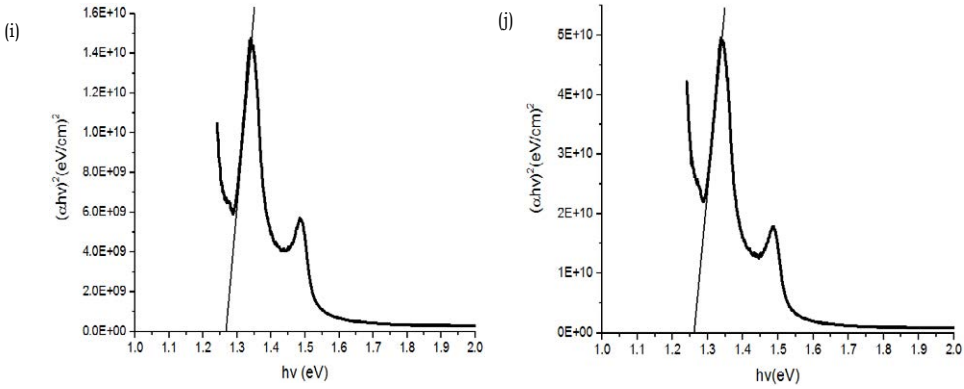

Figure 2: $(\alpha hv)^2$ versus hv of Cu_2CdSnS_4 Quaternary alloy nanostructures deposited on p-Si substrates with ultrasonic at **a)** room Temp, **b)** 200, **c)** 300, **d)** 400, and **e)** 500°C, and without ultrasonic at f room Temp, **g)** 200, **h)** 300, **i)** 400, and **j)** 500 °C. [38].

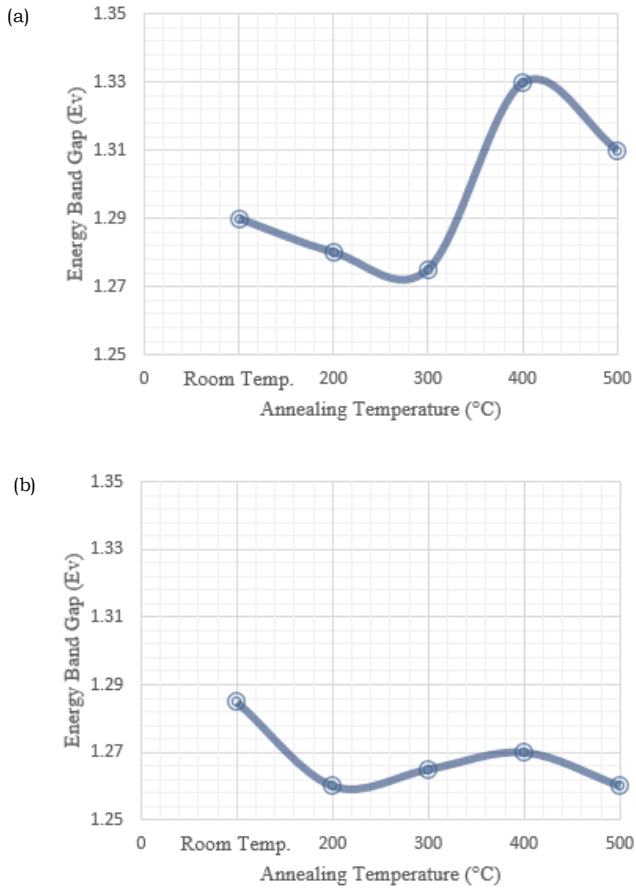

Figure 3: Fitted UV-vis plots of energy band gap of Cu_2CdSnS_4 Quaternary alloy nanostructures as a function of the annealing temperature **a)** with ultrasonic, **b)** without ultrasonic [38].

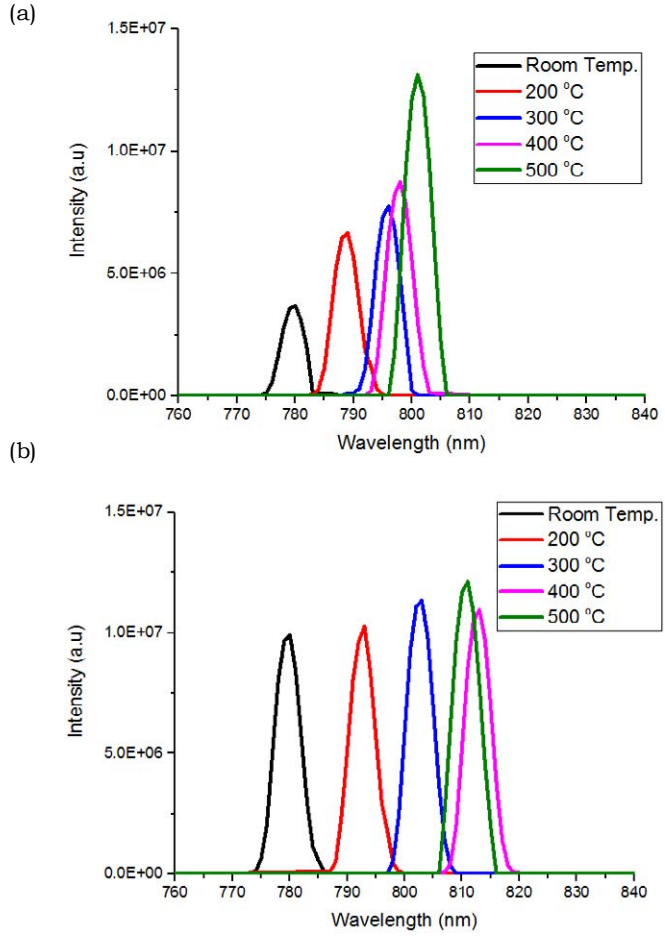

Figure 4: PL of Cu_2CdSnS_4 Quaternary alloy nanostructures as a function of the annealing temperature **a)** with ultrasonic, **b)** without ultrasonic [38].

materials for optoelectronic applications. The measured energy band gaps of Cu_2CdSnS_4 quaternary alloy nanostructures for UV-vis and PL spectroscopies are given in **Table 1**. There is a clear distinguished between E_g resulted from PL and UV-vis that is attributed to difference of instruments and ambient circumstances.

The optical properties of refractive index n is an important parameter in atomic interactions. From theoretical view point, it is related to local polarizability and density [24]. Different relationships between energy gap E_g and refractive index n have been recorded [25-32]. To validate our calculations, many relationships between E_g and n have been registered. Ravindra et al. [25] have presented a linear relationship between high frequency refractive index and band gap:

$$n = \alpha + \beta E_g \quad (4)$$

where $\beta = -0.62\ eV^{-1}$ and $\alpha = 4.048$. while, Herve and Vandamme [26] have inspired physics of dispersion and light refraction:

Annealing Temperature (°C)	E_g (eV) without ultrasonic			E_g (eV) with ultrasonic		
	UV-vis	***n***	ε_∞	**UV-vis**	***n***	ε_∞
Room Temp.	1.285	3.235[g]3.065[h]2.865[i]	10.46[g]9.39[h] 8.20[i]	1.29	3.24[g] 3.06[h] 2.86[i]	10.49[g] 9.36[h] 8.17[i]
200	1.26 1.49[a]	3.25[g] 3.07[h] 2.87[i]	10.56[g] 9.42[h] 8.23[i]	1.28	3.25[g] 3.07[h] 2.87[i]	10.56[g] 9.42[h] 8.23[i]
300	1.265 1.49[b]	3.245[g]3.068[h]2.865[i]	10.53[g] 9.41[h] 8.20[i]	1.275	3.257[g] 3.076[h] 2.875[i]	10.60[g] 9.46[h] 8.26[i]
400	1.27 1.48[c]	3.241[g]3.064[h]2.862[i]	10.50[g] 9.38[h] 8.19[i]	1.33	3.22[g] 3.04[h] 2.85[i]	10.36[g] 9.24[h] 8.12[i]
500	1.26 1.38[d] 1.35[e]	3.25[g] 3.07[h] 2.87[i]	10.56[g] 9.42[h] 8.23[i]	1.31	3.23[g] 3.05[h] 2.86[i]	10.43[g] 9.30[h] 8.17[i]
	PL	***n***	ε_∞	**PL**	***n***	ε_∞
Room Temp.	1.59	2.21[g] 2.90[h] 2.75[i]	4.88[g] 8.41[h] 7.56[i]	1.59	2.21[g] 2.90[h] 2.75[i]	4.88[g] 8.41[h] 7.56[i]
200	1.57 1.49[f]	3.07[g] 2.91[h] 2.76[i]	9.42[g] 8.46[h] 7.61[i]	1.57	3.07[g] 2.91[h] 2.76[i]	9.42[g] 8.46[h] 7.61[i]
300	1.54	3.09[g] 2.93[h] 2.79[i]	9.54[g] 8.58[h] 7.78[i]	1.56	3.08[g] 2.915[h] 2.768[i]	9.48[g] 8.49[h] 7.66[i]
400	1.52	4.01[g] 2.95[h] 2.81[i]	16.08[g] 8.70[h] 7.89[i]	1.55	3.087[g] 2.92[h] 2.77[i]	9.52[g] 8.52[h] 7.67[i]
500	1.53	4.00[g]2.945[h]2.805[i]	16.00[g] 8.67[h] 7.86[i]	1.54	3.09[g] 2.93[h] 2.775[i]	9.54[g] 8.58[h] 7.70[i]

Table 1: Measured energy band gaps correspond to refractive index and optical dielectric constant using Ravindra et al. [25], Herve and Vandamme [26] and Ghosh et al. [27] of Cu_2CdSnS_4 quaternary alloy nanostructures by using UV-vis and PL spectroscopies at different annealing temperatures. Ref. [22] Theo.; [b, c, d] Ref. [18] Theo.; [e] Ref. [17] Theo.; [f] Ref. [22] Exp.; [g]Ref. [25]; [h]Ref. [26]; [i]Ref.; [27].

$$n = \sqrt{1 + \left(\frac{A}{E_g + B} \right)^2} \tag{5}$$

where B= 3.4 eV and A= 13.6 eV. And, Ghosh et al. [27] had considered a different concept by considering the quantum-dielectric formulations of Penn [33] and Van Vechten [34]. Presenting, A (contribution from the valence electrons) and B (constant additive to the lowest band gap E_g), the meaning is:

$$n^2 - 1 = A / (E_g + B)^2, \tag{6}$$

where $B = 0.21E_g + 4.25$, $A = 25E_g + 212$ and (E_g + B) refers to the band gap of material. Therefore, the three models are for correlation of E_g and n. Also, calculated optical dielectric constant (ε_∞) was got using $\varepsilon_\infty = n^2$ [35]. The calculated values of n and ε_∞ are given in **Table 1**. It is shown that Ghosh et al. model is a suitable model for application.

Structural properties

The Cu_2CdSnS_4 (CCTS) quaternary alloy nanostructures have been investigated by XRD as shown in **Figure 5**. XRD patterns have provided information about the crystalline structure of nanoparticles as well as the crystallite size. By studying with ultrasonic patterns **(Figure 5a)**, the nanostructured CCTSs prepared at ambient temperature have ten peaks of major diffraction appeared at 2θ = 13.5808°, 15.8464°, 23.7231°, 28.2515°, 29.7159°, 29.9193°, 39.8234°, 43.5977°, 47.9415° and 48.9084° were belonged to (002), (101), (110), (100), (112), (004), (202), (114), (204) and (222), respectively. While, the nanostructured CCTSs prepared at 200 °C have ten peaks of major diffraction belonged to 2θ = 16.3054°, 29.8463°, 31.4023°, 33.8285°, 36.4505°, 39.8351°, 43.6715°, 47.9921°, 48.9813°and 57.8588° were attributed to (002), (112), (021), (101), (004), (202), (114), (204), (222) and (116). Whereas, the CCTS nanostructures deposited at 300 °C have three major diffraction peaks appeared at 2θ = 29.6737°, 47.84° and 48.9537° were attributed to (112), (204) and (222), respectively. Also, the nanostructured CCTSs prepared at 400 °C have seven peaks of major diffraction belonged to 2θ = 16.08°, 26.878°, 29.8635°, 39.8358°, 43.6052°, 47.9728°, and 48.9692° were referred to (002), (110), (112), (202), (114), (204) and (222). Lastly, the nanostructured CCTSs prepared at 500 °C have ten peaks of major diffraction belonged to 2θ = 12.2589°, 14.3791°, 17.9475°, 29.778°, 35.3549°, 39.8607°, 41.318°, 47.3837°, 48.9832° and 53.6095° were attributed to (110), (002), (101), (112), (004), (202), (114), (204), (222) and (116) planes, respectively.

On the other side, to investigate XRD patterns without using ultrasonic in **(Figure 5b)**, the nanostructured CCTS prepared at ambient temperature has one peak of major diffraction belonged to 2θ = 29.5961° was attributed to (112). While, the nanostructured CCTSs prepared at 200 °C have two peaks of major diffraction belonged to 2θ = 29.7836° and 39.8248° were referred to (112) and (114). Whereas, the nanostructured CCTSs prepared at 300 °C have four peaks of major diffraction belonged to 2θ = 29.9012°, 39.881°, 47.9995° and 49.0206° were attributed to (112), (114), (204) and (222). In addition, the CCTS nanostructures deposited at 400 °C have two major diffraction peaks appeared at 2θ = 10.554° and 29.5568° were attributed to (001) and (112). Lastly, the CCTS nanostructures deposited at 500 °C have nine major diffraction peaks appeared at 2θ = 21.9222°, 23.8988°, 29.9385°, 36.3869°, 39.9814°, 43.7231°, 48.0905°, 49.0561° and 57.9906° were attributed to (101), (110), (112), (202), (114), (220), (204), (222) and (224) planes, respectively. All the mentioned peaks are exactly matched with the tetragonal stannite structure of Cu_2CdSnS_4 that corresponding to the standard (ICDD PDF2008, 00-029-0537).

It is noticed that the highest peak at (112) plane for both types except the first peak at 500 °C for with ultrasonic. Additionally, it is noticed availability of peaks is with ultrasonic than without ultrasonic because of electron velocity difference. The lattice parameters a and c were found from XRD scheme of plane (112), according to system of tetragonal crystal. **Table 2** presents parameters, a and c with different structural parameters at different temperatures, with presence or without ultrasonic effect. The inter-planer distance (d) was calculated using Bragg's law [36];

$$d=\frac{n\lambda}{2\sin(\theta)} \tag{7}$$

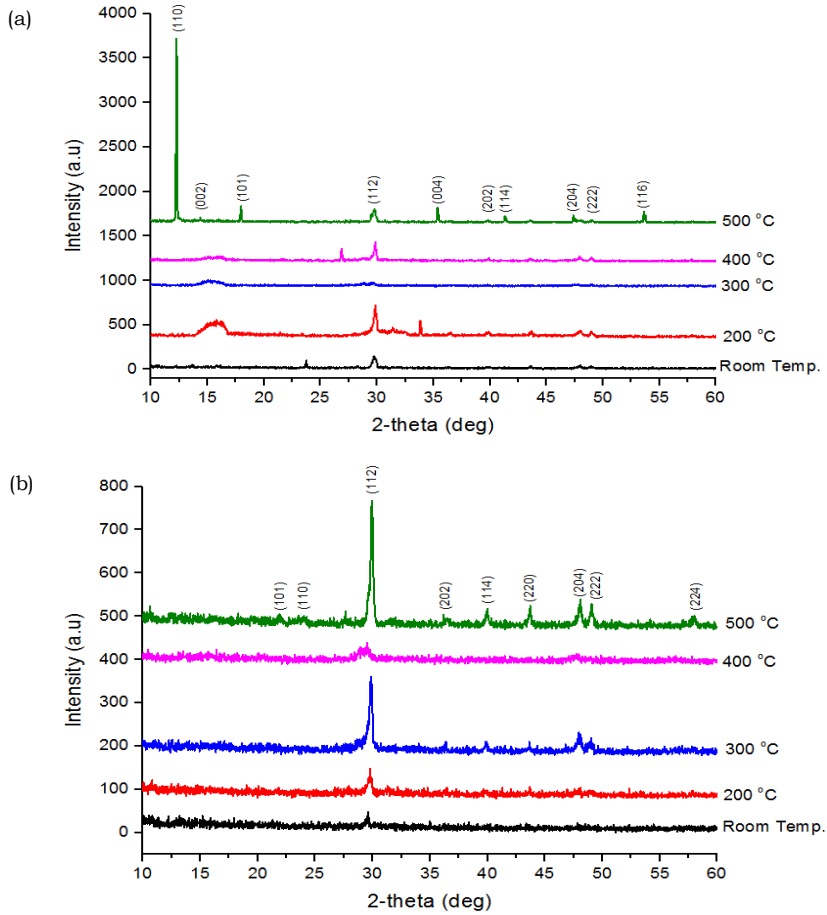

Figure 5: XRD patterns of Cu_2CdSnS_4 Quaternary alloy nanostructures deposited on p-Si at different annealing temperatures **a)** with ultrasonic, **b)** without ultrasonic [38].

Where λ is wavelength of XRD using (λ = 1.5406 Å) and θ is the Bragg's angle. Lattice constants a and c for tetragonal system were calculated from XRD patterns

$$\frac{1}{d^2}=\frac{h^2+k^2}{a^2}+\frac{l^2}{c^2} \tag{8}$$

Where hkl is Miller indices, a and c are the lattice constants. By combining eq's. (7) and (8), a and c can be calculated in terms of sinθ.

$$\sin^2\theta=\frac{\lambda^2}{4a^2}\left(h^2+k^2\right)+\frac{\lambda^2}{4c^2}\left(l^2\right) \tag{9}$$

The Scherrer's formula has been used to calculate the crystallite size (D) [37]

$$D=\frac{k\,\lambda}{\beta\cos\left(\theta\right)} \tag{10}$$

Where k is a constant, taken to be 0.94, and β is the full width at half maximum (FWHM) of the diffraction peak in radian. The dislocation density, strain and number of crystallites per unit area (N) for (112) plane as given in **Table 2** are calculated by the following equations.

$$\delta=\frac{1}{D^2} \quad (11)$$

$$\varepsilon=\frac{\beta\cos\theta}{4} \quad (12)$$

$$N=\frac{t}{D^3} \quad (13)$$

Where t is the thickness as indicated in **Table 2.**

T (°C)	2θ	Crystallite size (D) (nm)	full width at half maximum (FWHM)	Miller indices (hkl)	Interplaner distance (d) Å	Lattice constants (a and c)Å	Strain (ε)	Dislocation density (δ) (10^{14} lines/ m^2)	Number of crystallites particles/area (N)($x10^{15}$)	Thickness (t) (nm)
With Ultrasonic										
Room Temp.	29.71	43.7	0.1968	112	3.0065	a=5.2, c=10.41	0.047	5.23	1.607	136
200	29.84	43.9	0.196	112	2.99366	a=5.18, c=10.37	0.047	5.19	1.5	127
300	29.67	22	0.39	112	3.01068	a=5.2, c=10.43	0.094	20.6	3.193	34
400	29.86	109.12	0.0787	112	2.99197	a=5.18, c=10.36	0.019	0.83	0.00633	8.23
500	29.77	37.33	0.23	112	3.00037	a=5.19, c=10.39	0.055	7.17	0.392	20.4
Without Ultrasonic										
Room Temp.	29.59	29.8	0.288	112	3.0159	a=5.22, c=10.44	0.07	11.26	1.035	27.4
200	29.78	21.8	0.3936	112	2.99982	a=5.19, c=10.39 a=5.55, c=11.14[a]	0.095	21.04	98	1015.7
300	29.9	62.3	0.13776	112	2.98829	a=5.17, c=10.35 a=5.48, c=10.84[b]	0.033	2.57	1.42	344.6
400	29.55	18.1	0.47232	112	3.02232	a=5.23, c=10.46	0.114	30.52	11.28	66.9
500	29.93	43.6	0.1968	112	2.98465	a=5.16, c=10.34	0.047	5.26	0.52	42.7

Table 2: The structural parameters of Cu_2CdSnS_4 quaternary alloy nanostructures using XRD at different annealing temperatures.

[a]Ref. [22] Theo.; [b]Ref. [18] Theo.

Conclusion

Nanostructured Cu_2CdSnS_4 quaternary alloy was successfully prepared on p-Si wafer using sol-gel method under wide range of temperatures from room temperature to 500 °C. XRD results reveal that using ultrasonic in synthesizing the solution lead to introducing more peaks and as a result, the crystallite size increases. UV-vis and PL measurements demonstrate that the optical band gaps are 1.29-1.31eV and 1.59-1.54eV, respectively, which are quite close to the optimum band gap. The measured lattice constants are in accordance with available data in the literature. Ghosh et al. model is recommended model with ultrasonic effect at 400 °C. The resulted nanostructured Cu_2CdSnS_4 quaternary alloy is an absorbing layer for optoelectronic applications.

Acknowledgement

The author would like to thank to university for their support.

References

1. Wadia C, Alivisatos AP, Kammen D (2009) Materials availability expands the opportunity for large-scale photovoltaics deployment. Environmental Science & Technology 43: 2072-2077.
2. Peter lm (2011) Towards sustainable photovoltaics: the search for new materials. Philosophical Transactions of the Royal Society 369: 1840-1856.
3. Thiruvenkadam S, Jovina D, Rajesh A (2014) The influence of deposition temperature in the photovoltaic properties of spray deposited CZTS thin films. Solar Energy 106: 166-170.
4. Khan J, Arsalan M (2016) Solar power technologies for sustainable electricity generation - A review. Renewable and Sustainable Energy Reviews 55: 414-425.
5. Abermann S (2013) Non-vacuum processed next generation thin film photovoltaics: Towards marketable efficiency and production of CZTS based solar cells. Solar Energy 94: 37-70.
6. Liu CP, Chuang CL (2012) Fabrication of copper-indium-gallium-diselenide absorber layer by quaternary-alloy nanoparticles for solar cell applications. Solar Energy 86: 2795-2801.
7. Amiri O, Salavati-Niasari M, Farangi M (2015) Enhancement of Dye-Sensitized solar cells performance by core shell Ag@organic (organic=2-nitroaniline, PVA, 4-choloroaniline and PVP): Effects of shell type on photocurrent. Electrochimica Acta 153: 90-96.
8. Amiri O, Salavati-niasari M, Sabet M, Ghanbari D (2014) Sonochemical Method for Preparation of Copper Indium Sulfide Nanoparticles and their Application for Solar Cell. Combinatorial Chemistry & High Throughput Screening 17: 183-189.
9. Amiri O, Salavati-niasari M, Sabet M, Ghanbari D (2013) Synthesis and characterization of $CuInS_2$ microsphere under controlled reaction conditions and its application in low-cost solar cells. Materials Science in Semiconductor Processing 16: 1485-1494.
10. Sabet M, Salavati-niasari M, Ghanbari D, Amiri O, Yousefi M, et al. (2013) Synthesis of $CuInS_2$ nanoparticles via simple microwave approach and investigation of their behavior in solar cell. Materials Science in Semiconductor Processing 16: 696-704.
11. Amiri O, Salavati-niasari M, Rafiei A, Farangi M (2014) 147% improved efficiency of dye synthesized solar cells by using CdS QDs, Au nanorods and Au nanoparticles. RSC Advances 4: 62356-623561.
12. Li J, Zhang Y, Wang Y, Xue C, Liang J, et al. (2016) Formation of Cu_2ZnSnS_4 thin film solar cell by CBD-annealing route: Comparison of Cu and CuS in stacked layers SnS/Cu(S)/ZnS. Solar Energy 129: 1-9.
13. Cui Y, Wang G, Pan D (2012) Synthesis and photoresponse of novel Cu_2CdSnS_4 semiconductor nanorods. Journal of Materials Chemistry 22: 12471-12473.
14. Guan H, Zhao J, Wang X, Yu F (2013) Cu_2CdSnS_4 Thin film prepared by a simple solution method. Chalcogenide Letters 10: 367-372.
15. Guan H, Shi Y, Hou H, Wang X, Yu F, et al. (2014) Quaternary Cu_2CdSnS_4 nanoparticles synthesised by microwave irradiation method. Micro & Nano Letters 9: 251-252.
16. Li C, Cao M, Huang J, Wang L, Shen Y, et al. (2015) Facile synthesis of ultra-long Cu_2CdSnS_4 nanowires with wurtzite-derived structure. Materials Letters 140: 170-173.
17. Cao M, Li L, Fan W, Liu X, Sun Y, et al. (2012) Quaternary Cu_2CdSnS_4 nanoparticles synthesized by a simple solvothermal method. Chemical Physics Letters 534: 34-37.
18. Nie L, Liu S, Chai Y, Yuan R (2015) Spray pyrolysis deposition and photoresponse of Cu_2CdSnS_4 thin films. Journal of Analytical and Applied Pyrolysis 112: 363-368.
19. Guo H, Li Y, Fang X, Zhang K, Ding J, et al. (2016) Co-sputtering deposition and optical-electrical characteristic of Cu_2CdSnS_4 thin films for use in solar cells. Materials Letters 162: 97-100.
20. Zhang X, Chen D, Deng K, Lu R (20160 Band engineering of wurtzite-derived semiconductors Cu_2ZnSiS_4 and $Cu_2ZnSiSe_4$. Journal of Alloys and Compounds 656: 196-199.
21. Wang Y, Lou Y (2015) Radiant thermal conversion in 0.53 eV GaInAsSb thermo photovoltaic diode. Renewable Energy 75: 8-13.

22. Adegoke O, Nyokong T, Forbes P (2015) Structural and optical properties of alloyed quaternary CdSeTeS core and CdSeTeS/ZnS core–shell quantum dots. Journal of Alloys and Compounds 645: 443-449.

23. Kern W (1990) The Evolution of Silicon Wafer Cleaning Technology. Journal of the Electrochemical Society 137: 1887-1892.

24. Balzaretti N, Jornad J (1996) Pressure dependence of the refractive index of diamond, cubic silicon carbide and cubic boron nitride. Solid State Communications 99: 943-948.

25. Ravindra N, Auluck S, Srivastava V (1979) On the penn gap in semiconductors. Physica Status Solidi (b).

26. Herve P, Vandamme L (1995) Empirical temperature dependence of the refractive index of semiconductors. Journal of Applied Physics 77: 5476-5477.

27. Ghosh D, Samanta L, Bhar G (1984) A simple model for evaluation of refractive indices of some binary and ternary mixed crystals. Infrared Physics 24: 43-47

28. Al-Douri Y, Khachai H, Khenata R (2015) Chalcogenides-based quantum dots: Optical investigation using first-principles calculations. Materials Science in Semiconductor Processing 39: 276-282.

29. Al-Douri Y, Hashim U, Khenata R, Reshak A, Ameri M, Bouhemadou A, Rahim A, Arshad M (2015) AB initio method of optical investigations of $CdS_{1-x}Te_x$ alloys under quantum dots diameter effect. Solar Energy 115: 33-39.

30. Al-Douri Y (2003) Electronic and optical properties of $Zn_xCd_{1-x}Se$. Materials Chemistry and Physics 82: 49-54.

31. Al-Douri Y. Feng Y, Huan A (2008) Optical investigations using ultra-soft pseudopotential calculations of $Si_{0.5}Ge_{0.5}$ alloy. Solid State Communications 148: 521-524.

32. Al-Douri Y, Reshak A, Baaziz H, Charifi Z, Khenata R, Ahmad S, Hashim U (2010) An ab initio study of the electronic structure and optical properties of $CdS_{1-x}Te_x$ alloys. Solar Energy 84: 1979-1984.

33. Penn D (1962) Wave-number-dependent dielectric function of semiconductors. Physical Review 128: 2093-2100.

34. Vechten J (1969) Quantum Dielectric Theory of Electronegativity in Covalent Systems. I. Electronic Dielectric Constant. Physical Review 182: 891-895.

35. Samara G (1983) Temperature and pressure dependences of the dielectric constants of semiconductors. Physical Review B 27: 3494-3495.

36. Al-Douri Y, Khasawneh Q, Kiwan S, Hashim U, Hamid S, et al. (2014) Structural and optical insights to enhance solar cell performance of CdS nanostructures. Energy Conversion and Management 82: 238-243.

37. Al-Douri Y, Reshak A (2015) Analytical investigations of CdS nanostructures for optoelectronic applications. Optik 126: 5109-5014.

38. Ali A, Al-Douri Y, Ayub R, Ibraheam A (2016) Ultrasonic effect on optical, structural, topographical and morphological studies of Cu_2CdSnS_4 quaternary alloy nanostructures. Journal of Alloys and Compounds 686: 883-895.

Chapter 2

Copper Sulfide and Silver Sulfide Thin Films Prepared by Solid-vapor Reactions

M. Ortiz Díaz[1], H.S. Sánchez Rangel[2], J.F. Hernández Paz[3], I. Olivas Armendáriz[4], M. Ramos Murillo[5], C.A. Rodríguez González[6]*

[1,2,3,4,5,6]Instituto de Ingenieria Tecnologia, Universidad Autonoma de Ciudad Juarez, Ave del Charro #610 norte, Col. Partido Romero, C.P. 32320, Ciudad Juarez, Chihuahua, México

***Corresponding author:** C.A. Rodríguez González, Instituto de Ingenieria Tecnologia, Universidad Autonoma de Ciudad Juarez, Ave del Charro #610 norte, Col. Partido Romero, C.P. 32320, Ciudad Juarez, Chihuahua, México, E-mail: claudia.rodriguez@uacj.mx

Abstract

Currently, copper sulphide and silver sulphide thin films have been received a lot of attention from researcher. These films could be used for electronic, photonics, optoelectronic devices, solar cells, solar selective coatings, resistive switches, filament memories, and infrared detectors. Because of they have very unique properties (optical electrical, photocatalytical and photovoltaic properties), low cost and no toxicity. In this work, nanostructured copper sulphide and silver sulphide films were synthesized by using solid vapor reactions. Advantages and basic principles of this technique were discussed.

Keywords

Solid vapor reactions; Copper sulfide; Silver sulfide; Thin film; Solar cells

Introduction

Nowadays there is an extended interest on the research of different synthesis methodologies for copper sulfide and silver sulfide thin films. These materials are preferred for their excellent optical electrical, photocatalytical and photovoltaic properties as well as their low cost and no toxicity. They have been found to be potential candidates for electronic, photonics, optoelectronic devices among others. Solar cells, solar selective coatings, resistive switches, filament memories, infrared detectors are examples of applications for these materials. Numerous synthesis methodologies for these materials have been reported such as: Chemical Vapor Deposition, Ion Beam Deposition, Solid-Gas Reactions, Electrodeposition, Chemical Bath, Spray Pyrolysis and methodologies such as ADL and photochemical

Metal Chalcogenide Nanostructures: Characteristics and Synthesis, Edited by Ho Soon Min and Yarub Al-Douri

deposition that includes the silver or copper sulfidation by liquid or gas containing sulfur compounds such as H_2S [1-11]. Each methodology has advantages and disadvantages. Among the main disadvantages are excessive cost, toxicity, elevated synthesis temperatures, considerable number of by-products, annealing requirements at high temperatures after synthesis that limit the use of flexible substrates and films heterogeneity.

In this chapter, a review of the silver and copper sulfide thin films synthesis by solid vapor reaction is presented. This synthesis methodology has been used to obtain 2D and 3D nanostructures and its main advantages are: simplicity, low cost, low by product formation, low temperature and no-annealing requirements [12-15]. In section 1 the general principles of the solid vapor reaction are presented. Section 2 is a brief description of the Ag-S and Cu-S systems. The synthesis methodology is described in section 3 and the proposed reaction mechanisms are summarized in section 4. Section 5, and 6 describes the obtained morphological and optical properties, as well as the thickness of the films obtained from experimental variations. Finally, a summary and references are presented in sections 7 and 8, respectively.

The Solid Vapor Reaction: Basic Principles

The solid vapor reaction is considered a bottom-up processing technique since it goes from nano to macro. Among the four groups generally used to classify nanostructure synthesis techniques (spontaneous growth, template synthesis electrospinning and lithography), the solid vapor reaction is classified as spontaneous growth process [16].

This kind of processes are driven by the free Gibbs energy reduction or chemical potential. This is generally accomplished by a phase transformation, chemical reaction or stress relief. An anisotropic growth of three stages is required where each plane grows at different rates, crystal imperfections at specific directions occurs, and impurities in each plane are accumulated. Therefore, defects and impurities play an important role on the final product morphology [16].

The solid vapor reaction is a chemical reaction among reactants to produce crystalline phases with imperfections. The reactions and crystal growth is described by Cao 2004 [16] as follows:

1. Bulks´s growth species diffusion (for example, vapor or liquid phases) to the developing surface, which is considered to continue sufficiently rapid and therefore does not limit the process.
2. Adsorption and desorption of growth species onto and from the developing surface. This procedure can be rate constraining, if the supersaturation or amount of species is low.
3. Diffusion at the surface of the growth species that have been adsorbed. These species can leave the surface or form part of the crystal growth.
4. Surface growth. It occurs by incorporating the adsorbed growth species into the crystalline structure. If supersaturation of growth species occurs, this step will be limiting the growth rate.

5. Growth at the surface by irreversibly including the adsorbed species into the crystalline structure. At the point when an adequate supersaturation or a high concentration of growth species is available a process in which the development rate is limited occurs.
6. If there is presence of chemical by-products, they can desorb at the surface and then, the adsorption of the growth species can proceed.
7. By-products diffuses away from the surface creating vacancies for continuing the species growth. In this stage is adsorption and desorption which limits the reaction rate. **Figure 1** shows a schematic figure of the solid vapor reaction stages [16].

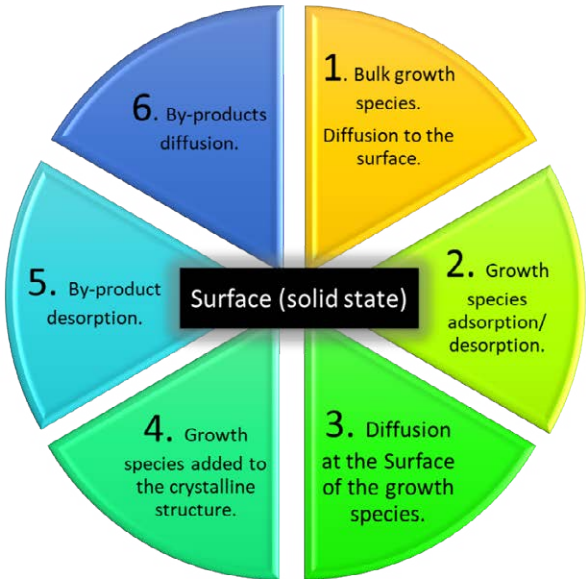

Figure 1: Solid vapor reaction stages.

Silver-sulfur (Ag-S) and copper-sulfur (Cu-S) systems

The thin films development for energy conversion and optoelectronic materials among other applications is of great interest. Low cost and non-toxic materials are required for these films and it is here where chalcogenides materials receive special attention because they fulfil these requirements and exhibit excellent electrical, photovoltaic, photocatalytical and optical properties [17, 18]. Copper sulfides poses various stoichiometric forms that are room temperature stable, including sulfur rich (CuS_2), copper rich (Cu_2S), and also some intermediate compounds such as (CuS, $Cu_{1.95}S$, and $Cu_{1.75}S$) as shown in **Figure 2** [19-23]. The reported band gaps of Cu_xS thin films typically lay in the range of 1.2 to 2.6 eV but are greatly dependable in the measuring method [24-29]. Covallite (CuS) is a p-type semiconductor with a hexagonal crystal structure ($P6_3/mmc$, a = 3.7938 Å, c = 16.341 Å, Z = 6) [30] which is stable up to approximately 500 °C.

Silver sulfide (Ag_2S) is known to be an ionic-electron conducting material capable of conducting both ions and electrons [32]. It has three different allotropic forms:

the α-Ag_2S phase called Acanthite presents a monoclinic crystalline structure (a = 4.23 Å, b = 6.91 Å, c = 7.87 Å, β = 99 °35) and a space group $P2_1$ / n. This phase is formed at room temperature and is stable at temperatures below 178 °C, at this temperature there is a transformation that gives rise to the allotropic form β-Ag_2S called Argentita with structure BCC (a = 4.88 Å), which is stable in the temperature range from 178 °C to 600 °C. The third known allotropic phase of silver sulphide is the γ-Ag_2S phase, which is stable over 600 °C and has an FCC structure [33].

The most stable phase corresponds to Acanthite (α-Ag_2S) and is considered an important semiconductor because it has a band of ~1eV at room temperature and has a relatively high absorption coefficient (approx. 104 cm-1) [34]. This compound can be used for the manufacture of optical and electrical devices such as photoconductors, photovoltaic cells, IR detectors, solar selective coatings A. 1988), actuators, among others [35, 36] **Figure 3.**

Solid-vapor reaction methodology

As mentioned before, some of the advantages of the solid vapor reaction methodology are simplicity, low temperature and very low by-product formation. This methodology allows the crystalline growth of nanostructures on different substrates containing the metal to be sulfurized. The methodology for obtaining copper sulphide and silver sulphide thin films includes the use of substrates

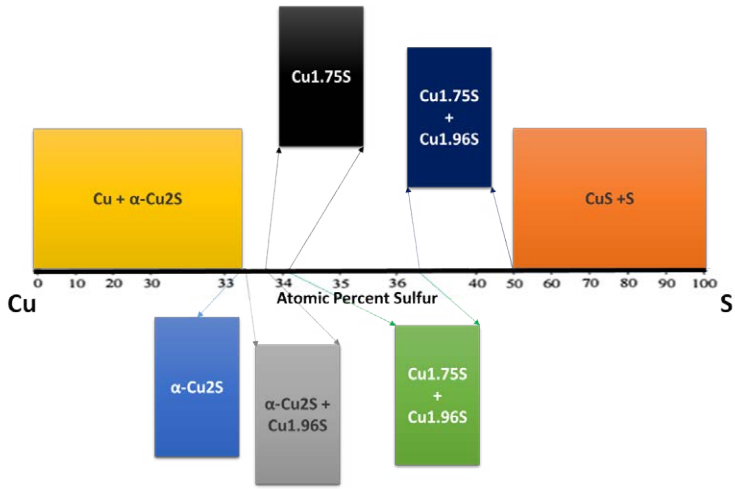

Figure 2: Cu-S phases at room temperature [31].

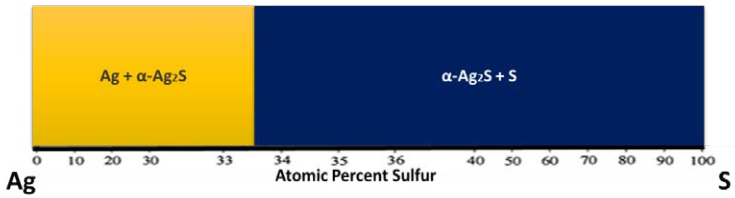

Figure 3: Ag-S phases at room temperature [37].

containing copper or silver. Copper films or silver films can be deposited on metallic, polymeric or glass substrates using a plasma sputtering coating technique using copper or silver targets. High purity targets should be preferred. Some research [12, 13] has shown that a simple sputtering coating for SEM analysis can be successfully used for this purpose. In these case, a fixed current of 20 mA was used for the process. Sputtering time was used to control the film thickness. For sulfidation, the samples were placed in a glass container along with two beakers containing 20 mL of D.I water each and 3 g of sublimed sulfur (99.97%). The system was closed with aluminium foil and sealed with aluminium tape. A reactive sulfur atmosphere was generated according to ASTM B809. The reaction was carried out for 3 h at 110 °C at atmospheric pressure. Sputtering deposition time and sulfidation time can be varied for tailoring the films properties. A schematic of the process is shown in **Figure 4**. Some results are presented in sections 5, 6 and 8.

Figure 4: Schematic drawing of the solid vapor reaction.

Resulting phases and reactions mechanisms

The resulting phases of the proposed solid vapor reactions for the Cu-S and Ag-S systems in this chapter are crystalline. No post-thermal treatments or annealing processes are required. **Figure 5** shows examples of CuS and Ag_2S thin films resulting from this synthesis methodology. Covellite and acanthite are the crystalline phases obtained for the respective systems mentioned above.

The mechanism of thin film silver sulfide formation by the solid vapor reaction could be represented by reactions 1 to 3. The silver sulfide formation does not depend of the water presence but it is reported that its presence can increase the reaction rate. Possibly forming more reactive sulfur compounds such as H_2S [38, 39]:

$$2Ag+S^{2-}=Ag_2S+2e^- \quad (1)$$

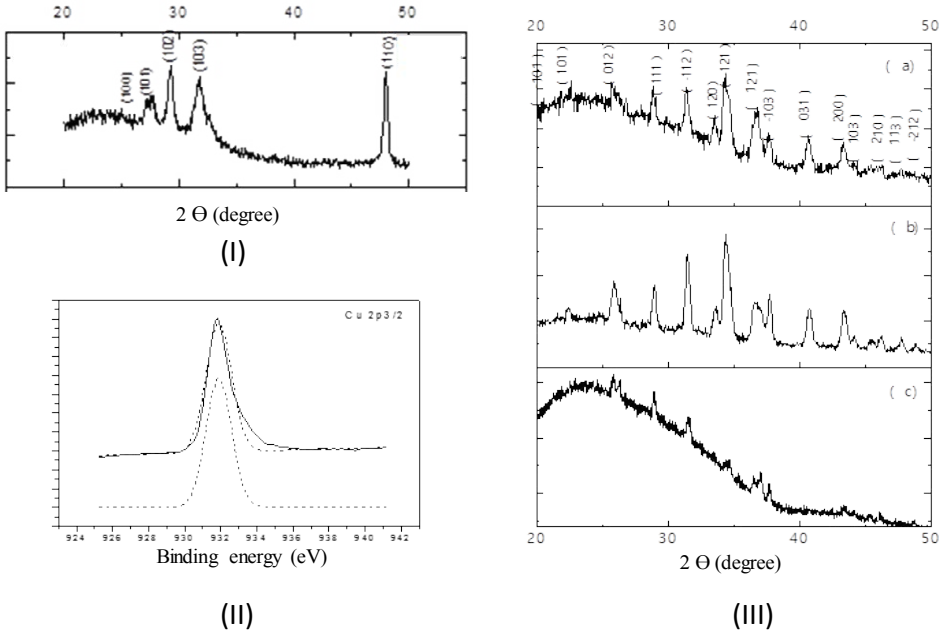

Figure 5: Example of the crystalline phases obtained with the solid vapor reaction thin films synthesis for the Cu-S and Ag-S systems. **(I)** Small angle XRD pattern of CuS thin film obtained on a glass substrate with a copper film generated by sputtering during 18 minutes [13], **(II)** Cu 2p3/2 XPS analysis of CuS thin film (binding energy correspond to CuS formation) [13] and **(III)** Small angle XRD pattern of **(a)** 2 minutes silver film, **(b)** and **(c)** small angle and XRD of a Ag2S film from a silver film deposition of 5 minutes. All films were prepared over glass substrates [12].

$Ag_2S+S^{2-}=Ag_2S_2+2e^-$ (2)

$2Ag+Ag_2S_2+2e^-=2Ag_2S$ (3)

A reaction between silver and the sulfur present in the vapor is developed. Probably, the sulfur excess in the atmosphere leads to the formation of an unstable Ag_2S_2 compound. The reaction continues with the movement of unreacted silver ions through the silver sulfide and reacting with the Ag_2S_2 and the sulfur in the atmosphere. Some research has shown that in the case where carbon monoxide (CO), carbonyl sulfide gas (COS) could be formed. Graedel et al. [38] propose that COS and silver react to form Ag_2S in a comparable manner that H_2S does it with silver. In summary, diverse mechanisms such as elemental adsorption and desorption occurring during the solid vapor reaction lead to the formation of the silver sulfide nanostructures. A sudden reaction between COS a silver may explain the observed discontinuities on the 3D nanostructures, this reaction could generate preferred crystal growth. This effect is explained in section 2.

The nanostructure formation is due to a solid vapor reaction and adsorption and desorption of the growing elements that come from the vapor phase occur causing the growth of t silver sulfide nanostructures. However, in this case open spaces are observed in the obtained 3D nanostructures which could be explained by a momentary reaction between the COS and the silver that could generate

a trunked path and a preferential growth according the effect of by-products in the crystal growing theory of nanostructures of solid-vapor reactions explained in section 2.

The proposed mechanism for the copper sulfide thin films synthesis is like the mechanism explained in the previous paragraph for the Ag_2S formation [15]. A sulfur rich atmosphere provides sulfur ions (S-2) that reacts with the Cu ions (Cu+) present on substrates forming the copper sulfide (CuS) film. The sublimed sulfur reaction provides a continuous presence of sulfur ions in the atmosphere which leads to the formation of a non-stable sulfur rich compound (e.g. CuS_x) on the film surface. This creates a species concentration difference that helps the copper diffusion from inner layers to the previously formed copper sulfide. The copper ions will react again with the atmosphere leading to the crystal growth of CuS. In this case, water presence and H_2S formation can increase the reaction rate [38, 39]. This process was applied onto glass substrates, but flexible substrates can be used as well.

$$Cu+S^{-}=CuS+e^{-} \quad (4)$$

$$Cu+S^{-}=CuS_x+e^{-} \quad (5)$$

$$Cu+CuS_x+e^{-}=CuS \quad (6)$$

Resulting thin films-thicknesses and microstructures of Cus and Ag_2s

According to the results obtained so far, it is possible to produce thin films of CuS in the range of 70 to 110 nm with the methodology presented in section 4. The effect of the solid vapor reaction on the thin films thickness is shown in **Figure 6**. The thickness increases due to the solid vapor reaction that promotes the layer

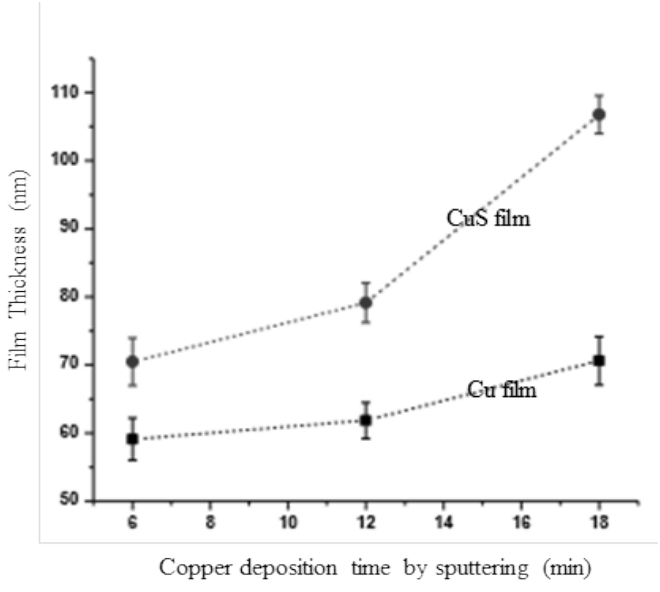

Figure 6: Effect of copper sputtering deposition time on the final CuS thin films thickness.

growth. Also, it is seen that the morphology of the CuS thin films surfaces depends on the initial thickness of the sputtered copper layer **(**See **Figure 7)**. A combined fine and coarse granular morphology is observed on samples with an initial copper layer thickness of 60 nm. Copper layers of 63 nm average thickness after being exposed to 3h of solid vapor reactions result exhibit similar fine grain size but the coarse grains change to smooth large areas. Smoother but porous surfaces were obtained with an initial copper layer of 70 nm average thickness. The observed changes in morphology can be attributed to copper availability, its diffusion and its reaction with sulfur ions (S^{-2}) during the solid vapor reaction.

The thin films morphology varies if a crystalline substrate is used instead of an amorphous one. Then, an ordered morphology is obtained because the growth process is oriented and directed by the substrate as shown in **Figure 8**. Structures are larger when deposition time increase because there is more copper to react and form the CuS structures. This is self-explanatory with **Figure 9**, where 3D nanostructures are obtained when copper substrates are used and the solid vapor reaction time is increased. At short time periods (2 h) and high magnifications, the effect of the crystalline substrate in the order of the resulting structure is easily observed where hexagonal bases growth and with the time are transformed in layered structures. Figure 10 shows the effect of the sputtering deposition time on the Ag2S thin films thickness. Also, in the Ag-S system thickness increases due to the layered growing mechanism of the solid vapor reaction [14, 15] **Figure 10.**

The Ag_2S thin films grain size homogeneity increases when the initial silver thickness increase but grain size decreases **(Figure 11)**. This behaviour can be explained in function of the amount of silver available on the substrate to react. Larger amounts favour the diffusion and nucleation process instead the grain growth. If the solid vapor reaction time increases **(Figures d, e, and f)**, grain growth is favoured and a coarse structure is observed. Larger grain islands or sections are observed because grains tend to coalesce with time.

Resulting CuS and Ag_2S thin films- optical properties

The measurement of thin films optical properties is basic for the understanding

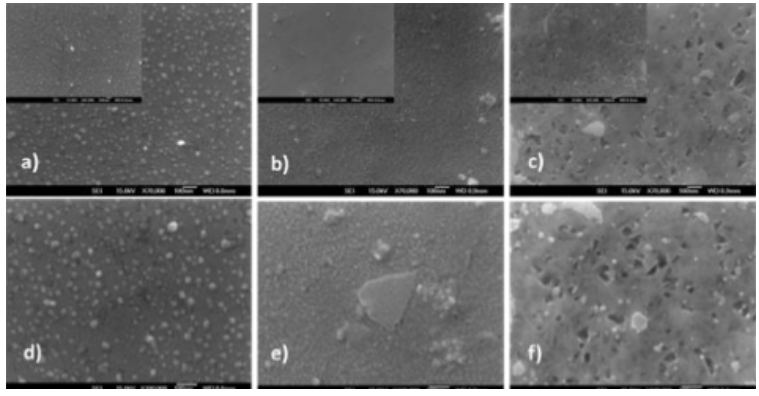

Figure 7: FE-SEM images of CuS thin film surfaces on glass substrate. **a), b)** and **c)** correspond to 6, 12 and 18min deposition time of Cu initial layer at low magnification; **d)**, **e)** and **f)** 6,12 and 18 min deposition time at higher magnification [13].

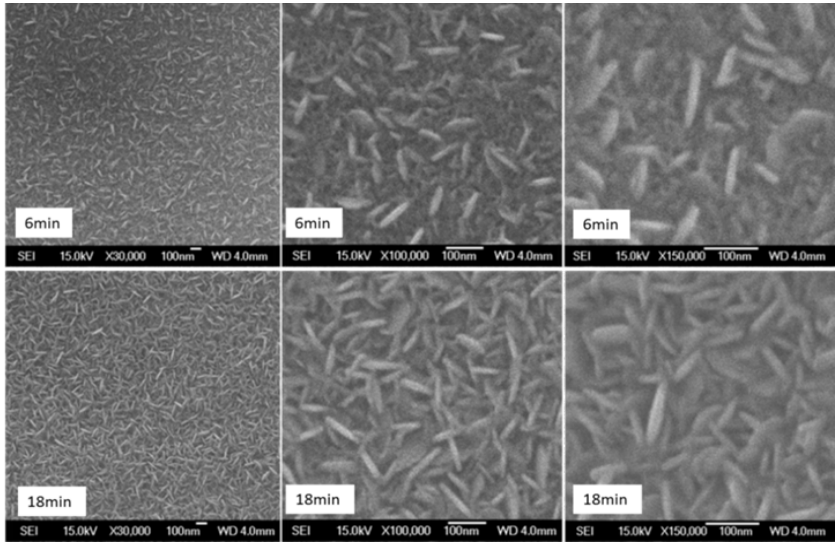

Figure 8: FE-SEM images of CuS thin film surfaces on crystalline acetate substrates.

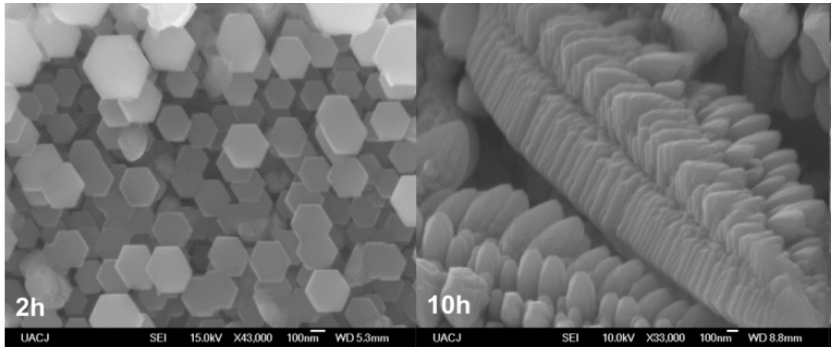

Figure 9: FE-SEM images of CuS structures on copper substrates synthetized by the solid vapor reaction.

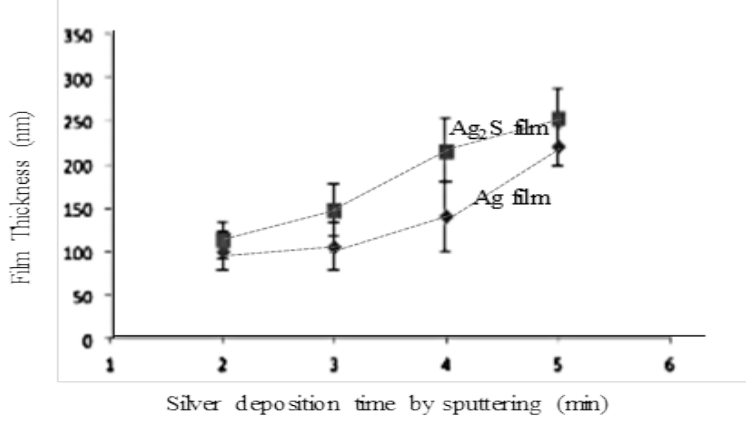

Figure 10: Effect of silver sputtering deposition time on the final Ag_2S thin films thickness.

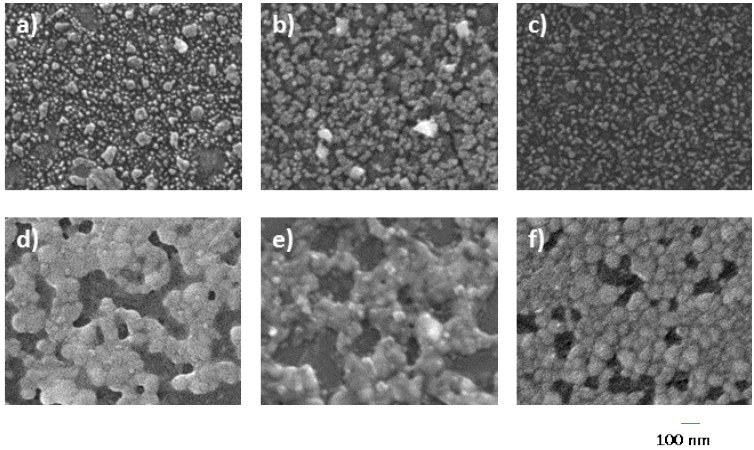

Figure 11: FE-SEM images of Ag_2S structures on glass substrates synthetized by the solid vapor reaction described in section 4. Initial silver average thickness film is **a)** and **d)** 90 nm, **b)** and **e)** 230 nm and **c)** and **f)** 280 nm. Solid vapor reaction time is 3h for **a), b)** and **c)** and 5 h for **d)**, **e)** and **f)**. Figures a, b and **c** are from reference [12].

of semiconductor thin films. Light transmission, absorption coefficients and band gaps are some of the properties that can be determined with these measurements.

Copper sulfide thin films synthetized by solid vapor reactions on glass substrates show adsorption edges from 441 to 448 nm wavelength ranges **(Figure 12)**. The maximum absorbance is observed from 350 to 400 nm which is in agreement with the reported values for this phase thin films synthetized by other methodologies [40]. Thin films absorbance increases as the thin films thickness increases.

Bandgaps of the samples were calculated using the $(\alpha h\nu)^2$ vs hv. The calculated values were in the range of 2.05 to 2.25 Ev **(Figure 13)**. As can be observed, the bandgaps decrease with the films thickness.

Covallite (CuS) thin films on flexible substrate (crystalline acetate) show similar optical properties despite morphologies are considerable different. The maximum absorbance values are also within 350 to 450 nm **(Figure 14)** and bandgaps between 2.12 to 2.25 eV **(Figure 15)**.

Bandgaps of CuS films on copper substrates synthetized by solid vapor reactions change. considerable since they absorb in a wide wavelength range. Values shown in **Figure 16** were calculated according to Kubelka-Munk´s equation and are similar to those reported for the bulk materials.

Regarding the Ag-S system optical properties, the absorbance of Ag_2S thin films on glass substrates increases significantly as a function of the increase in thickness **(Figure 17)**. The bandgaps values were calculated for each one of the samples of different sputtering times. Calculations were made for the direct and indirect transitions on the graphs of $(\alpha h\nu)^2$ vs hv for the case of the direct and $(\alpha h\nu)^{1/2}$ vs hv for the indirect transitions **(Figure 18)**. The ranges of values are between 1.7 to 2.6 eV depending on the thickness and these values are within those reported for the thin films of Ag_2S [40]. As expected, the values of the thicker films show the lowest values. The effect of the different thicknesses is greater than

the effect of the morphology (grain size or structures). The bangaps values for both systems allow applications in the field of solar radiation as solar absorbers or as optoelectronic devices.

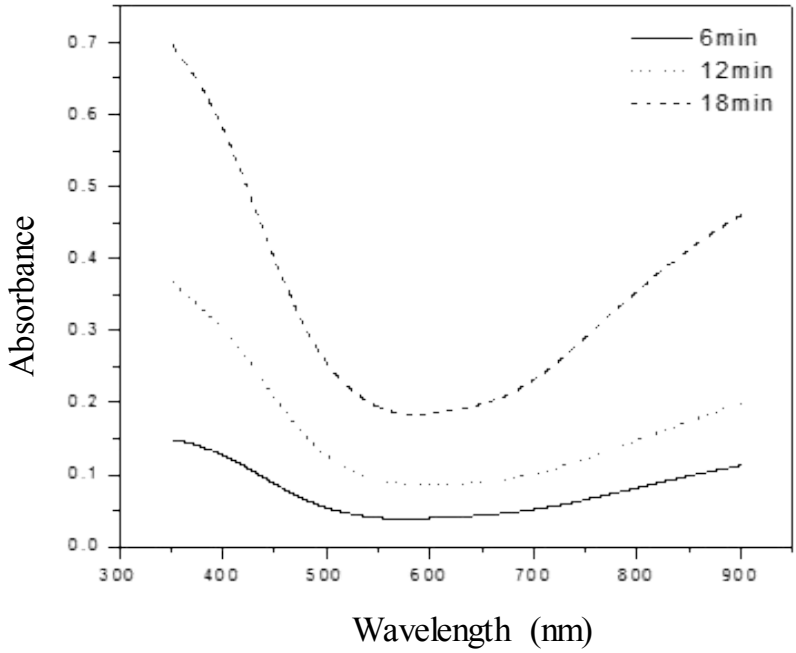

Figure 12: Absorbance of CuS thin film surfaces on glass substrate.

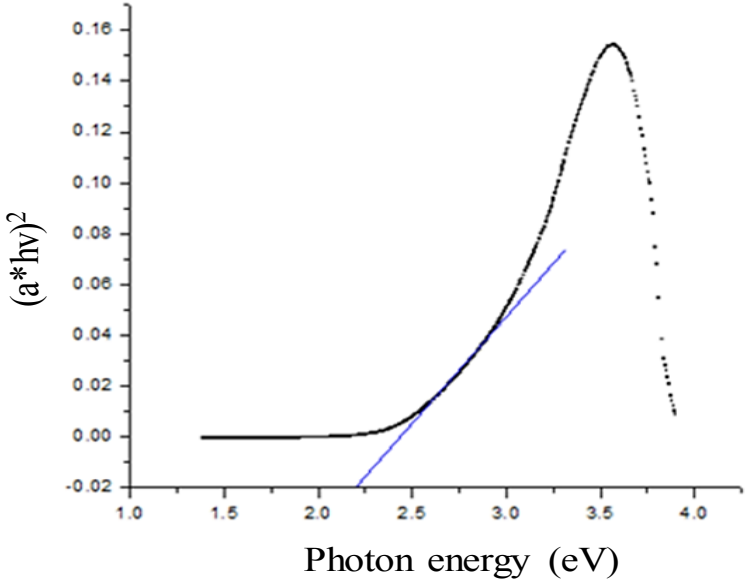

Figure 13: Example of the calculated bandgaps of CuS thin film surfaces on glass substrate.

Figure 19 shows the absorbance of Ag_2S thin film on glass substrates exposed to 5 h of solid vapor reaction time. As expected the transmittance value decreases and the absorbance value increases with respect to the thickness. However, the grain size is smaller in the samples with longer deposition time, which induces the dispersion of light reducing the transmittance of the film. On the other hand, the solid vapor reaction time increases the absorbance even though the grain size is large. This is because the effect of heterogeneity on the light scattering is greater and exceeds the effect of grain size **(Figure 20)**.

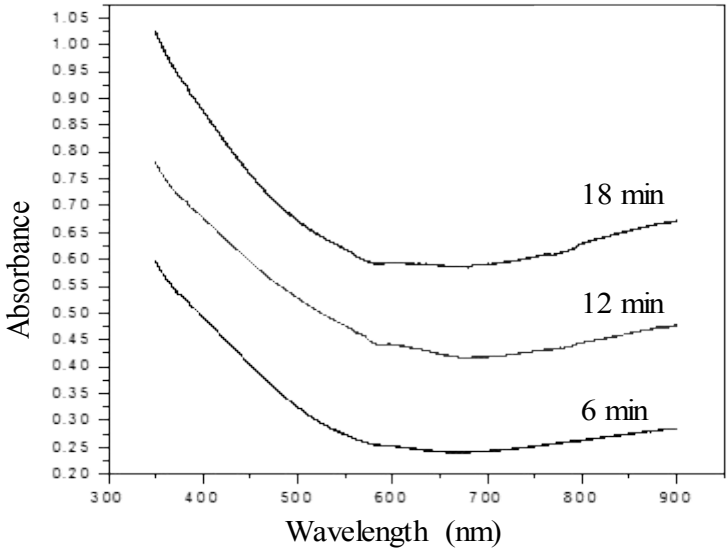

Figure 14: Absorbance of CuS thin film surfaces on flexible substrate.

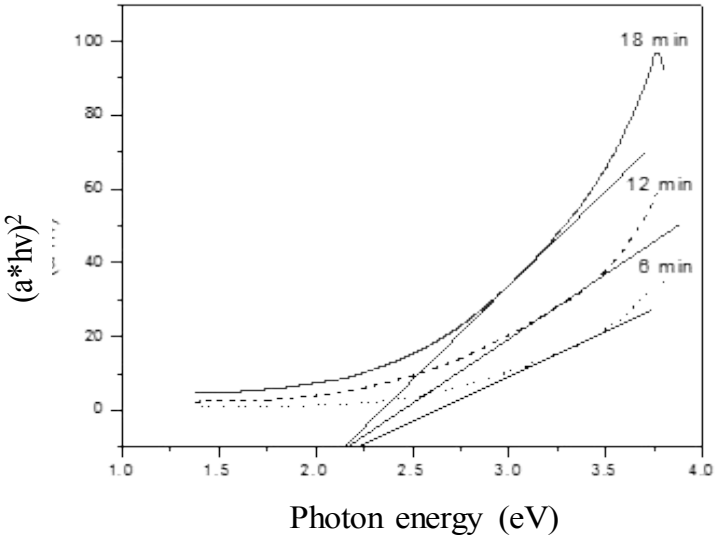

Figure 15: Example of the calculated bandgaps of CuS thin film surfaces on flexible substrate.

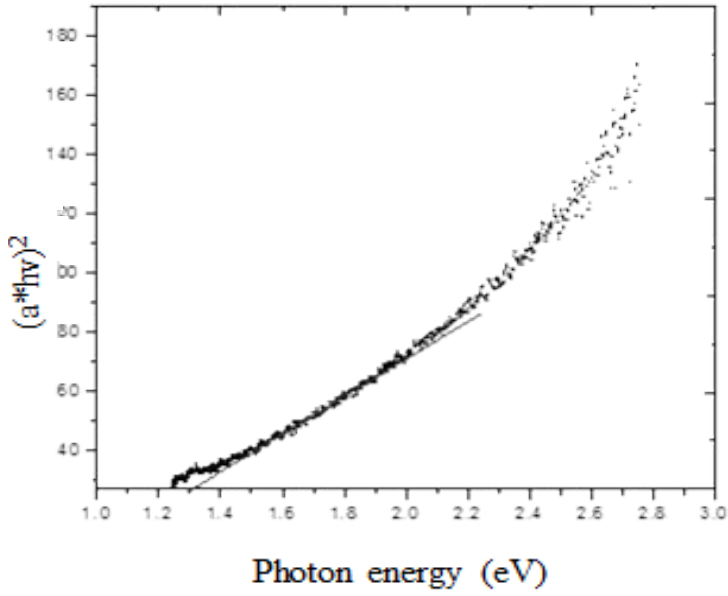

Figure 16: Example of the calculated bandgaps of CuS thin film surfaces on copper substrate. Values were calculated using the Kubleka Munk´s equation.

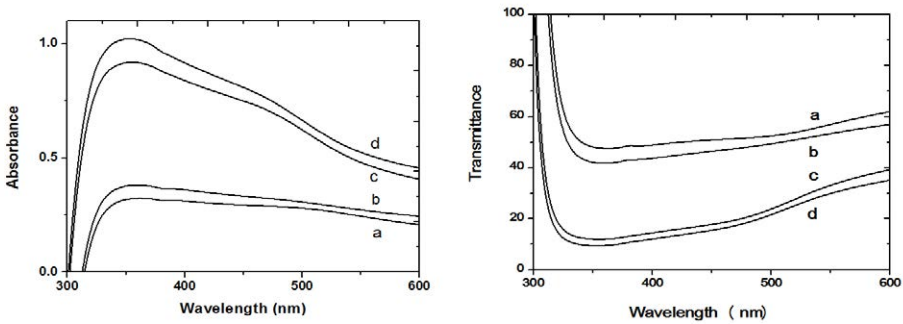

Figure 17: Absorbance and transmittance of Ag_2S thin films on glass substrates. Silver deposition time by sputtering was **a)** 2min, **b)** 3min, **c)** 4min y **d)** 5min. All samples were exposed to solid vapor reactions during 3h.

The change in the solid vapor reaction time allows tailoring optical properties in the system Ag-S. Absorbance after 3h of solid vapor reaction results in values below 40% in a wavelength range of 340-500 nm. If the solid vapor reaction time is increased up to 7 h. Absorbance values are around 90% in a wavelength range of 320-600nm. This gives the Ag_2S films promising properties as solar absorbers [29, 35, 41, 42].

Conclusion

The solid vapor reaction is considered a bottom-up processing technique that produces crystalline phases with imperfections through a chemical reaction

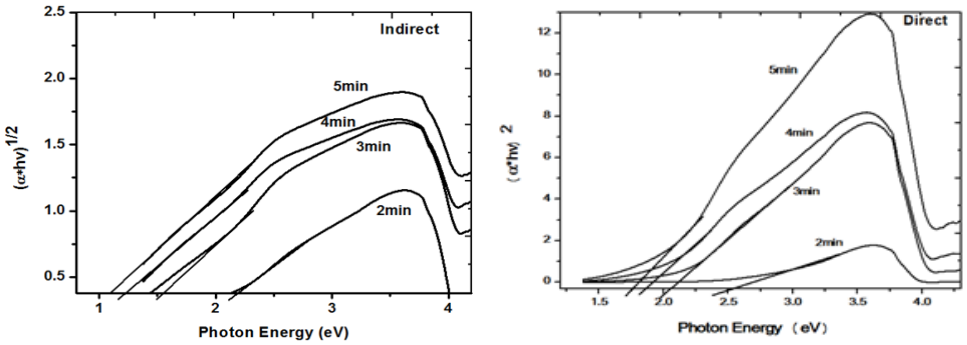

Figure 18: Bandgap of Ag2S thin films on glass substrates calculated from the direct and indirect transitions. Silver deposition time by sputtering was **a)** 2min, **b)** 3min, **c)** 4min y **d)** 5min. All samples were exposed to solid vapor reactions during 3h.

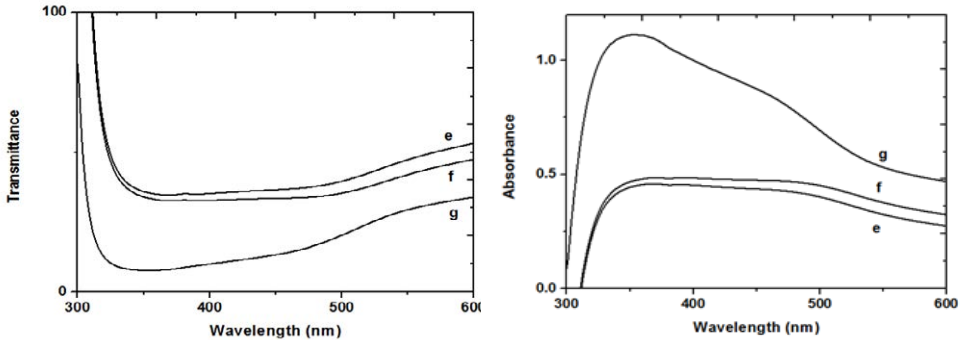

Figure 19: Absorbance and transmittance of Ag_2S thin films on glass substrates. Silver deposition time by sputtering was **a)** 2min, **b)** 3min, **c)** 4min y **d)** 5min. All samples were exposed to solid vapor reactions during 5h.

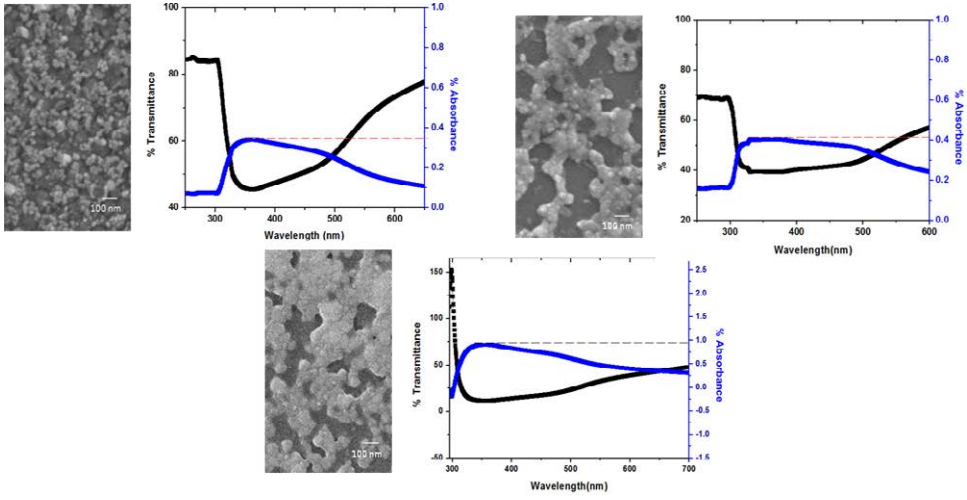

Figure 20: Absorbance and transmittance of Ag_2S thin films on glass substrates. Silver deposition time by sputtering was c) 4min, Solid vapor reactions times were 3h, 5h and 7h.

among reactants. This is an easy low temperature synthesis (110 °C), where the formation of secondary by-products is almost nil and results in crystalline CuS (Covallite) and Ag_2S (Acanthite) thin films over rigid or flexible substrates. The final film properties can be tailored with the reaction time, substrate materials and initial metallic films thickness.

The proposed mechanism for the thin films synthesis of copper and silver sulfide is through the reaction of the metallic ions of either copper (Cu^+) or silver (Ag^+) present in the substrates with a sulfur atmosphere (vapor) rich in sulfur ions (S^{-2}) which allows the formation of metallic sulfide phases. This process creates a species concentration gradient that allows the diffusion of metallic ions from within the thin film sample to the recently formed metallic sulfide in a continuous way, resulting in the formation and growth of crystalline metallic sulfurs.

Thin films thickness and morphology can be related to the available to diffuse metallic ions and reactive sulfur ions (S^{-2}) present during the solid vapor reaction. Ordered morphology is obtained when crystalline substrates are used. In systems where the amount of metallic material to be sulfurized during the solid vapor reaction is not limited, a layered growing mechanism is observed which results in crystalline metallic sulfide 3D nanostructures on the substrate.

Thin films optical properties such as band gaps, absorbance and transmittance vary considerably by changing these parameters. Therefore, another advantage of this methodology is the opportunity to design, in a very simple manner, the final films optical properties to fulfil the requirements of the currently highly demanding technological applications.

Acknowledgement

The author would like to thank to university for their support.

References

1. Panneerselvam A, Malik M, O'Brien P, Raftery J (2008) The CVD of silver sulfide and silver thin films from a homoleptic crystalline single-source precursor. Journal of Materials Chemistry 18: 3264-3269.

2. El-Nahass M, Farag M, Ibrahim E, Abd-El-Rahman S (2004) Structural, optical and electrical properties of thermally evaporated Ag_2S thin films. Vacuum 72: 453-460.

3. Sankapal BR, Mane RS, Lokhande CD (2000) A new chemical method for the preparation of Ag_2S thin films. Materials Chemistry and Physics 63: 226-229.

4. Wen X, Wang S, Xie Y, Li X, Yang S, et al. (2005) Low-temperature synthesis of single crystalline Ag_2S nanowires on silver substrates. The Journal of Physical Chemistry B 109: 10100-10106.

8. Rodríguez A, Nair M, Nair P (2005) Structural, optical and electrical properties of chemically deposited silver sulfide thin films. Semiconductor Science and Technology.

5. Akamatsu K, Takei S, Mizuhata M, Kajinami A, Deki S, et al. (2000) Preparation and characterization of polymer thin films containing silver and silver sulfide nanoparticles. Thin Solid Films 359: 55-60.

6. Dias C, Proenca M, Fernandes L, Tavares P, Vilarinho R, et al. (2016) Tuning the Stoichiometry of Ag_2S Thin Films for Resistive Switching Applications. Journal of Nanoscience and Nanotechnology 16: 2608-2612.

7. Vas-Umnuay P, Kim K, Chang C (2016) Growth kinetics of copper sulfide thin films by photochemical deposition. CrystEngComm 18: 6748-6758.

8. Schneider N, Lincot D, Donsanti F (2016) Atomic layer deposition of copper sulfide thin films. Thin Solid Films 600: 103- 108.

9. Sahraoui K, Benramdane N, Khadraoui M, Miloua R, Mathieu C, et al. (2014) Characterization of silver sulphide thin films prepared by spray pyrolysis using a new precursor silver chloride. Sensors & Transducers 27: 319-325.

10. Ortiz-Diaz M, Ramos-Murillo M, Elizalde-Galindo J, Enriquez-Carrejo J, Camacho-Montes H, et al. (2016) Absorbance and Current-Voltage Hysteresis Curve of Silver Sulfide Thin Films Synthetized By Solid-Vapor Reactions. Chalcogenide Letters 13: 201-206.

11. Rangel H, Castillo A, Hernández J, Paz J, Montes H, et al. (2015) Synthesis of copper sulfide (CuS) thin films by a solid-vapor reaction. Chalcogenide Letters 12: 381-387.

12. Martínez-Ruvalcaba I, Hernández-Paz J, Mancilla J, Ruiz P, Pérez C, García-Casillas P, Rodríguez-González C, et al. (2014) Optical properties of bio-inspired silver sulfide structures. Journal of Alloys and Compounds 586: S526-530.

13. Muniz-Lerma J, Hernández-Paz J, Farias-Mancilla J, Casillas P, González C, et al. (2012) Synthesis of hierarchical dorsal spine Ag_2S structures by a solid-vapor reaction: the effect of reagent gas composition. Journal of Nanomaterials.

14. Cao G, Wang Y (2011) Nanostructures and nanomaterials: synthesis, properties and applications. World Scientific.

15. Lai C, Lu M, Chen L (2012) Metal sulfide nanostructures: synthesis, properties and applications in energy conversion and storage. Journal of Materials Chemistry 22: 19-30.

16. Lai C, Huang K, Cheng J, Lee C, Hwang B, et al. (2010) Direct growth of high-rate capability and high capacity copper sulfide nanowire array cathodes for lithium-ion batteries. Journal of Materials Chemistry 20: 6638-45.

17. Puspitasari I, Gujar T, Jung K, Joo O (2007). Simple chemical preparation of CuS nanowhiskers. Materials Science and Engineering: B 140: 199-202.

18. Jiang C, Zhang W, Zou G, Xu L, Yu W, et al. (2005) Hydrothermal fabrication of copper sulfide nanocones and nanobelts. Materials Letters 59: 1008-1011.

19. Chen X, Wang Z, Wang X, Zhang R, Liu X, et al. (2004) Synthesis of novel copper sulfide hollow spheres generated from copper (II)–thiourea complex. Journal of Crystal Growth 263: 570-574.

20. Gong J, Yu S, Qian H, Luo L, Liu X, et al. (2006) Acetic acid-assisted solution process for growth of complex copper sulfide microtubes constructed by hexagonal nanoflakes. Chemistry of Materials 18: 2012-2015.

21. Tezuka K, Sheets W, Kurihara R, Shan Y, Imoto H, et al. (2007) Synthesis of covellite (CuS) from the elements. Solid State Sciences 9: 95-99.

22. Gadave K, Lokhande C (1993) Formation of Cu_xS films through a chemical bath deposition process. Thin Solid Films 229: 1-4.

23. Fatas E, Garcia T, Montemayor C, Medina A, Camarero E, et al. (1985) Formation of CuxS thin films through a chemical bath deposition process. Materials Chemistry and Physics 12: 121-128.

24. Varkey A (1989) Chemical bath deposition of Cu_xS thin films using ethylenediaminetetraacetic acid (EDTA) as complexing agent. Solar Energy Materials 19: 415-420.

25. Couve S, Gouskov L, Szepessy L, Vedel J, Castel E, et al. (1973) Resistivity and optical transmission of Cu_xS layers as a function of composition. Thin Solid Films 15: 223-231.

26. George J, Joseph K (1983) Amorphous films of CuS. Solid State Communications 48: 601-603.

27. Grozdanov I, Najdoski M (1995) Optical and electrical properties of copper sulfide films of variable composition. Journal of Solid State Chemistry 114: 469-475.

28. Evans H, Konnert J (1976) Crystal structure refinement of covellite. American Mineralogist 61, 996-1000.

29. Blachnik R, Müller A (2000) The formation of Cu_2S from the elements: I. Copper used in form of powders. Thermochimica Acta 361: 31-52.

30. Rickert H (1982) Electrochemistry of solids. Springer Berlin. New York, Heidelberg.

31. Madelung O, Rössler U, Schulz M (2001) Group IV Elements, IV-IV and III-V Compounds, Part a-Lattice Properties, Landolt–Börnstein–Group III Condensed Matter.

32. Dlala H, Amlouk M, Belgacem S, Girard P, Barjon D (1998) Structural and optical properties of Ag_2S thin films prepared by spray pyrolysis. The European Physical Journal Applied Physics 2: 13-16.

33. Shen H, Jiao X, Oron D, Li J, Lin H, et al. (2013) Efficient electron injection in non-toxic silver sulfide (Ag_2S) sensitized solar cells. Journal of Power Sources 240: 8-13.

34. Terabe K, Hasegawa T, Nakayama T, Aono M (2005) Quantized conductance atomic switch. Nature, 433, 47- 50.

35. Hiroaki O, Mark E, Erik MM (2016) ASM Handbook Volume 3: Alloy Phase Diagrams, ASM International, ISBN: 978-1-62708-070-5.

36. Graedel TE, Franey JP, Gualtieri GJ, Kammlott GW, Malm DL, et al. (1985) On the mechanism of silver and copper sulfidation by atmospheric H_2S and OCS. Corrosion Science 25: 1163- 1180.

37. Volpe L, Peterson PJ (1989) The atmospheric sulfidation of silver in a tubular corrosion reactor. Corrosion Science 29: 1179- 1187.

38. Grozdanov I (1995) Solution growth and characterization of silver sulfide films. Applied Surface Science 84: 325- 329.

39. Enríquez JP, Mathew X (2003) Influence of the thickness on structural, optical and electrical properties of chemical bath deposited CdS thin films. Solar Energy Materials and Solar Cells 76: 313-322.

40. Shiro T, Kanno T, Aratani K, Katsura Y, Ikenaga NO, et al. (2002) Promoting effect of sulfur compounds on the degradation of polyethylene. Energy & Fuels 16: 1314-1320.

Chapter 3

Chemical Bath Deposition Technique for Metal Chalcogenides

Prashant A. Chate[1]* Dattatray J. Sathe[2]

[1]Department of Chemistry, J.S.M. College, Alibag. (M.S.) India

[2]Department of Chemistry, KIT's College of Engineering, Kolhapur. (M.S.) India

***Corresponding author:** Prashant A. Chate, Department of Chemistry, J.S.M. College, Alibag. (M.S.) India, E-mail: pachate04@rediffmail.com

Abstract

A chalcogenide is a chemical substance including at least one chalcogen anion and at least one electropositive element. In the current scenario, there has been lots of attention in metal chalcogenides, due to their physical and chemical characteristics trade unexpectedly with particle dimension. There are some factors influence the quality of films such as deposition time, temperature, the role of complexing agent, pH, the concentration of solution. The growth and nucleation were explained. The advantage of chemical bath deposition method was discussed. The fundamental of chemical bath deposition technique was described.

Keywords

Thin film; Chemical bath deposition; Growth and nucleation; Chalcogenide; Band gap

Introduction

In the current scenario, there has been lots of attention in metal chalcogenides [1-3], due to their physical and chemical characteristics trade unexpectedly with particle dimension. Those substances are attracting significant attention because of their essential electronics and optical characteristics [4-6]. The physio-chemical characteristics of these substances are mostly relying upon method applied for the synthesis of the metal chalcogenide samples. It's miles vital to choose the appropriate methods for the preparation of metal chalcogenide.

A chalcogenide is a chemical substance including at least one chalcogen anion and at least one electropositive element. Even though all group sixteen elements of the periodic table are defined as chalcogens, the term chalcogenide is more frequently kept for sulfides, selenides, and tellurides, rather than oxides. The name is usually applicable to mean "ore former" from the Greek chalco "ore" and gen "formation".

Metal Chalcogenide Nanostructures: Characteristics and Synthesis, Edited by Ho Soon Min and Yarub Al-Douri

Oxygen and sulfur are nonmetals, and polonium, selenium and tellurium are semimetals. However, tellurium, in addition to selenium, is frequently considered to as a conductor when in elemental type. Chalcogens are obtained in the form of various minerals. The official oxidation state of the chalcogens is normally -2 in a chalcogenide however different charge and magnitude, like -1 in pyrite, may be observed. The maximum official oxidation state +6 is observed in sulfates, selenates and tellurates.

It appears from the Greek terms (chalkos, literally 'copper'), and (genes, born). Consequently, the chalcogens provide birth to, generate copper. Despite the fact that the factual significance of the Greek terms involves that chalcogen means copper-former, that is disingenuous due to the chalcogens have not anything to do with copper in specially. "Ore-former" has been endorsed as an enhanced transformation, together because of circumstance that larger amount of metal ores are chalcogenides, and because of the term chalcogen in ancient Greek was associated to metals and metal-bearing rocks. Chalcogenides have robust ability for application in photonics. Photo darkening were applied to manufacture waveguides, and a number of chalcogenides illustrate enormously high fast optical nonlinearities that could be applied for the entire optical switching and optical energy which may be in line to the mid-infrared telecommunications wavelengths.

The characteristics of metal chalcogenide are strongly reliant on the process of deposition. Chemical depositions [7-9] that occupy a restricted however slow precipitation is at the moment an attractive method because of its ease, cheapness and convenience for the synthesis of huge area compound. The preparative factors are simply convenient and enhanced orientation may be found out.

Deposition of metal chalcogenide applying chemical bath techniques [10-12] is at present drawing significant consideration since it is comparatively low-cost, easy and suitable for big area coating. Low temperature techniques [13-15] keep away using oxidation and corrosion of materials. Such processes were slow which provide higher orientation of grains having enhanced particle size. Relying upon preparative situations, film development may occur through ion via-ion deposition on the substances on the holding material or via adsorption of colloidal grain using the reactive mixtures on the holding materials. Any insoluble surface to which the solution has free access will be a suitable substrate for deposition. Applying such processes, compounds of different groups were deposited.

The vast flexibility supplied with the aid of the metal chalcogenide development techniques lets in the production of preferred topographical, geometrical, crystallographic, physical, and metallurgical microstructures into much less size and to have a look at the structure responsive characteristics. The characteristics are strongly reliant on the technique of preparation [16-18], the holder materials, pH, the preparation temperature, the pace of deposition and elemental combination. Precise appliances in present method demand sample characteristics like increasing optical reflection/ transmission, hardness, adhesion, non-porosity, higher mobility of charge transporters, insulating characteristics, stoichiometry, epitaxy, and point of reference in single crystal /crystalline samples.

Amongst a variety of preparation methods, the chemical bath methods are a smaller temperature, soft method for the development of metal chalcogenide.

It's far suitable when in compliance sample is desirable with conservation of the characteristics of the material under few monolayers. Compound semiconductors like Sb_2S_3 and Sb_2Se_3 are used in the Videocon television pick up tube and CdS and CdSe films in photoconductors and solar cells. The III-VI compound films especially GaAs and InSb have been used in galvanometric devices, while PbS, PbSe and HgS thin films have been used as IR detectors. Rapid progress in metal chalcogenide devices has helped for ICs of monolithic and hybrid microelectronics. Using chemical bath deposition, a number of binaries, such as CdS [19], CdSe [20], Bi_2S_3 [21], Bi_2Se_3 [22], PbS [23], PbSe [24], Ag_2S [25], MgSe [26], MnS [27], MoS_2 [28], ZnSe [29], ZnS [30], SnS [31] and ternaries such as $CuInS_2$ [32], $CuInSe_2$ [33], CdZnS [34], Cu_4SnS_4 [35], PbCdS [36], $CdZnSe_2$ [37], $Ni_3Pb_2S_2$ [38] have been deposited as thin films.

Chemical Bath Deposition (CBD)

Chemical bath deposition technique is oldest commercially used coating method. The method includes growing of film on any suitable substrate by dipping it in an appropriate solution of metal salt. The cation of respective metal, complexed with the appropriate complexing agent is allowable to react with chalcogen ion. The cations and anions are to produce gradually via rising temperature of reacting mixture. The ions so produced combine on the substrate via nucleation. The growth usually occurred by the ion-by-ion condensation process. The deposition may occur either by homogenous or heterogeneous chemical reaction.

The chemical bath deposition technique is mostly used for deposition of various elements [39, 40]. It is also known by various names as 'electroless plating' or 'chemical deposition (CD)', or 'chemical solution deposition (CSD)', or 'solution growth', or 'controlled precipitation'. The procedure of chemical bath deposition consists of the restricted precipitation of a compound from a solution on an appropriate substrate. In this technique, precipitation of the solid phase takes place because of the supersaturation in the reaction mixture. At a given temperature when the ionic product of reactants goes beyond the solubility product, precipitation takes place. While if the ionic product is not as much of as the solubility product, then the solid phase formed will dissolve reverse to the solution consequential in rejection net precipitation. This is the fundamental theory behind every chemical coating technique. The deposition occurs either by homogenous or heterogeneous chemical reaction.

CBD method is a technique to deposit metal chalcogenides samples and nanomaterials; it may be employed for huge area batch processing or continuous coating. Metal chalcogenide coating is the accuracy controlled immersion and elimination of a few substrates into a reactive mixture of liquid for the purpose of coating a film of material. A lot of chemical and nonmaterial manufacturing investigate initiatives in academic world and enterprise make use of the CBD technique.

In this process, when cationic and anionic solutions are mixed mutually and if ionic product beat or become equivalent to the solubility product, precipitation takes place as ions come together on the substrate and in the solution to develop nuclei. The process necessitates the occurrence of reagents that proceed as a supply of chalcogen ions and complexation of metal ions of attention whose equilibrium

stability make available a concentration of metal cation minute sufficient to generate the restricted homogeneous precipitation of the sample of the solid materials. This process is reliant upon factors such as reaction bath temperature, pH of the reaction mixture, a concentration of the reactant and reaction time. A complexing reagent is added to manage the hydrolysis of the metal ion [41, 42]. Such technique depends on the sluggish liberate of chalcogenide ions into acidic or basic solution in that the free metal ion is buffered at a low quantity. The quantity of free metal ion is maintained by the development of complex species consistent with the common reaction,

$$M^{2+} + A \longrightarrow M(A)^{2+}$$

At this time amount of the free metal ions at a particular temperature is corresponding to the expression concentration of product to the concentration of reactant is called as instability constant. The instability constant is unlike for dissimilar complexing agents. As the instability constant raise, larger number of ions will be free. The stability of the metal complex was too reliant on temperature and pH of the reactive mixture. Enhance in temperature of the reaction mixture will develop the complex less stable, while enhancing in pH commonly develops it more stable. Consequently, the amount of metal ions may be controlled via the quantity of a suitable complexing agent and the temperature of the reactive mixture. If a higher amount of sulfide or selenide ions be present locally such that the solubility product is increased, localized impulsive precipitation of a sulfide or selenide can take place as the case may be. Such conditions can be avoided by producing chalcogen ions gradually and consistently during the volume of the solution.

Nature of the reactants manipulates the composition of the deposition. Modify in the composition of the reaction mixture the segment of the ultimate deposition varies. The growth kinetics too depends on the type of reactants. For example, when metal sulfate is utilized to coat metal selenide samples applying sodium selenosulfide, the speed of coating reduce and the maximum thickness enhance. At this point, the sulfate ions acquire from the metal sulfate decrease a number of selenide ions. Deposition speed and maximum thickness begin with enhancing ionic quantity of the reactants. Nevertheless, at the higher amount, the precipitation becomes extremely quick, leading to reduce in sample thickness on the substrate.

In a typical reaction, the amount of metal ion diminishes with rising quantity of the complexing ions. As a result, the speed of reaction and therefore precipitation are decreases producing a larger terminal thickness of the sample. The deposition temperature is an additional parameter which manipulates the speed of reaction. As a temperature of the reactive mixture rises the breaking of the complex enhances. The kinetic energy of the molecules too boosts producing larger interaction among ions. This will consequence in enhance or reduce of maximum thickness, relying on the degree of supersaturation of the reactive mixture. When the pH value of the reactive mixture increases, the metal complex frequently happens to more stable, reduces the ease of use of liberated metal ions. Such conditions will reduce the reaction speed ensuing in greater maximum thickness. It was experiential that the sample characteristics have been extremely much dissimilar in the case of such samples when correlating with that of samples prepared using the alkaline bath. Generally, development of high-quality semiconductor metal chalcogenide samples

proceeds at a sluggish rate. This process is preferably suitable for producing homogeneous samples having the thickness in the range of 0.05- 0.3 μm in the majority of cases and infrequently to widen of few microns.

The advantages of chemical bath techniques [43, 44] over other techniques are discussed below:

1. It is an economical, modest and appropriate technique for greater region coating of metal chalcogenides.
2. The technique works at low temperature i.e. less than 80 ^{0}C.
3. There is no limitation on choice of substrate material as it operates at low temperature.
4. In this method, sample thickness and coating speed may be organized using fluctuating pH of a reactive solution, temperature and amount of reagents.
5. The oxidation or corrosion of the metallic substrate is avoided by using a low temperature.
6. Preparation of metal chalcogenide process is sluggish; it assists superior orientation of crystallites having enhanced granules structure.
7. Pinhole free and uniform deposits of complex shapes and sizes can be obtained due to intimate contact between the reacting solution and the substrate material used.
8. The basic building blocks are ions instead of atoms which maintain the stoichiometry of deposits.
9. The method does not use any toxic volatile constituents.
10. By using chemical bath deposition, the doped and mixed film structure can be obtained very easily by adding dopant solution directly into reaction bath.
11. In this method, an electrical conductivity of substrate material has no great importance.
12. This method can be used for deposition of elementary, binary, ternary or quaternary metal chalcogenides.
13. The technique is applicable for the deposition of highly insoluble compounds.
14. This technique does not necessitate complicated instrumentation.
15. This technique provides a minute thickness of the sample.

The mechanism of metal chalcogenide formation and the effect of various deposition parameters play a vital role in CBD process. The change in deposition conditions during the deposition process can result in different layers, e.g. compact inner layer and porous outer layer, in the film.

Factors Affecting Deposition of Metal Chalcogenides by Chemical Bath Deposition

The deposition of metal chalcogenide samples generally depends upon the amount of the precursor solution, the character of complexing agent, deposition temperature, deposition temperature and speed of substrate rotation.

Composition of precursor solution

The growth rate and feature of the deposited samples became significantly influences by the concentration of the reacting species [45, 46]. The samples prepared via applying small concentration are thin and non-uniform. This examination may be related to the inadequate supply of ionic species at such concentration levels. Alternatively, when an amount of the species was larger, the superiority and uniformity of the sample go on rising and the samples were thick. This is factual up to a definite level of concentration and afterward, saturation in the growth development was observed.

It is recognized that bath composition is significant in obtaining metal chalcogenide samples. By varying the composition of the reactive mixture, competition among the processes of homogeneous and heterogeneous nucleation could be changed to support metal chalcogenide development. The preparation of superior quality, adherent, specular and crystalline samples has frequently been associated with supersaturated mixture irrespective of the substrate. The development under such situation generates sulfide ions into an acidic solution, where the free metal ions are buffered. As a result, low amount of reactive mixture ingredients frequently favors the nucleation in the primary step. Through preparation procedure, 1.0- 3.0mM of ingredient concentration has been found out subsequent to numerous trials. Certainly, the reactive mixture amount plays a significant role in the substrate interaction with developing crystallites. For higher amount, the samples generated were thicker, representing stronger interaction. Under these conditions, the development processes develop into a cluster- via-cluster sooner than ion-via-ion nucleation. In contrast to the lower amount, the samples generated were excessively thin and non-uniform. This is due to the actuality that the requisite number of ionic species is not accessible in the reaction mixture to obtained enhanced quality samples.

Role of complexing agent

The complexing reagent is solitary of the preparation circumstances play a vital role in the methodology of the metal chalcogenides samples [47, 48]. A complexing reagent applied to attach metallic ions to keep away from the precipitation of the related compound. The creation of complexion is critical to manage the speed of deposition and to stay away from the instantaneous precipitation of the material in the reaction mixture. Metal chalcogenide sample coating is an adsorption procedure which consequences in the generation of material on the template. Metal chalcogenide sample creation takes place via the combination of ions free from complexed metal resource and chalcogen supply. The character of complexed metal ion is unstable and is correlated to the dissociation constant of metal-complex. The glycine complex has a lesser magnitude of stability constant in order that complexed metal ion may be ready free in acidic medium. Furthermore, glycine was applied to limit the hydrolysis of the metal ion and impart some stability to the reactive mixture that, if not experience quick hydrolysis and formation of solid materials.

In techniques, an aqueous solution of a metal complex when added to a solution of chalcogen bearing compound, formation of the solid compound of chalcogen take place under definite circumstances. When the precipitation is forbidden, the

material acquires prepared on uncontaminated substrates or further nucleating centers available in the reaction mixture. By choosing a suitable complexing reagent, the amount of the metal ions is maintained via the quantity of the complexing reagent. The kinetics of development of a metal chalcogenide sample in this procedure is estimated via the ion-via-ion coating of the chalcogenide on nucleating location on the dipped faces. In the beginning, the film development speed is insignificant due to an induction time is requisite for the creation of important nuclei as of a homogeneous system onto an uncontaminated face. On one occasion nucleation take place, the speed increases quickly awaiting the speed of coating equals the speed of dissolution. Therefore, the sample achieved a maximum thickness. The metal ion amount diminishes with rising amount of the complexing ions. Therefore, the speed of reaction and consequently precipitation is reduced generating to a greater maximum thickness of the sample.

Deposition temperature

The speed of chemical reaction in the reactive mixture may too be prejudiced by the bath temperature. As temperature enhances dissociation of the complex raise, therefore, the kinetic energy of the reacting ions also raises leading to larger interaction among ions and subsequent deposition at volume nucleation centers of the substrate [49, 50]. These will consequence in increase or decrease of terminal thickness, depending on the extent of super saturation of the solution of the bath. Reaction mixture temperature has a significant outcome on crystal dimension. In the majority cases, larger temperatures permit larger granule growth while lower temperatures yield extremely minute nuclei in a solution that are thermodynamically unstable. Nevertheless, if the cluster is smaller than the critical nucleus dimension, subsequently there is the probability that the nucleus will redissolve. In a large amount cases, dip process may be applied to cautiously manage the crystallinity of the metal chalcogenide sample semiconductors by adjusting the preparation temperature. The life span of the nucleus will then reliant on its dimension and as well on the temperature; lower temperatures will sluggish the redissolution stage. Thus smaller temperature enhances the possibility that a subcritical nucleus will ultimately develop to a stable mass before redissolving.

Deposition time

Deposition period is one of the significant factors that influence metal chalcogenide sample deposition in technique [51, 52]. In the majority cases, it has an immense influence on structural, morphological and optical characteristics of metal chalcogenide films sample. Larger deposition rates and greater metal chalcogenide thicknesses are frequently accompanied by powdery deposits and be deficient of specular reflection.

Greater deposition period resulted in thicker films samples that led to comparatively low absorbency in the absorption spectrum. Such samples show low absorption in the higher wavelength region. The thickness consequence is noticed in the long wavelength area of the spectra where interference effects occur. The interval of the sample deposition became too studied.

Process of precipitation in the solution phase

There are the two steps involved in the process of precipitation in the solution phase.

Formation of a nucleus

The circumstance of supersaturation only is not an adequate reason for a system to commence to crystallize. Before crystal may grow there ought to be present in the solution numerous microscopic solid bodies, embryos, nuclei or seeds that operate as a center of crystallization. Nucleation can take place concurrently or it can stimulate artificially. It is not constantly possible, though, to make a decision whether a system has nucleated of its own accord or it has made so under the influence of a few outside stimuli. Nucleation may frequently be induced by agitation, mechanical shock, friction and intense pressures inside solutions and melts. The unpredictable effects of exterior influences like electric and magnetic fields, spark discharge, ultraviolet light, X-rays, γ-rays, sonic and ultrasonic emission have too been studied over numerous years however so far not any of such process has established any important applications in significant crystallization practice. It is recommended that the nucleation caused via scratching the surface of the container could be the consequence of nucleation.

At the current occasion, there is no common agreement on nucleation nomenclature. The term primary will be kept for the entire cases of nucleation in systems that do not consist of crystalline substance. Alternatively, nuclei frequently create in the vicinity of crystals available in a supersaturated system; such performance will be considered as secondary nucleation.

Precisely how a stable crystal nucleus is developed inside a homogenous fluid is unknown with any degree of certainty. The development of crystal nuclei is an even more complicated technique to predict. Not only have the ingredient molecules to coagulate, oppose the affinity to redissolve, although they have to become orientated into an unchanging lattice.

If a solution consists of no uncontaminated particles or crystals of its own nature, the nucleus may only be generated via homogeneous nucleation. If foreign surfaces are available in the system, it is likely for a liquid to develop on those surfaces nuclei at less supersaturation related to the case of homogeneous nucleation. This procedure is known as heterogeneous nucleation. It has been found out that nuclei take place still at extremely low supersaturation. When crystals of same substance are present and it works as attrition agents or seed crystals then such nuclei are referred as secondary nuclei.

Nucleation is the beginning of a first-order phase alteration by that an unstable step changes into a further stable one. Such a phase alteration takes place when an early system originally in equilibrium is unstabilized by the change of an exterior factor such as the temperature or the pressure. If the perturbation is small sufficient, the system remains stable although relatively stays metastable. In diffusive alterations, the system then develops through the nucleation, the growth and the coarsening of a second stage.

An origin of nucleation representations is the fact, that fraction of the collisions among molecules cause a bond breaking and formation among the molecules. The familiar Arrhenius relation provides the temperature related to the reaction rate unstable. The equation involved a multiplier associated with the collision speed known as the frequency parameter and the exponent function part. The exponent function illustrates the portion of reactive collisions of the entire collisions. The

reactive fraction correlates exponentially with the expression of the necessary energy level known as activation energy and the product of the kinetic gas constant and absolute temperature.

The nucleus can be defined as the smallest amount of ions or molecules necessary for producing a secure second stage in contact with an aqueous phase. The speed of formation of nuclei in the reactive mixture depends on the extent of super saturation. The speed of nucleation enhances exponentially in highly supersaturated reaction mixture i.e.

Speed of nucleation = K (Q-S)x.

Where K and x are the constants and x is less than 1.

Growth

Metal chalcogenide go through numerous dissimilar steps throughout growth [53, 54], every step affecting the resultant sample microstructure and therefore its physical characteristics in some, now and then irreversible, ways. A number of processes occur at the same time as the nuclei developed and become grains. Atoms incessantly connect to, either directly from the vapor or as diffusing adatoms, and separate from the granules with a positive overall growth speed for granules. To understand the processes taking place it is helpful to first consider what happens to a number of in a different way sized granules on a surface with no any coating occurs. Atoms will continuously separate from attaching grains with no net modify in dimension for some isolated granules. Any given grain will consequently be bounded via a two-dimensional cloud of adatoms at any given moment. Lack of involvement of an atom from a granule is more likely the smaller the grain is as the binding energy for surface atoms related on the grain curvature, which is inversely related to the grain dimension. The adatom density approximately small grains will consequently be higher than around large grains. If two granules of dissimilar dimension are located close to each other there will be a gradient in the adatom density among the granules creating a driving force for diffusion from higher adatom density areas around the minute grain to the lower adatom density regions near to the bigger grain. This consequence in an overall loss of atoms for the minute grain and an overall gain of atoms for the bigger granules which will accelerate as the dimension dissimilarity develops bigger in a process called as Ostwald ripening. The crystallographic orientation of the granules is more or less arbitrary at the initial steps of growth if not the substrate works as a crystallographic template. It should be noted that the surface locally may be periodic on non-crystalline substrates and act as a template in the extremely in the early hours of sample growth. The initial orientation of the grain may be energetically adverse with regard to the equilibrium arrangement of the grain. The grain will, in that case, be restructured as it develops bigger unless the configuration is kinetically frozen. High energy surfaces will reshuffle unless there are kinetic limitations, in that case, they may develop in a way that alters the surface to a further favorable structure. The surface area of low energy surfaces usually enhances though the surface area of neighboring surfaces reduce as high energy surfaces will develop themselves out of existence.

The growing islands will ultimately meet. Immediately two islands are close sufficient to relate they will commence restructuring to decrease the energy in

the systems. Impinges islands will distort elastically, touch and create a grain boundary thereby trading surface energy for interface energy and strain energy. Atoms will disperse, mostly along the grain surface as bulk diffusion is some orders of magnitude slower, into the neck between the grains to minimize their chemical potential by moving from regions with a positive curvature to the neck which has a negative curvature. Surface diffusion carries on modifying the grain form until the new grain attains its equilibrium shape. Dimension dissimilarity among the coalescing grains will guide to a growth of the bigger granules at the expense of the smaller because of the larger curvature of the smaller granules. One of the effects of island coalescence is that the areas fraction of the surface covered via deposited material reduces. These newly released surfaces are frequently large adequate to permit for nucleation of a novel generation of islands, called as secondary nuclei.

The growth mode and consequently the surface topography throughout epitaxial growth are determined by the interaction among material transportation between dissimilar atomic layers, the interlayer transport, and the nucleation of fresh islands. The surface of some single crystal in spite of the crystal is macroscopic or a solitary granule in a polycrystalline sample, have atomic steps alienated by flat terraces. Film growth takings in one of four primary growth modes step flow growth, layer-by-layer growth, mound formation or self-affine growth relying on the preparation situation.

Step flow growth, happen when diffusion is quick related to deposition and the distance among surface steps is lesser than the regular distance between nuclei. In preference to creating fresh nuclei on the terrace adatoms connect to the step edges ensuing in the sideways growth of the terraces. Though step flow is the mainly probable when interlayer diffusion is infinite it is too, in principle, possible when interlayer diffusion restricted as it may continue through adatom attachment to the ascending stage merely.

If the average distance among nuclei is lesser than the terrace breadth nucleation will occur on the terraces. Growth will continue in a layer-via-layer style, as long as interlayer diffusion is quick sufficient to permit for atoms coated on top of the islands to overcome the step edge barrier prior to they encounter other atoms and form nuclei on top of the island. These atomically high islands will grow and coalesce to approximately fully cover the underlying atomic layer prior to nucleation happen on top of the islands and the cycle begins once more.

Greater substrate temperatures or low step edge barriers are requisite for layer-via-layer growth to not break down. Mountain generation, arise when interlayer transport of adatoms is suppressed sufficiently for adatoms to be trapped on a peak of islands and facilitate nucleation of a fresh atomic layer, moreover because of low deposition temperature or the occurrence of a high step-edge barrier. The constant nucleations of fresh layers on an apex of islands will consequence in substantial surface roughness subsequent to deposition of an only some atomic layers of substance.

The surface roughness will remain to build up for the period of the deposition and may outcome in high levels of surface roughness for thicker samples. Intralayer diffusion is reserved when the substrate temperature is extremely low consequential in coating atoms sticking relatively where they land. This growth

mode is known as self-affine or hit-and-stick growth. Though self-affine growth consequences in quite some surface roughness on the atomic scale it is arbitrary and does not develop a great deal with rising sample thickness.

The growth mode of a sample is not only changed by temperature and step-edge barriers but also via different parameters like deposition speed and bombardment by energetic element. It is, for instance, probable to bring a layer-via-layer such as growth mode by applying extremely high immediate deposition rates. The high deposition speed generates a high density of little islands that limits the quantity of another layer nucleation because of island dimensions lesser than the critical dimension desirable for nucleation. Energetic bombardment raises inter and intra-layer mass transportation in numerous paths and may consequently to give rise to a layer via layer resembling or step-flow resembling growth, under circumstances where it usually doesn't occur.

In model layer-via-layer growth, a layer is finished prior to nucleation of a fresh layer initiate. In such case, growth on succeeding layers would basically be indistinguishable to growth on preceding layers. In realism, nevertheless, nucleation on higher layers establish before the previous layer has been finished and the surface found to roughen. This roughening transition depends on the growth circumstances and the substance structure. Simultaneously, the average lateral feature dimension raises in higher layers that we will mention as coarsening of the face.

The next stage is the growth of the constituent part previously there in the reaction mixture, for ionic solids.

$(AB)_n + A^+ + B^- \leftrightarrow (AB)_{n+1}$

$(AB)_{n+1} + A^+ + B^- \leftrightarrow (AB)_{n+2}$

Wherein, n is the numeral of cation and anion necessary for forming steady compound $(AB)_n$. The speed of growth is related to the super saturation.

Rate of growth = K x a (Q-S).

Wherein, 'a' is the surface region of exposed substance and K is invariable, that is the characteristic of specific precipitation. But the super saturation is retaining at small level throughout the procedure, the precipitation takes place, rather than film development. Due to this, a large number of nucleation centers are formed, upon which growth may take place. As a consequence, not any of the particles grows extremely bigger and a colloidal suspension consisting of a thinly alienated particle is produced. In such similar circumstance, colloidal particle approaches mutually and stick each other. The consequential solid is known as coagulation. Colloidal particles once coagulated have dissimilar characteristics as of polycrystalline substances, because the units are available in an irregular manner.

Metal chalcogenide growth process

Three vital phases that comprise a typical metal chalcogenide synthesis process are (i) creation of the appropriate molecular, ionic or atomic type, (ii) transport of these species in the direction of templates throughout a solvent, then (iii) amount on the template, by using chemical reactions, to produce a solid compound. Derived

from the variety of investigational and theoretical studies a universal image of the step-via-step growth procedure is as follows: Developed molecular, ionic or atomic types, condense on template, fall their speed typical to templates (make existing striking energy is low) and are essentially coated on template exterior.

Adsorbed species and templates are not in equilibrium and travel over template exterior. In this procedure they act together between themselves, generating larger cluster. Such clusters or the bunch as they are referred, are thermodynamically unsteady and can have a tendency to desorbs in time, relying on the preparation circumstances. If the preparations factors are like that a cluster has a collision with other adsorbed group prior to getting desorbed, it begins rising in dimension. Succeeding to achievement a certain critical mass, cluster grow into thermodynamically constant and formation of nucleus hurdle may have overwhelmed. Such stage relating the generation of stable, chemisorbed, critical sized nuclei is known as the nucleation step.

Critical nucleus formation takes place in minute amount and saturated nucleation concentration became attained. Quantities of nucleus as well as typical nucleus dimension rely on innumerable factors. A nucleus may develop mutually parallel to template via diffusion of adsorbed species, and vertical to it via direct impingement of striking species. Generally, though, the speed of lateral development at such step is much greater than upright development. The developed nuclei are known islands. The subsequently step in the procedure of film generation is the coalescence step, in that the minute islands begin coalescing with all other in an effort to decrease the template surface area. Such affinity to give larger islands is called as agglomeration. It became improved by raising movement of adsorbed species. In few cases, generation of fresh nuclei can take place on region recently exposed as a result of coalescence. Bigger islands develop mutually, parting channels and holes of exposed templates.

Shape and size of samples at this step varies as of irregular island category to porous nature. Satisfying of minute gaps in island consequences in generation of totally unbroken films. Therefore, statistical procedure of nucleation, surface diffusion managed the development of the three-dimensional nuclei, and generation of a net type shape and size and their succeeding filling to provide an uninterrupted film, such procedure composes development technique. Island nature is the mainly general growth method, accessible in approximately every practical case. Excluding under particular situation, structural as well as morphological particulars of dissimilar islands are arbitrarily dispersed. Such islands contact one another throughout growth, granule junctions and different types of imperfection are included into thin films because of inequality of geometrical alignments as well as structural modifications.

If the granules are arbitrarily oriented, the sample shows a ring kind diffractogram and is supposed to be crystalline. Although the orientation of dissimilar islands is the identical throughout, as for attaining under particular preparation circumstances, on appropriate single crystal material, a single crystal sample is not achieved. As an alternative, the film made up of single crystal granules oriented parallel to one another and associated with low angle grain junctions. These films illustrate diffraction patterns resembling those of single crystal.

Metal chalcogenide growth modes

Metal chalcogenide growth manner in materials as an account in literature may be distinguished in three modes. Volmer–Weber or island growth [55], Frank–Van der Merwe or layer-by-layer growth [56], and Stranski–Krastanov or mixed type growth.

When the small dimension steady clusters nucleus formation on templates and develop into the three-dimensional island. Single basic clarification of such development performance is that species being coated are further tightly attached to each other. This is frequently circumstance once thin sample and templates are unlike substance. There is some instance of this performance in the development of oxide samples on O^{-2} templates, although such growth manner is normally detected once conducting and semiconducting samples are developed on oxide templates.

The contradictory properties of Volmer– Weber, nevertheless, take place when the expansion of the small dimension nucleus happens in two dimensions consequential in the generation of planar sheets. In layer-via-layer development, the prepared species are further tightly bounded to template than one another and every layer is increasingly less strongly attached than the preceding layer. Such consequence extends incessantly until the bulk attaching strength is attained. A usual pattern obtained of such epitaxial development of thin films on semiconducting and oxide substrate. The area of oxide sample growth has increased capability to maintain material through Volmer–Weber and other comparable growth modes.

Stranski–Krastanov mode is the ultimate growth system that is an amalgamation of the layer-via-layer and island growth. In such growth manner, subsequent to generating one or other monolayers in a layer-via-layer manner, sustained layer-via-layer growth happen to actively disapproving and islands commence to form. This type of development is moderately universal. This observed in a numeral of metal-metal and metal-semiconductor systems. These dissimilar growth modes may be explained in brief by means of easy thermodynamic theory for nucleus formation as well as growth of samples. As well as these three recognized traditional epitaxial development manners reveal overhead, 4 dissimilar growth modes like step flow mode, columnar growth, screw-island growth, and step bunching.

In columnar growth manner Volmer-Weber development style, pillar of single-island clots to generate a continuous sample. Merging of developed islands and columnar growth is the reason for a higher concentration of imperfection such as grain junctions, dislocations, empty space, antiphase junctions, etc.

Step flow approach is obviously separate from layer-via layer development in Frank–Van der Merwe mode. Unidirectional step flow is encouraged by templates disorientation. Such idea is frequently applied to keep away from island generation, its amalgamation as well as subsequent columnar development in epitaxy using gaseous medium.

Step bunching is found out once a larger number of stages move by means of greater phase rates above growth surface. Via variations, next stages catch up by means of previous stages and formerly shift together as doublet; triplet and so on. At large, macro stages which may exceed the thickness of 1000's of monostage.

The micro steps origin dissimilar inclusion rates of contamination and dopants because of locally changing growth rate.

Coalescence of a greater numeral of preliminary growth islands can guide to screw dislocations because of the layer formation ensuing in spiral-island growth mode. This has been found in the high-temperature superconductor metal chalcogenide samples. The Frank–Van der Merwe growth mode happens due to ions or molecules of coated material is more strongly bind to the template than each other. In the contradictory case, the coated ions or molecules are further extremely bound to one another compare to templates, island, or Volmer–Weber mode consequences. An in-between circumstance, layer in addition to island, otherwise Stranski–Krastanov growth approach is commonly frequent.

In approximately every practical case, the growth happens by island generation. Subsequent to a continuous sample is created; anisotropic growth occurs normal to the templates in the type of cylindrical columns. The preliminary nucleation density estimates the lateral grain dimension or crystallite dimension. Nevertheless, if recrystallization occurs throughout the coalescence steps, the lateral granules dimension is greater than average division of the preliminary nucleus. Average amount of granules/ unit area of sample are lesser related to quantity of early nucleation. The grain dimension typical to the template is equivalent to the sample thickness. For thicker samples, re-nucleation happens at face of formerly grown granules, and every upright column develops multi granularly with probable variation as of regular development.

Prerequisite of the Metal Chalcogenide Materials

Nature of substrate

Substrates play a vital role in deposition technique [57, 58]. Besides providing mechanical support to the coating method, influences on the topographical properties of the developing layer and on the optical and electrical characteristics of the metal chalcogenide samples. For the alternative of an appropriate substrate, the significant criteria should be used for their assortment. Substrates must have high-quality mechanical strength. It should be stable in a reactive bath. It should be smooth. Rough, spongy, voids and other irregularities influence the local current allocation. Metals were extensively applied as substrates due to their superior conductivity, effortless availability, lesser price and comparative simplicity of managing.

The substrates used to deposit metal chalcogenide were micro-glass slides of the size 75 x 25 x 2 mm, and polished stainless steel strips. The stainless steel substrates were polished using emery cloth and a polishing paper of zero number. The metal chalcogenide deposited on amorphous glass substrates were used to study properties; while the film deposited on stainless steel was used for photoelectrochemical studies.

Substrate clean-up

Substrate cleaning involves a very imperative part in the preparation of metal chalcogenide samples. A significant influence exerted via the substrate on sample development is throughout its cleanliness. The well wiped cleaned substrates are essential for the deposition. Substrate clean-up is performed earlier than putting in

the substrate inside the reactive bath. The substrate acts as a mechanical hold for the sample. For durable stability of metal chalcogenide sample, it is very important that no chemical actions happen that could transform the characteristics of the sample. The substrates have to perform certain necessities such as its mechanical strength and there should be sufficient bond of the sample to the substrate not only at ordinary temperature but also throughout comparatively huge temperature alter. It ought to also accomplish the practical necessities, like the probability of vacuum processing and the accessibility and price of the substrates. The most extensively applied substrates for crystalline metal chalcogenide samples are glass, fused silicon and ceramics.

Innumerable methods were applied for clean-up the substrates. Chemical clean-up is mainly generally applied and various techniques have been tried. In recent times vapor degreasing and ultrasonic cleaning, normally in a continuous flow of deionized water were applied in many instances in amalgamation with chemical clean-up. An essential segment of cleaning is the procedure used for drying the substrate subsequent to ultimate washing.

If drying agents such as acetone are utilized recontamination can occur unless extremely pure agents are employed. Even wipe up with a clean fabric can disappear a residue. Consequently, drying is normally accomplished in a vapor degreaser followed via blowing off the lasting moisture with compressed, filtered air or nitrogen. An analogous extent of cleanliness has been achieved via heating the substrate to 1500 ^{o}C or greater although breaking of a crystalline substrate in a vacuum or melting the face of the substrate can take place. As a result, these methods are not applicable to the entire substrate materials or substrates of greater dimension and they necessitate an apparatus. It is complicated to evaluate the techniques quantitatively as minor dissimilarity in a process and the feature of the process itself may modify the outcome significantly. For that reason, every experimenter must estimate his/her process sooner than adopting a recipe.

The tainted material exterior gives nucleation location providing the development that consequences heterogeneous sample. The amorphous material has been heated in concentrated chromic acid for approximately forty-five minutes and rinsed a number of times with double distilled water to do away with substances on the face. The substrates have been washed, by means of placing in acetone subsequently distilled water. The material has been once more kept in detergent solution and eventually kept in double distilled water. All the substrates have been stored in an airtight bottle consists of double distilled water for long period earlier than apply. The stainless steel plates had been first washed with a detergent solution after which polished with the aid of emery material.

The careful cleaning of the substrates is a key for obtaining good quality metal chalcogenide. All the substrate strips were boiled in a chromic acid bath for about 30 minutes and washed with water in order to remove adsorbed impurities on the surface. The strips were then decreased, by washing with acetone followed by distilled water. They were further dipped in a detergent solution and lastly washed with double distilled water. All the substrates were kept in an airtight container containing double distilled water for a long time before use. The stainless steel substrates were first degreased with a detergent solution and then polished (mirror smooth) with an emery cloth.

Preparations of the Solutions

All the solutions were exclusively prepared in double-distilled water and the basic chemicals used were of AR grade. All the solutions were kept in air tight bottles. The desired concentration of a particular substance is done on the basis of gram mole weight.

Instrumentation of Classical Chemical Bath Deposition Method

A schematic diagram of chemical bath deposition method is displayed in **Figure 1**. The experiment setup consists of an ice bath/oil bath, a dust proof chamber, a reaction vessel, a substrate holder and a motor etc.

A dust proof chamber

It is made of plywood with its dimensions 2.5 x 0.9 x 0.15 m. In order to provide the clean and contaminant less environment for deposition of the samples, hollow pipe outlet at the top of the chamber is fitted with an exhaust fan. During the metal chalcogenide deposition, any evolved gasses exhausted by using an outlet.

Ice bath

A metallic container containing crushed ice was used as a bath. The container was insulated with thermocol in order to prevent the thermal loss to surroundings. A thermometer (1/10th) was used to measure the temperature of the bath.

A reaction vessel

A reaction vessel was 250/100-mL capacity Borosil make glass beaker. The beaker was fitted with an ice bath by means of a suitable ring stand. Individual

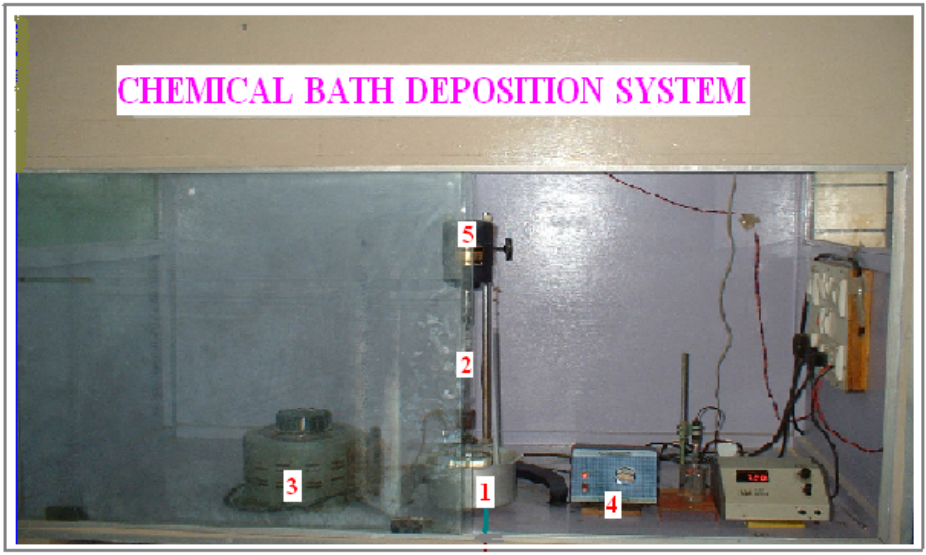

Figure 1: Schematic diagram of chemical bath deposition system. [**1**.Container **2**. Substrate holder **3**.Temperature controlling assembly with sensor indicator **4.**Speed controller **4**.Rotating motor].

solutions were cooled first to 278 K and then processed. The reaction mixture was maintained in the range of 278-293 K temperature in the ice bath.

A substrate holder

The substrates like non-conducting glass or stainless steel plates were mounted on specially designed 'substrate holder' and its schematic view is as shown in **Figure A** substrate holder is a circular disc, made up of Bakelite material. The thickness of the holder is about 10 mm and its diameter less than the diameter of the beaker so that the substrate attached to substrate holder can move freely in the reaction mixture in a beaker. The disc has four slots to fix substrates with the help of screw in such a fashion that each of the substrates is exactly perpendicular to the next. This substrate holder is fitted to a synchronous universal motor so that the substrate can be rotated in a reaction mixture. The motor is mounted on a drilling machine stand and the level of a stand is adjusted in such a way that about 80% portion of the substrate dips into the reaction vessel. The desired speed

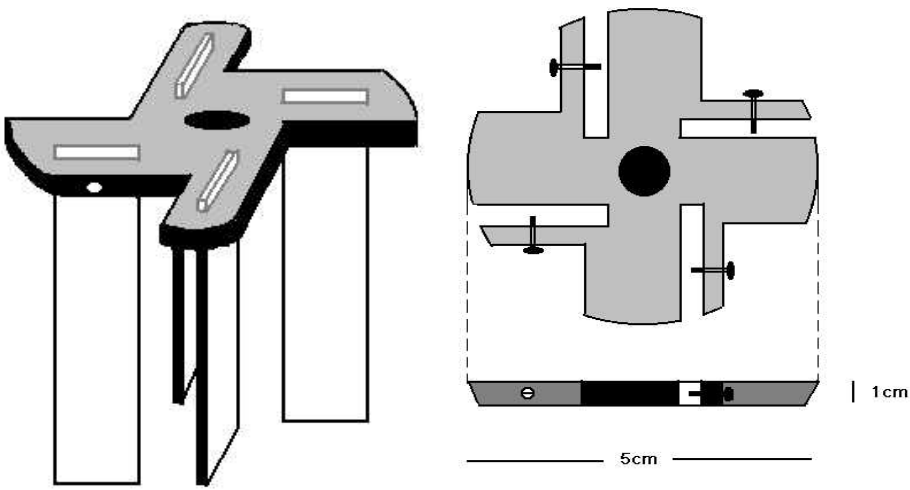

is maintained with the help of a regulator. Thus, the steady and proper churning of the solution in the reaction vessel is possible and helps in depositing uniform films with a better orientation of the crystallites.

Instrumentation of Modify (Automatic) Chemical Bath Deposition Method

In classical Chemical bath deposition technique has large numbers of operators and handling problems. We plan to modify classical CBD into Automatic- CBD. In modified (automatic) CBD method we are designing in portable size device to help of electronics and the mechanical mechanism to enhance accuracy and result.

This modified (automatic) CBD unit includes temperature sensor unit, controller, substrate rotates the motor, electronic circuit, oil bath/water bath, display, Acrylic substrate holder, condition setup button, Switch on the On/ off button etc. We can perform experiments in the temperature range 27 ^{0}C to 135 ^{0}C which is controlled by temperature sensor. The speed of stirrer and speed

of substrate rotation sets in limit of one to hundred rpm. A deposition time of the material adjusts from a minute to 5 hours, which can extend to 24 hours. In the experimentation, initially, fill oil or water in the bath up to mark. Generally, use a water bath to avoid contamination of the fumes liberated by oils. Hold precursor in a water bath and dipping templates that were maintained straight up somewhat slanted in reaction mixture of automatic chemical bath Unit has shown **Figure 2**.

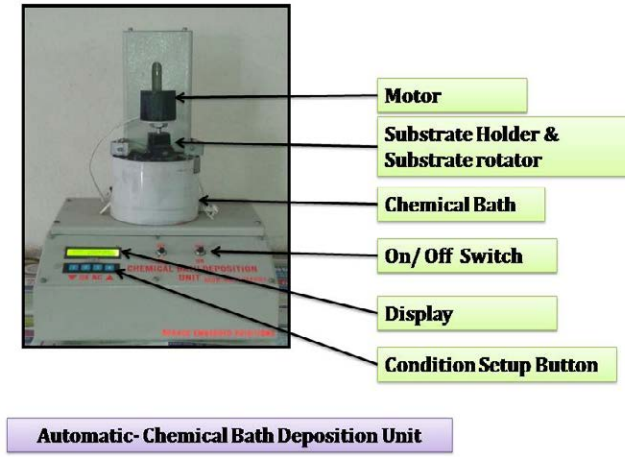

Figure 2: Automatic chemical bath deposition unit.

Temperature of reaction components maintains (^{0}C), rate of revolution of templates adjust in rpm, and programing for coating and string rate of reactants (rpm) fixed on unit. After setting all parameters, press OK button on the Automatic-Chemical Bath Unit. The unit can be automatically stopped after completion of time. Then the substrates have been detached and wash away numerous times by means of water. Deposited templates became dried naturally.

Conclusion

Chemical bath deposition technique is very common technique in order to produce thin films. This technique has many adavantages such as cheaper method, low temperature is required to prepare large area of sample. Binary, ternary and quaternary nano structured thin films have been prepared by many researchers. The ontained films have been characterized by using various tools.

Acknowledgement

The author would like to thank to university for their support.

References

1. Halim K, Yunus A, Ali FY, Yakup U, Ayhan C, et al. (2018) Investigation of the usage possibility of CuO and CuS thin films produced by successive ionic layer adsorption and reaction (SILAR) as solid lubricant. Surface and Coatings Technology 344: 522-527.

2. Kamala KS, Ebin B, Indra S, Song Z, Randy JE, et al. (2018) Nanocomposite $(CuS)_x(ZnS)_{1-x}$ thin film back contact for CdTe solar cells: Toward a bifacial device. Solar Energy materials and Solar Cells 186: 22-35.

3. Ho SM (2015) Chalcogenide thin films prepared using chemical bath deposition method. Research Journal of Applied Sciences, Engineering and Technology 11: 1058- 1065.

4. Montes MI, Campos E, Luna M, Cruz J, Sanchez TG, et al. (2018) Development of phase pure $CuSbS_2$ thin films by annealing thermally evaporated CuS/Sb_2S_3 stacking layer for solar cell applications. Materials Science in Semiconductor Processing 80: 74-84.

5. Ho SM (2016) A scanning electron microscopy investigation of semiconductor metal chalcogenide thin films: a review. Der Pharma Chemical 8: 13-16.

6. Monohorn S, Anuar K, Ho SM, Nagalingam S (2010) Synthesis of PbSe thin film by chemical bath deposition and its characterization using XRD, SEM and UV-Vis spectrophotometer. Makara of Science Series 14: 117- 20.

7. Nair PK, Nair MTS, Garcia VM, Arenas OL, Pena Y, et al. (1998) Semiconductor thin films by chemical bath deposition for solar energy related applications. Solar Energy Materials and Solar Cells 52: 313-344.

8. Garcia JA, Baez MR, Lerma M (2013) Chemical bath deposition of PbS thin films on float glass substrates using a $Pb(CH_3COO)_2$-NaOH-$(NH_2)_2$CS-$N(CH_2CH_2OH)_3$-CH_3CH_2OH definite aqueous system and their structural, optical and electrical/photoelectrical characterization. Thin Solid Films 534: 126-131.

9. Saravanan N, Ho SM, Anuar K, Kelvin, (2011) Composition, morphology and optical characterization of chemical bath deposited ZnSe thin films. European Journal of Applied Sciences 3: 75-80.

10. Benattou H, Benramdane N, Berouaken M (2017). Thin film bismuth (III) sulfide/zinc sulfide composites deposited by spray pyrolysis. Results in Physics 7: 3847-3852.

11. Nagalingam S, Ho SM, Anuar K, Tan WT (2011) Influence of pH on the properties of chemical bath deposited Ni_4S_3 thin films. Bangladesh Journal of Scientific and Industrial Research 46: 243-246.

12. Gouda L, Yelameli RA, Ramasesha SK (2012) Correlation between the solution chemistry to observed properties of CdTe thin films prepared by CBD method. Journal of Modern Physics 3: 1870-1877.

13. Shyju TS, Anandhi S, Indirajith R, Gopalakrishnan R (2010) Effects of annealing on cadmium selenide nano crystalline thin films prepared by chemical bath deposition. Journal of Alloys and Compounds 506: 892-897.

14. Dhandayuthapani T, Girish M, Sivakumar R, Sanjeeviraja C, Gopalakrishnan R, et al. (2015) Tuning the morphology of metastable MnS films by simple chemical bath deposition technique. Applied Surface Science 353: 449-458.

15. Anuar K, Ho SM, Tan WT, Sharif A, Nagalingam S, et al. (2010) Preparation and studies of chemically deposited Cu_4SnS_4 thin films in the presence of complexing agent Na_2EDTA. Indian Journal of Engineering & Materials Sciences 17: 295-298.

16. Martinez MA, Guillen C, Herrero J (1999) Cadmium sulphide growth investigations on different SnO_2 substrates. Applied Surface Science 140: 182-189.

17. Kuchkarov KM, Razykov TM, Chris F, Ergashev BA, Yuldoshov RT, et al. (2015) Research of the morphological and structural properties of CdTe films obtained by chemical molecular beam deposition for thin film solar cells. Applied Solar Energy 51: 314-318.

18. Anuar K, Ho SM, Tan WT, Atan S, Kuang Z, et al. (2009) Effect of deposition period and bath temperature on the properties of electrodeposited Cu_4SnS_4 films. Solid State Science and Technology 17: 226-237.

19. Lisco F, Kaminski PM, Abbas A, Bass K, Bowers JW, et al. (2015) The structural properties of CdS deposited by chemical bath deposition and pulsed direct current magnetron sputtering. Thin Solid Films 582: 323-327.

20. Olmos JAG, Armando G, Anan L, Thomas M, Carlos V, et al. (2015) CBD synthesis and characterization of CdSe nanostructured thin films. ECS Transactions 64: 29-33.

21. Brindha R, Devi KBR (2014) Structural and optical properties of chemical bath deposited Bi_2S_3 thin films. International Journal of ChemTech Research 6: 5632-5637.

22. Phok S, Fatima AW, Shifaa M, Saeed A (2014) Growth of Bi_2Se_3 films by chemical bath deposition at room temperature. MRS Online Proceeding Library Archive 1630.

23. Ho SM, Anuar K, Tan WT (2013) The role of bath temperature in aqueous acidic chemically PbS films. Journal of Basic and Applied Scientific Research 3: 353-357.

24. Anuar K, Tan WT, Dzulkefly KA, Haron MJ, Ho SM, Shanthi M, Saravanan N (2010) Preparation and characterization of PbSe thin films by chemical bath deposition. Jurnal Kimia 4:1-6.

25. Nunez A, Nair MTS, Nair PK (2011) Absorber films of Ag_2S and $AgBiS_2$ prepared by chemical bath deposition. Volume 730 (Symposium V-Materials for Energy Storage, generation and Transport. 730-V5.14.

26. Ubale AU, Sakhare YS (2013) Physical properties of MgSe thin films grown by chemical bath deposition method: effect of molar concentration of $MgCl_2$. Indian Journal of Physics 87 1183-1187.

27. Kassim A, Ho SM (2010) Deposition and characterization of MnS thin films by chemical bath deposition method. International Journal of Chemistry Research 1: 1-5.

28. Sargar SB, Sathe DJ, Chate PA, Sandi ZD, Kite SV, et al. (2016) Synthesis and characterization of MoS_2 thin films deposited by automatic CBD method. International journal of Scientific Research and Education 4: 5455- 5460.

29. Anuar K, Ho SM, Tan WT, Atan S, Kelvin, Nagalingam S, et al. (2011) Chemical bath deposition of ZnSe thin films: SEM and XRD characterization. European Journal of Applied Sciences 3: 113-116.

30. Kassim A, Tan WT, Ho SM, Saravanan N (2011) Deposition and characterization of ZnS thin films using chemical bath deposition method in the presence of sodium tartrate as complexing agent. Pakistan Journal of Scientific and Industrial Research 54: 1- 5.

31. Anuar K, Ho SM, Atan S, Jelas H, Saravanan N (2011) Chemical bath deposition of SnS thin films: AFM, EDAX and UV-Visible characterization. Oriental Journal of Chemistry 27: 1375-1381.

32. Bini S, Bindu K, Lakshmi M, Kartha CS, Vijayakumar KP, et al. (2000) Preparation of $CuInS_2$ thin films using CBD Cu_xS films. Renewable Energy 20: 405-413.

33. Chauhan SM, Chaki SH, Deshpande MP, Tailor JP, Ankurkumar J, et al. (2018) Characterization of CBD deposited $CuInSe_2$ thin film. Materials Science in Semiconductor Processing 74: 329-335.

34. Sanap VB, Pawar BH (2011) Study of chemical bath deposited nanocrystalline CdZnS thin films. Journal of Optoelectronics and Biomedical Materials 3: 39-43.

35. Anuar K, Saravanan N, Tan WT, Atan S, Kuang Z, et al. (2009) Effect of Deposition Period and pH on Chemical Bath Deposited Cu_4SnS_4 Thin Films. Philippine Journal of Science 138: 161-168.

36. Mudhafar AM, Mousa AM, Ponpon JP (2009) Optical and optoelectric properties of PbCdS ternary thin films deposited by CBD. Journal of Semiconductor technology and Science 9, 117-123.

37. Chaitali SB, Vishvanath BG, Suvarta DK, Khot KV, Rohini RK, et al. (2016) Rapid formation of ternary $CdZnSe_2$ chalcogenide thin film by microwave assisted chemical bath deposition. Macromolecular Symposia 362: 60- 64.

38. Ho SM (2015) Morphological studies of $Ni_3Pb_2S_2$ thin films by means of scanning electron microscopy technique. International Journal of Applied Chemistry 11: 363-369.

39. Subramaniam EP, Rajesh G, Muthukumarasamy N, Dhayalan V (2014) Solar cells of Cu_2ZnSnS_4 thin films prepared by chemical bath deposition method. Indian Journal of Pure and Applied Physics 52: 620-624.

40. Ho SM (2017) X-ray photoelectron spectroscopy studies of metal chalcogenide thin films: a review. Inorganic Chemistry-An Indian Journal 12: 109-112.

41. Fekadu GH, Francis KA, Tizazu A, Isaac N, Robert KN, et al. (2015) Synthesis and characterization of CdSe nanocrystalline thin film by chemical bath deposition technique. International Journal of Thin Films Science and Technology 4: 69-74.

42. Anuar K, Tan W, Abdullah H, Jelas M, Saravanan N, et al. (2009) Chemical bath deposition of NiSe thin films from alkaline solutions using triethanolamine as complexing agent. Oriental Journal of Chemistry 25: 813-816.

43. Xavier RJ, Prema AA, Sahayaraj PA, Pragathiswaran C, Dharmalingam V, et al. (2016) The properties of chemical bath deposited cadmium sulfide thin films with the effect of ammonia salt concentration. Advances in Applied Science Research 7: 178-182.

44. Anuar K, Tan WT, Ho SM, Teh XY (2011) Deposition and characterization of tin sulphide thin films by chemical bath deposition technique. International Journal of Applied Chemistry 7: 175-182.

45. Safonova M, Mellikov E, Mikli V, Kerm K, Revathi N, et al. (2015) Chemical bath deposition of SnS thin films from the solutions with different concentrations of tin and Sulphur. Advanced Materials Research, 1117: 183-186.

46. Gumus C, Gode F, Guneri E, Ulutas C, Kirmizigul F, et al. (2010) Properties of p-type SnS thin films prepared by chemical bath deposition. Chalcogenide Letters 7: 685-694.

47. Shin SW, Oh HP, Pawar SM, Moon JH, Kim JH, et al. (2010) Effect of complexing agent and annealing atmosphere on properties of nanocrystalline ZnS thin films. Journal of Nanoscience and Nanotechnology 10: 3686-3690.

48. Ke H, Duo S, Liu T, Zhang H, Fei X, et al. (2014) Effect of second complexing agent of N_2H_4 on the optical and structural properties of ZnS thin films. Key Engineering Materials 591: 297-300.

49. Biswajit G, Singh B, Pushan B, Das S (2016) Nucleation and growth of CBD-CdS thin films on ultrathin aluminium layers and annealing induced doping. Optik- International Journal for Light and Electron Optics 127: 4413-4417.

50. Kokotov M, Gar H (2010) Influence of selective nucleation on the one step chemical bath deposition of CdS/ZnO and CdS/ZnS composite films. Chemistry of Materials 22: 5483-5491.

51. Zhou L, Tang N, Wu S, Hu X, Xue Y, et al. (2011) Influence of deposition time on ZnS thin films performance with chemical bath deposition. Physics Procedia 22: 354-359. Abdallah B, Ismail A,

52. Zetoun W (2018) Effects of deposition time on the morphology, structure, and optical properties of PbS thin films prepared by chemical bath deposition. Journal of Nanomaterials.

53. Maske D (2016) Growth and characterization of CdS thin films by chemical bath deposition. International Journal of Scientific and Research Publications 6: 264-266.

54. Kostoglou M, Andritsos N, Karabelas AJ (2000) Modeling thin film CdS development in a chemical bath deposition process. Industrial & Engineering Chemistry Research 39: 3272-3283.

55. Vashistha IB, Sharma MC, Sharma SK (2016) Post annealing treatment of zinc sulphide thin film as a buffer layer for solar cell application. Journal of Surface Engineering 33: 299-304.

56. Shinde MS, Ahirrao PB, Patil IJ, Patil RS (2011) Studies on nanocrystalline ZnS thin films prepared by modified chemical bath deposition method. Indian Journal of Pure & Applied Physics 49: 765-768.

57. Aguilera A, Marquez F, Trujillo G, Galan V (2014) Influence of CdS thin films growth related with the substrate properties and conditions used on CBD technique. Energy Procedia 44: 111-117.

58. Kumar TP, Sherwood D, Bosco E, Kumar S (2012) influence of substrate on the structural, surface photoluminescence and computed three dimensional nanocrystal shapes of CBD-CdS thin films. Journal of Computational and Theoretical Nanoscience 9: 947-952.

Chapter 4

Properties of Thin Films Deposited on Different Substrates: A Review

Ho Soon Min*

Centre for Green Chemistry and Applied Chemistry, INTI International University, Putra Nilai, 71800, Negeri Sembilan, Malaysia

***Corresponding author:** Ho Soon Min, Centre for Green Chemistry and Applied Chemistry, INTI International University, Putra Nilai, 71800, Negeri Sembilan, Malaysia, E-mail: soonmin.ho@newinti.edu.my

Abstract

Nanostructured thin films (binary, ternary and quaternary) have been prepared using different deposition techniques. During the deposition process, films were deposited onto various clean substrates such as soda lime glass, indium tin oxide coated glass and stainless steel. These substrates are used for several different industrial and scientific applications. The choice of an appropriate substrate depends on cost production, the properties of desired thin films and the deposition conditions. Experimental results indicate that the polycrystalline nanostructured films have different properties based on the substrate.

Keywords

Thin films; Substrates; X-ray diffraction; Solar cells.

Introduction

In recent years, the investigation of nanostructured semiconductor thin films for use in solar cells [1-4], optoelectronic device [5, 6], electrochemical capacitor [7, 8], electroluminescent device [9, 10], light emitting diodes [11, 12], electrochromic display devices [13], heterogeneous catalyst [14], gas sensor [15], and anti-ferromagnetic layers [16] has been reported by many researchers. A number of techniques are used (including chemical and physical method) in the growth of high quality thin films under different deposition parameters. Fluorine doped tin oxide glass, plastic, mica, titanium, microscope glass slide, soda lime glass, stainless steel and indium tin oxide coated glass are widely employed (as substrates) for the deposition of various metal chalcogenide thin films. The choice of an appropriate substrate is very important and depended on several factors (thermal, mechanical electrical property and production cost).

In this work, preparation of thin films using different substrates such as indium tin oxide coated glass, stainless steel and soda lime glass was reported. XRD,

Metal Chalcogenide Nanostructures: Characteristics and Synthesis, Edited by Ho Soon Min and Yarub Al-Douri

AFM, SEM, EDAX, UV-Visible spectrophotometer were applied for characterizing the deposited films.

Literature Survey

Soda lime glass substrate

Soda lime is consisted of sodium oxide (15%), silicon dioxide (70%- the highest composition), lime (9%) and other compounds (to improve specific properties [17]). The general properties such as electrical, thermal and mechanical behaviors were shown in **Table 1**. It is notable for its chemically stable (up to 90 °C), good insulator, good transmission, hard and inexpensive [18] glass (compared with silica glass). Currently, it is widely employed for tubes, bottles, plates, light bulbs [19], rods, window panes, and glassware components.

The preparation of zinc oxide thin films on soda lime glass by using sol gel technique has reported by Perez et al. 1999 [20]. Experimental results show the physical and chemical properties can be controlled under various annealing temperatures (100-450 °C). The formation of ZnO and sharp absorption edge (380 nm) could be detected of films annealed at 200 °C as shown in XRD pattern and UV-Vis spectra. It is clearly seen that the grain size and refractive index values increase with increasing annealing temperature. Soda lime glass substrate was used (as substrate) for the ZnO films deposition under various concentrations of Zn^{2+} ions by using sol gel method. Surface morphology and band gap values were observed to reduce as the concentration of zinc ions increases [21]. ZnO films were synthesized using sol gel method in the amorphous phase at temperature of 100 °C [22]. Intense near band edge emission was detected as the obtained films were studied using the photoluminescence tool. Synthesis of Al-doped ZnO films on soda lime glass using sol gel method has been described by Li et al. 2012 [23]. As-deposited films were polycrystalline with (002) oriented crystallites of hexagonal wurtzite structure. The annealed films show high transmittance in the UV region and conductivity value, indicating annealing treatment improved the surface quality of films. TiO_2 films were deposited on to various substrates using sol gel method [24]. XRD data support that anatase and brookite could be found

Mechanical properties	
Properties	**Value**
Elastic Modulus	70 GPa
Knoop Hardness	570
Poisson Ratio	0.23
Shear Modulus	29 GPa
Tensile Strength	180 MPa
Thermal properties	
Specific Heat Capacity	720 J/kg.K
Thermal expansion	9 µm/m.K
Thermal conductivity	1.1 W/m.K
Electrical properties	
Dielectric strength	13 kV/mm
Dielectric constant	7.3

Table 1: Mechanical, thermal, and electrical properties of tempered soda lime glass.

for the films deposited on glass pre-covered with the SiO_2 and soda lime glass, respectively. Experimental findings highlighted that the brookite crystal phase structure showed superhydrophilic properties, meanwhile anatase structure indicates much better photoinduced activity.

Electron beam evaporation method was used to prepare CZTS films in the specific atmosphere (nitrogen + Sulphur vapor), 2 hours and 560 °C. The photovoltaic device performance shows PCE of 1.8 % and fill factor of 0.38 were observed [25]. The successful preparation of Cu_2ZnSnS_4 (CZTS) films using evaporation technique has been reported by Schubert et al. 2011 [26]. The thin films deposited at 550 °C, using sulphur pressure (3 x 10^{-3}Pa) indicate copper rich as shown in EDX spectroscopy. Power conversion efficiency reaches 4.1 % with open circuit voltage of 541 mV. Cubic structure with (111) as prominent diffraction peak was observed in zinc sulphide films prepared using liquid phase atomic layer epitaxy method on soda lime glass [27]. The growth rate increased (0.7 to 2 Å/cycle) with increase in solution concentration of zinc chloride (0.1 to 0.2 M) and Na_2S solution (0.05 to 0.1 M). Close spaced sublimation method was used to produce cadmium telluride thin films on soda lime glass [28]. The power conversion efficiency and fill factor of the fabricated solar cell are 15.5 % and 76.6 %, respectively. ZnO films of different thicknesses (256-627 nm) and band gap values (3.26-3.3 eV) were prepared using pulsed laser deposition in an oxygen reactive atmosphere [29]. The films show high transmittance (90 %) in the visible region. Also, they found that increase the resistivity with decrease the substrate temperature and the increase of oxygen pressure based on electrical measurements.

The growth of zinc oxide films using spin coating deposition method in the presence of zinc acetate and monoethanolamine, isopropanol [30]. The band gap of hexagonal wurtzite structure of films is 3.5 eV and show high transparency (more than 70 %). The growth of SnO_2 films on soda lime glass via spin coating method was investigated using photoluminescence technique [31]. Intensified peaks in 400 and 430 nm represent oxygen vacancies in samples and tin interstitials, respectively. Thermal co-evaporation was used to prepare $CuGaSe_2$ films with average diameter of about 1 μm [32]. Tandem cell was fabricated, power efficiency of 7.4% and open circuit voltage of 1.18V was observed.

Chemical bath deposition of zinc sulphide films was carried out in acidic conditions, at 80 °C in the presence of disodium salt of ethylenediaminetetraacetic acid [33]. X-ray photoelectron (XPS) and field emission scanning electron microscopy (FESEM) investigation shows the presence of only Zn-S bonding, compact morphology and agglomerated clusters for the films prepared at pH 5, 5.5. and above 6, respectively. Stoichiometric films were obtained with thicknesses from 30 to 220 nm, in the pH range from 5 to 6.5 meanwhile the band gap energy diminishes from 3.91 to 3.78 eV. ZnS films of different thicknesses (few to 100 nm) were produced on soda lime glass using chemical bath deposition method in the presence of ammonia and acetic acid, thioacetamide [34]. The obtained films were reported to have band gap of 3.6 eV and cubic structure. Staring materials such as $CuSO_4$, $ZnSO_4$, $SnSO_4$ and $Na_2S_2O_3$ were used to produce CZTS films using photo chemical deposition technique. As-deposited films were annealed by furnace (300-500 °C) under specific atmosphere conditions (nitrogen or N_2+H_2S). Based on the XRD studies, the structural of films was improved by heat treatment

(peaks became sharp). EDAX investigations show that the grown films (nitrogen atmosphere) have very low amount of Sulphur. However, reduce of compositional ratio of Sulphur could be suppressed in the N_2+H_2S atmosphere [35].

Cu_2ZnSnS_4 (CZTS) films were grown on soda lime glass using ultrasonic spray pyrolysis method have shown a band gap of 1.5 eV with high absorption coefficient [36]. Hence, kesterite semiconductor can be employed as absorber layers of photovoltaic cell. Spray pyrolysis method has been used to synthesis CZTS films [37] in the range 643-683 K. All the films are polycrystalline and the lattice parameters are observed to be a=0.542 and c=1.085 nm. The band gap obtained could be in the range of 1.4 to 1.45 eV. Chemical spray technique was applied to prepare low resistivity polycrystalline ZnO: Al films at 500 °C under various types of solvents (ethanol, methanol, isopropanol). The films prepared with ethanol presented a uniform morphology while broad distribution of size could be seen by using methanol and isopropanol [38].

In_2O_3-ZnO thin films were synthesized onto different substrates using R.F. magnetron sputtering method [39]. The films prepared using soda lime glass generally present poor resistance to moist heat and rough uniformity if compared to other substrate (corning glass), due to the diffusion of alkali metal from soda lime glass. Al-doped ZnO films have been prepared onto soda lime glass using magnetron sputtering show hexagonal structure with polycrystalline [40]. These films show high transmittance (85-90%) in visible region, and resistivity of 1.6-2 mΩcm. Further, the highest carrier concentrations were reached for the annealed films (350 °C) in vacuum.

CZTS films were synthesized via vapor phase sulfurization on soda lime glass present band gap of 1.45-1.6 eV [41]. Open circuit voltage (735 mV) and conversion efficiency (2.62%) were determined from solar cell consisted of Al/ZnO: Al/CdS/ CZTS/Mo-SLG. Higher electrical conductivity and open circuit voltages could be observed for the Cu (In, Ga) Se_2 films deposited on soda lime glass [42]. Because of increased net acceptor density in this substrate. Braunger and co-workers [43] have described the effect of sodium on the growth of Cu (In, Ga) Se_2 films. The obtained results reflect that sodium-polyselenides were formed during the film formation and oxidation.

Stainless steel substrate

Stainless steel has a unique property such as high resistance to corrosion (form thin layer on the surface) because of the presence of at least 10.5% chromium (most important element). It is thin, inert and invisible film also contains other elements including silicon (to increase resistance to oxidation process), cobalt (to increase hardness), nickel (to enhance austenitic structure), carbon (to increase mechanical strength), copper (to promote corrosion resistance in acidic condition), manganese (to improve hot ductility), titanium (to increase ferritic structure), vanadium (to enhance hardness), sulphur (to increase machinability), cerium (to improve resistance to high temperature corrosion), niobium (to improve ferritic structure) and molybdenum (to enhance formability property). The applications of stainless steel including oil & gas industry, food industry, textile industry, sinks and kitchen equipment.

Stainless steel was used as substrate to prepare ZnS films at 800 mV (SCE) for 15 minutes, at pH 14 [44]. The synthesized electrodeposited ZnS films show flower like morphology with an average grain diameter of 55-60 nm. Raman spectrum revealed that the presence of two peaks at 463 (longitudinal optical phonon peak) and 287 nm (transverse optical phonon). FTIR spectra show the stretching vibration of C-O group (1067, 1402 cm^{-1}) and stretching of ZnS bond (685 cm^{-1}). Na_2S and $ZnSO_4$ solution were used as starting materials to synthesis ZnS films through pulsed electro deposition technique [45]. The uniform grain size of cubic structure about 13 Å, spread all over the surface. The ZnS films deposited in electrolytic bath ($ZnSO_4$, $Na_2S_2O_3$) were brown, greenish-gray in colour. Based on the XRD patterns, the observed intensity increases are due to an increase in deposition time from 10-40 minutes [46]. Electro deposited ZnS films prepared in acidic conditions indicate uniform surface, well adherence and fibrous morphology [47]. The obtained electro deposited As_2Se_3 thin films are black in color. XRD data show that the as-deposited and annealed films (in nitrogen atmosphere, 2 hours, 200 °C) have polycrystalline nature. However, annealed films have bigger grain size while as-deposited films consisted of porous and many pin holes according to SEM studies [48]. Electrodeposition of SnS films in electrolytic bath contains $SnSO_4$, KSCN, Na_2SO_4 in the potential range from -560 to -590 mV (saturated calomel electrode) indicated progressive nucleation model [49]. The band gap of polycrystalline films is about 1.38 eV. Electrodeposition technique for the preparation of Bi_2Te_3 thin films at pH 2, 297 K, deposition potential of -170 mV (SCE) has been described by Thorat et al. 2018 [50]. These films were deposited by using starting materials such as sodium tellurite and bismuth nitrate. XRD patterns fit a rhombohedral structure with some major diffraction peaks such as (101), (015), (1010), (110), (205) and (125). EDS spectrum displays that the formation of pure and stoichiometric films with Bi/Te atomic percentage ratio is 0.73. The influence of deposition time on the properties of films was investigated. They conclude that micro strain (2.25-1.47 X 10^{-3}) and dislocation density (4.83-2.46 X10^{-3}) reduce, while fill factor (0.2896-0.3979), crystallite size (18-33 nm) and efficiency of solar cell (0.0288-0.0987%) increase with increasing deposition time up to 300 seconds.

The XRD data show triclinic phase in Cu_2SnS_3 films was prepared using chemical bath deposition method on stainless steel [51], which is consistent with the Raman spectra (286, 320 cm^{-1}). The annealed films have small spherical grains and band gap of 1.31 eV. Formation of Cu_2S (as secondary phase) in annealed films could be supported in Raman technique. Photoelectrochemical (PEC) parameters of fill factor, efficiency, open circuit voltage and short circuit current of as-deposited and annealed films were 0.48 & 0.65, 0.11 & 0.21 %, 222 & 253 mV, 550 & 738 μA, respectively. Morphology studies reveal that as-deposited films present uniform, spherical, smooth, compact and small rock type crystallites [52]. Meanwhile, agglomeration of nanoparticles into larger particles and construction of cracks –free could be seen in the annealed films (1 hour, 300 °C, 800 torr). Tin chloride, triethylamine (complexing agent) and sodium thiosulfate were used to deposit SnS using chemical bath deposition method [53]. Specific change in morphology can depend on deposition time such as 1 (micro-flower) and 4 hours (spherical grain). They also highlighted that the films thickness (575-754 nm) and crystalline sizes are increase as the deposition time increases from 1 to 3 hours.

Cu (In, Ga) Se_2 thin films were deposited on stainless steel (as substrate). XRD investigation revealed the major diffraction peak which is indexed (220) plane [54]. Meanwhile, predominant peaks correspond to (112) as the films deposited onto molybdenum/soda lime glass, indicating that the different compensation ability (between sodium and iron elements).

Indium tin oxide glass substrate

Indium tin oxide coated glass (ITO) contains tin, indium and oxygen. Physical vapor deposition, sputter deposition and electron beam evaporation technique were used to prepare ITO glass. The obtained glass is colourless, transparent and large band gap (4 eV). Other properties such as high electrical conductivity, low sheet resistance (70-100 Ω/sq), high transmittance value (about 86%), make them attractive for electronic ink industry, solar cell, electroluminescence device, transparent conductive coating, optoelectronic applications, research and development purposes.

The synthesis of cadmium sulphide thin films on to ITO glass substrate has been investigated [55] under agitation process. Substrate (ITO slide) was hold in oscillatinf tool (oscillate at 37 Hz). The clean CdS thin films (without colloidal precipitate) with constant rate deposition could be observed. The effect of deposition time on the properties of CdS was studied [56]. They described that film thickness (7.5 to 13.7 nm) increased linearly with deposition time (20 to 50 minutes). However, the band gap of CuS films reduces (2.9 to 2.45 eV) as the time was increased [57]. The influence of bath temperature (50 to 90 °C) on the properties of ZnS films was reported [58]. They conclude that an increase of the amount of the precipitate, and the rate of precipitation reduces at high temperature. The influence of precursor (zinc nitrate, zinc chloride) on the chemical bath deposited ZnS films was conducted in the pH range from 10-10.6 [59]. Favorable conditions (zinc nitrate) are met as the films show higher band gap, better transparency and surface morphology. In_2S_3 films were prepared using chemical bath deposition method [60]. The obtained films have great potential to be absorber materials in solar cell application due to band gap (1.5 eV). Glass slide was used as substrate during the deposition of indium sulfide films [61]. Optical studies reveal that greater band gap values (2.4-2.79 eV) could be found (porosity of surface morphology) as compared to ITO glass slide (2.32-2.29 eV). CuS binary thin films grown on ITO glass using chemical bath deposition method [62]. Atomic force microscopy images indicate these films are spherical have uniform particle size.

Electro deposition technique has been used to prepare zinc sulfide thin films [63]. The obtain results reflect that more peaks (at longer time, such as 30 min) and bigger grain size (potential becomes more positive) could be found as indicated in XRD and SEM. Electrodeposited CdS films were produced at 90 °C [64]. Thicker films formed and higher growth rate could be detected at lower pH. The influence of deposition time on the properties of CdS films was investigated [65]. Optical studies indicated that absorption edges (465 nm) become more significant and shift to lower energy as the deposition time was increased. with increasing deposition time.

SnS thin films have been prepared on ITO glass using electro deposition method. There are some highlighted results such as better crystallinity and

smaller band gap value [66] could be seen at higher bath temperature (if compared to lower temperature). Stoichiometric SnS (Sn/S ratio was nearly 1:1) films [67] and orthorhombic structure could be detected for the films prepared at deposition potential (-0.95 V and -1 V versus Ag/AgCl). The influence of concentration of EDTA was carried out. SnS and Sn_2S_3 phase [68] were formed as the EDTA/Sn^{2+} is 1/1, and the EDTA/Sn^{2+} is less than 0.5, respectively.

The influence of deposition potential (-0.65, -0.7, -0.71 and -0.72 V versus saturated calomel electrode) on the properties of CdSe films were studied [69]. Compositional analysis revealed that nearly stoichiometric CdSe films were detected at potential of -0.7 V. Morphology studies indicate that these films are smooth, compact, uniform with smaller grain size. They also reported that CdSe films with different grain sizes (ranging from 80-150 nm) were produced under various pH values [70]. Cubic phase of CdSe films were synthesized by Sarangi and Sahu [71]. It is clear that crystalline size (7-19 nm) varied according to different deposition conditions as calculated from the grazing angle X-ray diffraction (GXRD) measurement.

Ternary compounds such as $CuInSe_2$ films produced in the presence of complexing agent [72]. Improvement in film quality could be achieved by using triethanolamine (less than 0.1 M). However, weak intensity in XRD patterns as concentration was greater than 0.1 M. The growth of smooth, and stoichiometric $CuInSe_2$ films [73] was observed at -0.55V versus SCE, pH 3 in the presence of benzotriazole (1 mM BTA). The influence of deposition time (5, 10, 15 and 20 minutes) on the structure of $CuInSe_2$ films was studied. XRD data revealed that single phase and secondary phase (In_2Se_3) appeared for the films deposited for 20, and other deposition times [74].

Quaternary semiconductor films of Cu_2ZnSnS_4 (CZTS) have band gap energies (1 to 1.5 eV) and high absorption coefficient (more than 10000 cm^{-1}). Chemical bath deposited Cu_2ZnSnS_4 films exhibited conversion efficiency of 1.34 % and the band gap was 1.5 eV [75]. P-type semiconductor with band gap of 2 eV was successfully produced using electro deposition method at room temperature, as shown in photoelectrochemical behavior [76]. There are some disadvantages of ITO glass. For example, large scale production, expensive and short supply of indium.

Conclusion

Binary, ternary and quaternary compound semiconductor thin films were successfully deposited onto various substrates. Selection of substrate (soda lime glass, indium tin oxide glass and stainless steel) is important to ensure the quality of films. The properties of films depend on the type of substrate used during the deposition process. The obtained films have band gap of 1.5 eV, which could be used in solar cell applications.

Acknowledgement

INTI INTERNATIONAL UNIVERSITY is gratefully acknowledged for the financial support of this work.

References

1. Meglali O, Bouraiou A, Attaf N, Aida MS (2018) $CuInTe_2$ thin films synthesis using one step electro deposition process: structural, optical and electrical characterization. Applied Physics A 124.
2. Ho SM (2015) Scanning electron microscopy study of surface morphology of Ni_3Pb2S_2 thin films. Asian Journal of chemistry 27: 3851-3853.
3. Mahjoubi S, Bitri N, Abaab M, Ly I (2018) Effect of copper concentration on the characteristics of Cu_2ZnSnS_4 (CZTS) thin films. Materials Letters 216: 154-157.
4. Mohd JH, Anuar K, Ho SM, Tan WT, Atan S, et al. (2009) Effect of deposition period and bath temperature on the properties of electodeposited Cu_4SnS_4 films. Solid State Science and Technology 17: 226-237.
5. Cruz JS, Hernandez SAM, Delgado FP, Angel OZ, Perez RC, et al. (2013) Optical and electrical properties of thin films of CuS nanodisks ensembles annealed in a vacuum and their photocatalytic activity. International Journal of Photoenergy.
6. Ubale AU, Choudhari DM, Kantale JS (2011) Synthesis of nanostructured Cu_xS thin films by chemical route at room temperature and investigation of their size dependent physical properties. Journal of Alloys and Compounds 509: 9249-9254.
7. Pang SC, Chin SF, Ling CY (2011) Preparation and characterization of self-assembled manganese dioxide thin films. Journal of Nanotechnology.
8. Yano M, Suzuki S, Masaru M, Ohgaki M (2013) Electrode properties and microstructures of MnO_2 nanosheet thin films as cathodes for electrochemical capacitors. Solid State Ionics 233: 32-37.
9. Luo Y, Bian J (2010) Room temperature ultraviolet electro luminescence from ZnO based homo-junction device. 2010 Symposium on Photonics and Optoelectronics.
10. Yoshioka K, Egawa S, Kobayashi T, Baba T, Sugimoto K, et al. (2007) ZnO films fabricated by spin coating and their application to UV electroluminescent devices. Physica Status Solidi C: Current Topics in Solid State Physics 4: 162-165.
11. Mahmoud A, Walid I, Abdelhamid E (2018) Low cost inorganic white light emitting diode based on submicron ZnO rod arrays and electrodeposited Cu_2O thin film. Materials Science in Semiconductor Processing 81: 44- 47.
12. Kunio I, takahiro K, Shunsuke O, Takuma K, Shoichi N, et al. (2013) ZnS-based ZnSTe:N/n-ZnS light emitting diodes. Applied Physics Express.
13. Yunus A, Tuba, C (2015) Fabrication and characterization of NiO thin films prepared by SILAR method. Journal of Alloys and Compounds 625: 144-148.
14. Chtouki T, Soumahoro L, Kulyk B, Bougharraf H, Kabouchi B, et al. (2017) Comparison of structural, morphological, linear and nonlinear optical properties of NiO thin films elaborated by spin coating and spray pyrolysis. Optik-International Journal for Light and Electron Optics 128: 8-13.
15. Taskopru T, Turan E, Zor E (2016) Characterization of NiO films deposited by homemade spin coater. International Journal of Hydrogen Energy 41: 6965-6971.
16. Ukoba KO, Inambao FL, Eboka AC (2018) Review of nanostructured NiO thin film deposition using the spray pyrolysis technique. Renewable and Sustainable Energy Reviews 82: 2900-2915.
17. Zheng K (2013) Recycled glass concrete, 1st edition, In eco-efficient concrete. Woodhead Publishing, Cambridge: United Kingdom.
18. An R, Li Y, Dou Y, Fang Y, Yang H, et al. (2004) Laser micro hole drilling of soda lime glass with femtosecond pulses. Chinese Physic Letters 21: 2465-2468.
19. Ashby MF (2013) Material Profiles 2nd edition. In materials and the environment, Elsevier: New York, United States.
20. Perez R, Sandoval O, Sandoval S, Marin J, Calvan A, et al. (1999) Influence of annealing

temperature on the formation and characteristics of sol gel prepared ZnO films. Journal of Vacuum Science & Technology A 17.

21. Thongsuriwong K, Amornpitoksuk P, Suwanboon S (2013) Structure, morphology, photocatalytic and antibacterial activities of ZnO thin films prepared by sol-gel dip coating method. Advanced Powder Technology 24: 275-280.

22. Seung H, Lee Y, Hwang K (2008) Photoluminescence of ZnO layer on commercial glass substrate prepared by sol-gel process. Ceramics International 34: 1237-1239.

23. Li J, Xu J, Xu Q, Fang G (2012) Preparation and characterization of Al doped ZnO thin films by sol-gel process. Journal of Alloys and Compounds 542: 151-156.

24. Novotna P, Krysa J, Maixner J, Kluson P, Novak P, et al. (2010) Photocatalytic activity of sol gel TiO_2 thin films deposited on soda lime glass and soda lime glass pre-coated with a SiO_2 layer. Surface and Coatings Technology 204: 2570-2575.

25. Hideaki A, Aya M, Yuki K, Tatsuhiro S, Kazuo J, et al. (2008) Preparation of Cu_2ZnSnS_4 thin films by sulfurization of stacked metallic layers. Thin Solid Films 517: 1457-1460.

26. Schubert B, Marsen B, Sonja C, Thomas U, Klenk R, et al. (2011) Cu_2ZnSnS_4 thin film solar cells by fast co-evaporation. Progress in Photovoltaics 19: 93-96.

27. Seppo L, Tapio K, Markku L (1994) Growth of ZnS thin films by liquid phase atomic layer epitaxy (LPALE). Applied Surface Science 75: 70-74.

28. Naba RP, Yan Y (2013) Fabrication and characterization of high efficiency CdTe based thin film solar cells on commercial SnO_2: F-coated soda lime glass substrates. Thin Solid Films 549: 30-35.

29. Tsoutsouva MG, Panagopoulos CN, Papadimitriou D, Fasaki I, Kompitsas M, et al. (2011) ZnO thin films prepared by pulsed laser deposition. Materials Science and Engineering: B 176: 480-483.

30. Winfield RJ, Koh LHK, Shane O, Crean GM (2007) Excimer laser processing of ZnO thin films prepared by the sol-gel process. Applied Surface Science 254: 855-858.

31. Feng G, Wang SF, Lu MK, Cheng XF, Liu SW, et al. (2004) Luminescence of SnO_2 thin films prepared by spin coating method. Journal of Crystal Growth 262: 182-185.

32. Nishiwaki S, Siebentritt S, Walk P, Lux MC (2003) A stacked chalcopyrite thin film tandem solar cell with 1.2 V open circuit voltage. Progress in Photovoltaics 11: 243- 248.

33. So RK, Seung WS, Doo SC, Moholkar AV, Moon J, et al. (2010) Effect of pH on the characteristics of nanocrystalline ZnS thin films prepared by CBD method in acidic medium. Current Applied Physics 10: S473-477.

34. Liudmila VM, Igor K, Rudiger S, Nurdin A, Mathias S, et al. (2005) Composition and properties of ZnS thin films prepared by chemical bath deposition from acidic and basic solutions. Physica Status Solidi C 2: 1206-1211.

35. Moriya K, Watabe J, Tanaka K, Hisao U (2006) Characterization of Cu_2ZnSnS_4 thin films prepared by photo chemical deposition. Physica Status Solidi C 3: 2848-2852.

36. Tejas P, Nagaraju J (2011) Effect of sodium diffusion on the structural and electrical properties of Cu_2ZnSnS_4 thin films. Solar Energy Materials and Solar Cells 95: 1001-1004.

37. Kumar YBK, Babu GS, Raja VS, Bhaskar PU (2009) Preparation and characterization of spray deposited Cu_2ZnSnS_4 thin films. Solar Energy Materials and Solar Cells 93: 1230-1237.

38. Suarez H, Maldonado A, Olvera M, Reyes A, Perez R, et al. (2002) ZnO: Al thin films obtained by chemical spray: effect of the Al concentration. Applied Surface Science 193: 52-59.

39. Hong J, Rhee B, Kim H, Je K, Kang Y, et al. (2004) Enhanced properties of In_2O_3-ZnO thin films deposited on soda lime glass due to barrier layers of SiO_2 and TiO_2. Thin Solid films 467: 158-161.

40. Guillen C, Herrero J (2010) Optical, electrical and structural characteristics of Al: ZnO thin films with various thicknesses deposited by DC sputtering at room temperature and annealed in air or vacuum. Vacuum 84: 924- 929.

41. Katagiri H, Kotoe S, Tsukasa W, Hiroyuki S, Tomomi K, et al. (2001) Development of thin film solar cell based on Cu_2ZnSnS_4 thin films. Solar Energy Materials and Solar cells 65: 141-148.

42. Ruckh M, Schmid D, Kaiser M, Schaffler R, Walter T, et al. (1996) Influence of substrates on the electrical properties of Cu(In, Ga)Se_2 thin films. Solar Energy Materials and Solar Cells 41-42: 335- 343.

43. Braunger D, Hariskos D, Bilger G, Rau U, Schock HW, et al. (2000) Influence of sodium on the growth of polycrystalline Cu(In, Ga)Se_2 thin films. Thin Solid Films 361-362: 161-166.

44. Dhaygude HD, Shinde SK, Dubal DP, Lohar GM, Fulari VJ, et al. (2015) Electro synthesis of nanoflower like ZnS thin films and its characterizations. Journal of Materials Science: Materials in Electronics. 3529-3537.

45. Kulkarni HR (2017) Synthesis, characterization and optical properties of ZnS thin films. International Advanced Research Journal in Science, Engineering and Technology 4: 11-15.

46. Patil JS, Dhasade SS, Thombare JV, Fulari VJ (2014) Structural, morphological and optical studies of ZnS thin films produced by electro deposition method. Journal of Shivaji University (Science & technology) 41: 1-3.

47. Anuradha BB, Wagh BG, Lokhande CD (2013) Structural properties of single step electrochemically deposited ZnS nanofibers. AIP Conference Proceedings.

48. Torane AP, Bhosale CH (2003) Electro deposition of As_2Se_3 thin films. Materials Research Bulletin 38: 847- 855.

49. Medhat MK, Mervat MI (2011) Electrochemical deposition and characterization of SnS thin films. Journal of Sold State Electrochemistry 15: 683-688.

50. Thorat JB, Mohite SV, Bagade AA, Shinde TJ, Fulari VJ, et al. (2018) Nano crystalline Bi_2Te_3 thin films synthesized by electro deposition method for photo electrochemical application. Materials Science in Semiconductor Processing 79: 119-126.

51. Shelke HD, Kim JH, Lokhande CD, Lokhande AC (2017) Photoelectrochemical (PEC) studies on Cu_2SnS_3 (CTS) thin films deposited by chemical bath deposition method. Journal of Colloid and Interface Science 506: 144-153.

52. Patil AM, Kim JH, Lokhande CD, Shelke HD, Lokhande AC, et al. (2017) Cu_2SnS_3 thin film: Structural, morphological, optical and photoelectrochemical studies. Surfaces and Interfaces 9: 238-244.

53. Lokhande AC, Patil AM, Shinde PA, Shelke HD, Lokhande CD, et al. (2017) Electrochemical super capacitor properties of SnS thin films deposited by low cost chemical bath deposition route. International Journal of Engineering Research and Technology 10: 914- 922.

1. Li B, Zhang Y, Wang H, Wang B, Wu L, et al. (2012) Preferred orientation of Cu(In, Ga)Se_2 thin film deposited on stainless steel substrate. Progress in Photovoltaics.

54. Salazar YA, Patino R, Pena JL, Cauich W, Oliva AI, et al. (2006) Physical properties of CdS/ITO thin films growth by CBD technique with substrate oscillating agitation. Brazilian Journal of Physics 36: 1058-1061.

55. Ordaz-Flores A, Bartolo-Perez P, Castro-Rodriguez R, Oliva AI (2006) Annealing effects on the mass diffusion of the CdS/ITO interface deposited by chemical bath deposition. Revista Mexicana De Fisica 52: 15- 19.

56. Anuar K, Tan WT, Saravanan N, Khor LK, Ho SM, et al. (2010) Effects of deposition time on the chemical bath deposited CuS thin films. Journal of Nepal Chemical Society 25:2-8.

57. Yamaguchi K, Yoshida T, Lincot D, Minoura H (2003) Mechanistic study of chemical deposition of ZnS thin films from aqueous solutions containing zinc acetate and thioacetamide by comparison with homogeneous precipitation. The Journal of Physical Chemistry B 107: 387-397.

58. Antony A, Murali KV, Manoj R, Jayaraj MK (2005) The effect of the pH value on the growth and properties of chemical bath deposited ZnS thin films. Materials Chemistry and Physics 90: 106-110.

59. Asenjo B, Guillen C, Chaparro AM, Saucedo E, Bermudez V, et al. (2010) Properties of In_2S_3 thin films deposited onto ITO/glass substrates by chemical bath deposition. Journal of Physics and Chemistry of Solids 71: 1629-1633.

60. Bansode S, Kapadnis R, Wagh V, Kale S, Pathan H, et al. (2014) Comparative studies on physico-chemical properties of indium sulfide films deposited under different deposition conditions by chemical bath deposition. Chemistry & Chemical Technology 8: 441-444.

61. Sangamesha MA, Pushpalatha K, Shekar GL, Shamsundar S (2013) Preparation and characterization of nanaocrystalline CuS thin films for dye sensitized solar cells. ISRN Nanomaterials.

62. Anuar K, Saravanan N, Ho SM, Noraini K (2010) XRD and AFM studies of ZnS thin films produced by electro deposition method. Arabian Journal of Chemistry 3: 243-249 (2010).

63. Stephen D (1993) Studies of the cathodic electro deposition of CdS from aqueous solution. Electrochimica Acta 38: 2395-2403.

64. Sisman I, Alanyahoglu M, Demir U (2007) Atom-by-atom growth of CdS thin films by an electrochemical co-deposition method: effects of pH on the growth mechanism and structure. The Journal of Physical Chemistry C 111: 2670-2674.

65. Cheng SY, Chen GN, Chen YQ, Huang CC (2006) Effect of deposition potential and bath temperature on the electro deposition of SnS film. Optical Materials 29: 439-444.

66. Cheng SY, He YJ, Chen GN (2008) Structure and properties of SnS films prepared by electro deposition in presence of EDTA. Materials Chemistry and Physics 110: 449-453.

67. Cheng SY, He YJ, Chen GN, Cho EC, Conibeer G, et al. (2008) Influence of EDTA concentration on the structure and properties of SnS films prepared by electro deposition. Surface and coatings Technology 202: 6070-6074.

68. Shen CM, Zhang XG, Li HL (2005) Influence of different deposition potential on morphology and structure of CdSe films. Applied Surface Science 240: 34-41.

69. Shen CM, Zhang XG, Li HL (2001) Effect of pH on the electrochemical deposition of cadmium selenide nanocrystal films. Materials Science and Engineering B 84: 265-270.

70. Sarangi SN, Sahu SN (2004) CdSe nanocrystalline thin films: composition, structure and optical properties. Physica E: Low dimensional Systems and Nanostructures 23: 159-167.

71. Whang TJ, Hsieh MT, Kao YC, Lee SJ (2009) A study of electrodeposition of $CuInSe_2$ thin films with triethanolamine as the complexing agent. Applied Surface Science 255: 4600-4605.

72. Beyhan S, Suzer S, Kadirgan F (2007) Complexing agent effect on the stoichiometric ratio of the electrochemically prepared $CuInSe_2$ thin films, Solar Energy Materials and Solar Cells 91: 1922-1926.

73. Meglali O, Attaf N, Bouraiou A, Aida MS, Lakehal S, et.al, (2014) One step electro deposition process of $CuInSe_2$: Deposition time effect. Bulletin of Materials Science 37: 1535-1542.

74. Subramaniam EP, Rajesh G, Muthukumarasamy N, Thambidurai M, Asokan V, Velauthapillai D (2014) Solar cells of Cu_2ZnSnS_4 thin films prepared by chemical bath deposition method. Indian Journal of Pure & Applied Physics 52: 620-24.

75. Jafarov MA, Nasirov EF, Jahangirova SA (2014) Preparation of nanosized CZTS structures for solar cells. International Journal of Engineering Innovations and Research 3: 741-745.

Chapter 5

Preparation Techniques of Thin Films by Physical and Chemical Vapor Deposition

A.Ayeshamariam[1]*, M.Jayachandran[2]

[1]Department of Physics, Khadir Mohideen College, Adirampattinam, 614701, India

[2]Department of Physics, Sethu Institute of Technology, Pullor, Kariapatti, 626 106, India

***Corresponding author:** A.Ayeshamariam, Department of Physics, Khadir Mohideen College, Adirampattinam, 614701, India, E-mail: aismma786@gmail.com

Abstract

In the last two decades, there are several physical and chemical deposition methods have been used to produce nanostructured thin films. Researchers have concluded that both methods present certain advantages over conventional methods and showed promising potential for the deposition process. Thin film technology employs new forms of transparent materials deposited at low temperature on conducting and non-conducting substrates. Researchers have defined that thin film layer is a material ranging from a fraction of a nanometer to a micrometer. In this work, physical vapour deposition, chemical vapour deposition and chemical solution deposition technique were discussed. Basic principles of these deposition techniques were highlighted.

Keywords

Thin film technology; Semiconductor; Deposition method; Substrate

Introduction

Thin Film

Thin film technology utilizes new forms of transparent materials deposited at low temperature on conducting and non-conducting substrates. Thin film layer is a material ranging from a fraction of a nanometer to a micrometer [1-3]. Extensive research has been conducted by many researchers [4-7] and experimental findings have been published in literature reviews [8-10].

Typical steps in making thin films

1. Emission of particles from source (heat, high voltage).
2. Transport of particles to substrate (free vs directed).

Metal Chalcogenide Nanostructures: Characteristics and Synthesis, Edited by Ho Soon Min and Yarub Al-Douri

3. Condensation of particles on substrate.

Thin film preparation notes

In the last two decades physical and chemical deposition methods of thin film were developed. Both methods present certain advantages over conventional methods and showed promising potential for the deposition process. A number of experimental conditions should be optimized before these depositions to produce nanostructures with high quality scientific relevance. The process should be performed in a vacuum or similarly controlled atmosphere in order to avoid interaction between vapour and air.

Preparation Methods

There are many preparation methods available. They are broadly classified into three areas as follows:

1. Physical Vapour Deposition
2. Chemical Vapour Deposition.
3. Chemical Solution Deposition.

Physical vapour deposition

There are numerous methods of physical vapour deposition including thermal evaporation, electron beam evaporation, pulsed laser evaporation, molecular beam epitaxy, ion plating, and activated reactive evaporation. The objective of this deposition process is to transfer atoms from a source to a substrate where film formation and growth follow automatically. However, limitations include the need for a highly controlled vacuum environment and costly instrumentation.

Physical Vapour Deposition (PVD) is a vapourization coating technique involving the transfer of material on an atomic level [11]. PVD process is carried out under vacuum conditions, in which material vapourized from a source is transported in the form of vapour through a vacuum or low pressure gas environment to the substrate where it condenses. There are four basic PVD techniques to prepare the thin films, two of which are discussed below.

Electron beam evaporation technique

Electron beam physical vapour deposition (EBPVD) is a form of physical vapour deposition in which a target anode is bombarded with an electron beam given off by a charged tungsten filament under a tight vacuum. The electron beam causes atoms from the target to transfer into the gaseous phase. The atoms then precipitate into solid form, coating everything in the vacuum chamber with a thin layer of the anode material. EBPVD yields a high deposition rate (0.1 µm /min to 100 µm /min) at relatively low substrate temperatures, with very high material utilization efficiency as shown in **Figure 1.**

Vacuum evaporation

Vacuum evaporation is one of the oldest and simplest techniques. The pressure used for normal evaporation is about 10^{-5} torr [12]. When evaporation is carried out in a vacuum, the evaporation temperature is considerably lowered and the

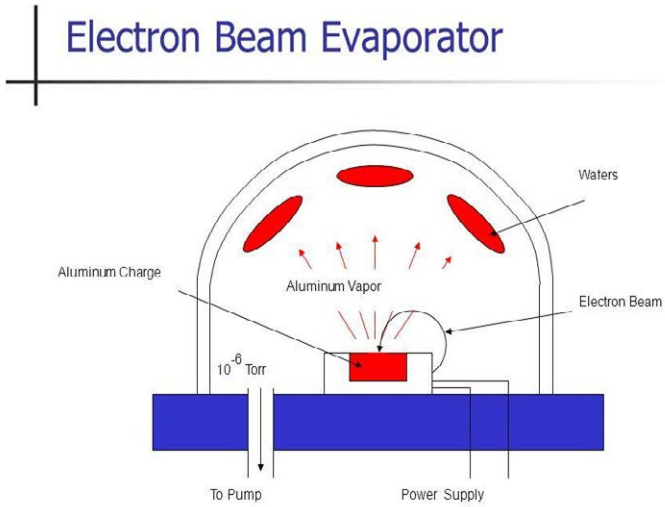

Figure 1: Electron beam evaporation technique.

incorporation of oxides and other impurities is very much reduced. This also ensures a straight line path for the vapor emitted from the source, a usual working source-to-substrate distance of 10-50 cm. Vapor sources of different types: hairpin, wire helix, dimpled foil, dimpled foil with oxide coating, wire basket, indirectly heated crucible is used for the evaporation depending on the evaporant material.

Sputtering

Coordination action of individual components for the integrated functional structures was obtained by ejecting the material from a target and then deposited onto a substrate such as a glass plate, Silicon wafer or any conducting ITO/SnO_2 plates. With wide energy distribution, up to 10 of eV were ejected from the target. At high gas pressure, the ions collide with the gas atoms that act as a moderator and condense after undergoing a random walk. Surface supported systems or clusters can be obtained via this method for the reduction of metals in usually big clusters of more than 10^{14} atoms. The sputtering gas is often an inert gas such as Ar [13]. For efficient momentum transfer, the atomic weight of the sputtering gas should be close to the atomic weight of the target. For sputtering light elements, neon or argon are used while for heavy elements Kr or Xe are preferable. Reactive gases can also be used to sputter compounds as the target to deposit the thin film to enhance their properties.

Sputter deposition

The sputtering deposition system is made by fastening the sputter cathode via a vacuum con-flat flange and/or fittings to the vacuum chamber [14] **Figure 2**.

Sputter deposition is used for obtaining thin films [15-18] of metallic crystals. Ejected material from the target, ionized atoms or clusters of atoms, travel to the substrate where the material is deposited. The plasma chamber must be arranged such that a high density of ions strike the target containing the material to be

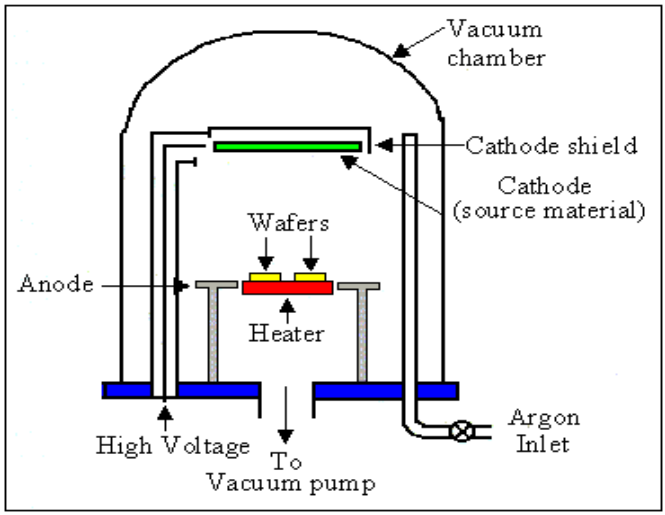

Figure 2: DC sputtering technique.

deposited. When an energetic ion strikes the surface of the material four things might happen:

a. Ions with low energy may bounce off from the target.

b. Ions with energy<10 keV may get adsorbed.

c. Ions with energy>10 keV, may penetrate many layers. They lose energy in the process and the released energy might affect changes in the physical structure. Substrate atoms and clusters of atoms will be ejected from the surface.

For very high energies (i.e., much greater than the energies corresponding to chemical bonds) like those used in implantation, chemical bonding processes can be largely ignored. The target can simply be considered as a collection of atoms. Secondary electrons might be knocked off from the target material.

Figure 3 shows the sputtering chamber in which a base pressure of $\sim 10^{-4}$ pa is maintained by an oil diffusion pump, and the sputtering gas (an inert gas like Ar) is introduced into the chamber at a pressure of ~0.1-1 pa. The target material is bonded to one electrode and the substrate to another electrode in a parallel plate capacitor configuration. Usually the target is at the bottom in the sputter mode so that loose powders of the material can also be employed in process. Sputtering is induced by applying a high DC voltage to the target. However, DC sputtering is only feasible for target materials that are metallic in nature. A wide variety of thin films can be made with little film contamination and at a high deposition rate by the low-pressure sputtering technique.

There are various types of sputtering such as reactive sputtering, magnetron sputtering, and ion beam sputtering. In reactive sputtering, the sputtered atoms yield the desired material, In magnetron sputtering, the sputtered atoms move in the presence of a magnetic field. The magnetic field is used to deflect the electrons from striking the substrate. This helps to prevent the unnecessary heating of

the substrate. These are DC magnetron and RF magnetron sputtering routes. In ion beam sputtering, an ion beam source is used for sputtering. Along with the configuration shown in the Fig, magnetron is used for DC magnetron sputtering. In RF magnetron sputtering, a separate RF source is used as shown in **Figure 4** hence the target material may be of any nature.

In magnetron sputtering, a magnetic field is superposed to the cathode and glow discharge, which is parallel to the cathode surface. The electrons in the glow discharge show cycloidal motion, and the center of the orbit drifts in the direction of Ex B with the drift velocity of E/B, where E and B denote the electric field in the discharge and the superposed transverse magnetic field respectively. The magnetic field is oriented such that these drift paths for electrons from a closed loop. This electron-trapping effect increases the collision rate between the electrons and the sputtering gas molecules. This enables one to lower the sputtering gas pressure as low as 10^{-5} torr, but more typically 10^{-2} torr. In this system, the magnetic field increases the plasma density which leads to increases in the current density at the cathode target, thereby effectively increasing the sputtering rate at the target. Due to working pressure, the sputtered particles traverse the discharge space without collisions, which results in a high deposition rate [19].

The difference in the mobilities of the ions and the electrons causes a positive ion sheath to develop close to the target cathode, floating at a negative potential relative to the plasma. Because of this field, ions are extracted from the plasma and accelerated to strike the target, resulting in the sputtering of the target material. The secondary electrons produced, upon entering the region of crossed electric (E) and magnetic (B) fields, are trapped in orbits that permit long travel distances

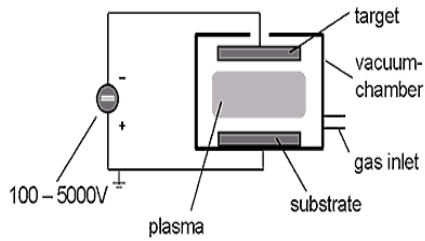

Figure 3: Sputtering mechanism with sputtering chamber.

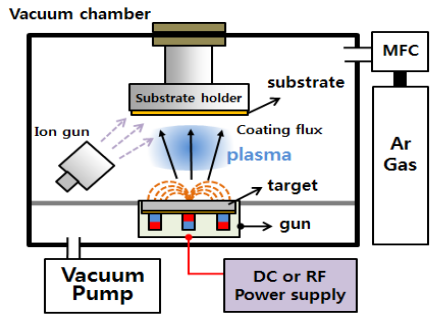

Figure 4: RF sputtering with RF sources.

close to the cathode. In the zones of efficient electron trapping, the electron density reaches a critical value, at which the ionization probability due to trapped electrons is at a maximum. This means that a higher rate of secondary electron production by high energy positive ions is not necessary for effective sputtering.

The basic operation of a magnetron cathode is somewhat altered in the case of RF magnetron sputtering. At frequencies less than 10 kHz, an ion sheath will not be formed; therefore, 13.56MHz frequency is generally used for RF sputtering. It should be noted that since the applied RF field appears between two electrodes, an electron escaping from the inter-electrode space as a result of random collision will no longer oscillate in the RF field. Therefore, these electrons will not have sufficient energy to cause ionization and will be lost to the glow. If a magnetic field is applied parallel to the RF field, it will constrain the electrons without being lost to the flow, thus improving the efficiency of the RF discharge. A magnetic field is more important in RF sputtering than it is for the DC case. A grounded metal shield is placed close to the other side of the metal electrode to extinguish the glow on the electrode side and to prevent sputtering of the metal electrode.

Planar magnetron RF sputtering

At present, the planar magnetron is indispensable for the fabrication of semiconductor devices. The planar magnetron sputtering consists of a water-cooled cathode made of copper on which planar targets of any material bound to a copper backing plate can easily be screw-mounted. The cathode is insulated from a water-cooled aluminum shield with a Teflon spacer and is kept in position using a stainless-steel nut. The magnets are mounted outside the shield. The whole assembly is affixed to a stainless-steel base plate, which is placed in a bell jar in which sputtering is carried out. The discharge voltage is 300V to 800V using which the maximum sputtering yield per unit energy is obtained.

If the process is continued, surfaces near the impact are covered with a layer of concrete dust. In sputtering, the “steel balls” are ionized atoms. The “wall” is a plate of the material to be sputtered, called a target. The sputtering process takes place in an evacuated chamber. Ar is introduced, then ionized in the chamber which contains the substrate and the target of the film material to be sputtered. The target is maintained at a negative potential relative to the positively charged argon atom. The positive ion accelerates towards the negative charge, striking the target with sufficient force to remove target material. The argon atom does not become imbedded in the target. Rather, it slams into it like a metal ball onto a wall and tears off some of the target material. Since the chamber is maintained at a vacuum, the liberated material settles on everything in the chamber, mainly the substrates.

In a traditional planar magnetron, the magnetic flux on the cathode surface is terminated to the magnetic core. The magnetron is called a balanced magnetron. When an additional magnetic flux is superposed to the balanced magnetron, the magnetron is called an unbalanced magnetron. Several types of modified magnetron sputtering systems are proposed based on the unbalanced magnetron system. In the balanced magnetron, energetic electrons escape from the primary magnetic trap near the cathode surface. These electrons go to the anode. In the unbalanced magnetron, the excess magnetic field lines trap the escaping energetic electrons

that make ionizing collisions. Secondary plasma is generated near the substrates. The incident flux of ionized particles increases in the unbalanced magnetron. The incident ionized flux modifies the film-growing process similarly to ion-assisted deposition.

Ion beam sputtering

This is another useful film deposition technique affording independent control of the ion beam energy, as well as the density of the bombarding ions. The ion beam generated at an ion source is extracted into a high vacuum chamber and directed at the target material, which is sputtered and deposited on a nearby substrate. The directionality of the beam allows the angle of incidence (on the target) and angle of deposition (on the substrate) to be varied. This technique holds several advantages over conventional sputtering such as low background pressure and greater isolation of the substrate from the ion production process.

Reactive sputtering

In reactive sputtering, the sputtered metal from the target reacts with the gas present to form the compound. In some cases, reactive gas is added to make up for a constituent in the film and this process is also treated as a case of reactive sputtering. "Target poisoning" can occur as well; in this case, the gas reacts with the target during sputtering and a compound is formed on the surface of the target, causing the sputtering rate to drop considerably as a result of the exposure to ion-bombardment of the compound as opposed to the target material. The effect of target poisoning on sputter deposition depends on the specific metal & reactive gas combination and the properties of the compound on the surface layer.

Reactive ion beam sputtering

This is a modification of the ion beam sputter deposition technique and differs from other reactive deposition methods in that the reactive ion can be introduced in two ways: ain ion beams or in a gaseous phase. In the former, the compound film is formed by the sputtering of the compound or target component of the binary compound with the reactive ion beam or a mixture of inert and reactive ions. Alternatively, when sputtering is done by one ion source, the reactive ion beam from another source is directed on to the growing film on the substrate. In the latter, film formation is accomplished with the inert gas exposed to the target in the presence of the reactive gas, which is admitted near the substrate.

Chemical vapor deposition

Chemical Vapor deposition (CVD) is a chemical reaction which transforms precursors, which are gaseous molecules, into solid materials of thin film or power on a substrate's surface. The process is widely used to fabricate semiconductor devices. Flow rate, input concentration, deposition temperature, pressure and reactor geometry are process variables controlling the deposition of films. A basic CVD system for the deposition of thin films involves three fundamental processes: transportation of the reactants to the site of reaction, provision of activation energy for reaction and removal of by-product gases and vapors.

Electro deposition

It is an electrochemical process [20-22] in which the anode and cathode are immersed in a suitable electrolyte and the passage of electric current deposits the material on the cathode. A variety of insulators, semiconductors [23-26] and alloy films have been prepared by electrodeposition.

Electroless deposition

Electroless deposition is a film deposition process in which no electrode potential is applied, unlike electrodeposition. The chemical reduction can be done without a catalyst, for example, as in a silver coating on glass using a reducing agent for silver nitrate, or with a catalyst, as in the case of reduction of $NiCl_2$ by sodium hypophosphite, the metal being deposited on nickel itself. The metal acts as a catalyst here. Electroless deposition or chemical bath deposition is simple [27-29], cheaper [30-32] and applicable to large-area deposition experiments [33-35].

Electron beam evaporation

Electron beam evaporation method is used for preparing TiO_2 thin films. The temperature of the evaporant material can be raised by electron bombardment instead of resistive heating. In this technique, an electron bean is accelerated through a potential of 5kV to 10 kV and focused on the material. The electrons lose their kinetic energy as heat, and the temperature at the focused spot can rise to 3000 °C. At such a high temperature, most of the refractory metals and metal oxides can be evaporated. Since the temperature is high only at the focused spot, the rest of the material remains cool. Since the input power can be very high 5kV to 10 kV, extremely high rates of evaporation (a few microns/sec) can be achieved, even for materials with high melting points. The electron gun used for evaporation consists of a heated W filament for electron emission. The filament is normally shielded to prevent any sputtering by the vapor species and gaseous ions. Depending on how these emitted electrons are accelerated, the guns are called work-accelerated or self-accelerated. Work-accelerated guns are limited and can be operated only at voltages <10 kV. If a separate anode is used with an aperture to allow passage of the electron beam, the gun is classified as self-accelerated. These guns can be used at higher voltages and are most commonly used. In both the e-guns, electrostatic or electro-magnetic focusing is used to focus the electron beam. The beam can be focused sequentially onto one or more hearths situated between the role pieces. This enables multi-hearth evaporation by scanning the beam. If the evaporated material is transported through reactive gas such as O_2 plasma, the deposition technique is called activated reactive evaporation.

Pulsed laser deposition

In this technique the solid target material is converted to vapour by focusing a laser pulse on the target as shown in **Figure 5**. The ablated material is deposited on the substrate. Laser ablation is a term used to describe the removal of moistures and impurities from the target surface. The phenomenon involves laser heating leading to rapid evaporation, direct chemical bond breaking, exfoliation of chip-away particulate due to mechanical recoil force, thermal and non-thermal ionization and plasma formation associated with the above process etc. When light

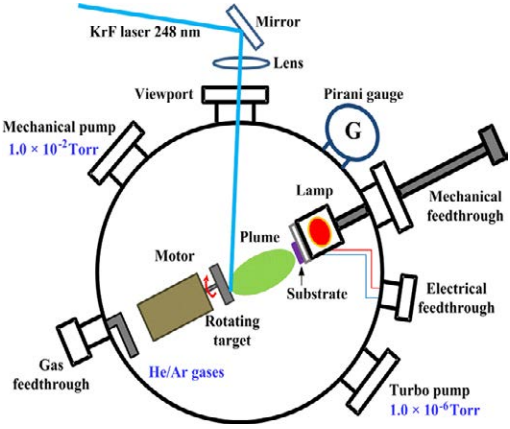

Figure 5: Pulsed Laser Depositions.

falls on the target surface, it is absorbed by electrons and the lattice. The adsorbed energy is instantly coupled into electronic excitations, and the heating effect is instantaneous. Hence the laser heating effect becomes localized and results in substantial increases in temperature. A laser fluence of $1J/cm^2$ of 10 ns duration dumps an instantaneous power of 10^8 $Watts/cm^2$ on the target surface. Under this high power the high temperature several non-thermal mechanisms are triggered.

The ablated material, whether from thermal [36] or non-thermal phenomena [37], can be condensed onto a surface as thin film. This process is generally called Pulsed Laser Deposition (PLD). The nanosecond or sub-second laser pulses cause the entire process of laser ablation to take place in nanoseconds. Hence the stochiometric transfer of the target composition can be achieved more rapidly when compared to other techniques. In principle, almost any material including ceramic dielectrics, semiconductors, or even complex biomolecules can be deposited in the thin film form by this technique.

However, more volatile species like oxygen (in oxide semiconductors) may exhibit deficiencies in the deposited film, especially at higher substrate temperature, due to the reduced sticking co-efficient of these elements. Such a deficiency can be compensated by either using a background or additional evaporation source of the volatile species near the substrate.

Chemical vapour deposition

Chemical Vapour Deposition (CVD) is the process whereby reaction precursors in vapour phase react either homogenously in the gas phase or heterogeneously at the solid-gas interface at the substrate [38, 39]. This produces a composition different from that of the starting precursor materials. The precursor molecules can be made to decompose by means of heat (pyrolysis), absorption of light (photolysis) or in electric plasma formed in the gas. Vapour deposition is enhanced by laser in some cases. Thermal CVD is the most commonly used method. Typical reactions to grow semiconducting crystals are given below:

$$SiH_4\ (gas) \rightarrow Si\ (solid) + 2H_2\ (gas)$$

$$Ga(CH_3)_3\ (gas) + AsH_3 \rightarrow GaAs\ (solid) + 3CH_4$$

For silicon dioxide, deposition can be achieved via the reaction of silane at 200-500 °C using an N_2 carrier gas, ie.

$$SiH_4 + 2O_2 \rightarrow SiO_2 + 2H_2O$$

For silicon nitride, at 750-850 °C, the reaction is affected in the presence of NH_3

$$3SiH_4 + 4NH_3 \rightarrow Si_3N_4 + 12H_2$$

For polysilicon, a reaction takes place with silane at 500-800 °C

$$SiH_4 \rightarrow Si + 2H_2$$

The **Figure** shows the apparatus used for CVD with vertically mounted substrates as silicon wafers. In some cases, laser may be used to assist the decomposition of the carrier gas. This is known as Laser Assisted Chemical Vapour Deposition (LACVD). This method has been used to produce nanowires shown in **Figure 6**.

Plasma enhanced chemical vapour deposition (PECVD)

Energy sources other than heat can be used to initiate molecular level deposition in CVD. One obvious alternative source is light photons (typically in the UV region of the electromagnetic spectrum) with energy sufficient to break (or severely weaken) intramolecular chemical bonds. It can cause direct dissociation or facilitate dissociation within gas phase collisions. For example, photolysis of disilane (Si_2H_6) leads to high quality films of amorphous hydrogenated silicon, Si-H.

Another energy source that can be used to promote CVD is associated with electrical plasma. In many cases the rates of reaction are drastically affected in the presence of plasma, the source of energetic electrons. The **Figure** shows typical arrangement employed for the purpose. CVD is carried out in the presence of plasma. Plasma is a partially ionized gas. Plasma is characterized by the density of electrons and their average energy. The glow discharge plasma usually has energy ~1-100eV and its typical densities are 10^{14}-$10^{18}/m^3$. If the inlet flow of gas contains molecules AB made of atoms A and B, the types of processes that occur in the plasma characterized as follows:

Dissociation: $e^* + AB \; f \; A + B + e$
Atomic Ionisation: $e^* + Af \; A^+ + e + e$

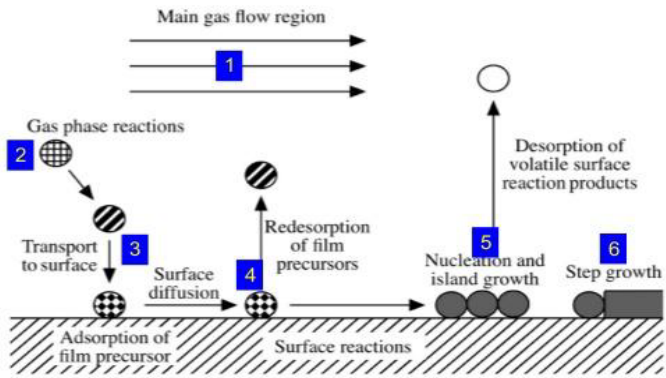

Figure 6: Chemical Vapor Deposition.

Molecular Ionisation: $e^* + AB \rightarrow AB^+ + e + e$

Atomic Excitation: $e^* + A \rightarrow A^+ + e$

Molecular Excitation: $e^* + AB \rightarrow AB^+ + e$

Here the superscript (*) refers to species whose energy is much larger than the ground state. Dissociated atoms or molecular fragments are called radicals. Radicals have incomplete bonds and are extremely reactive.

The efficiency of PECVD can be enhanced by the application of a magnetic field [40, 41]. A magnetic field can be used to increase the density of electrons by preventing the ion-electron recombination. This also brings down the effective temperature of the substance, heating of which is prevented from ion bombardment shown in **Figure 7**.

Molecular beam epitaxy

Molecular beam epitaxy (MBE) has become a reliable and versatile technique for growing epitaxial thin films of semiconductors [42-44], metals and alloys by impinging thermal energy beams of atoms or molecules onto a heated substrate under ultra-high vacuum (UHV) conditions. Compared to the well-established techniques of liquid phase epitaxy (LPE) and vapour phase epitaxy (VPE), the advantageous characteristic features of MBE are as follows **Figure 8**.

- The slow growth rate is about 0.1-2.0 μm/hr. It permits very precise control of layer thickness in the submicron and nano-meter range.
- The reduced growth temperature, eg.500-600 °C for GaAs, is favorably low enough to not disturb the compositional or doping profiles of the films because of negligible bulk diffusion.

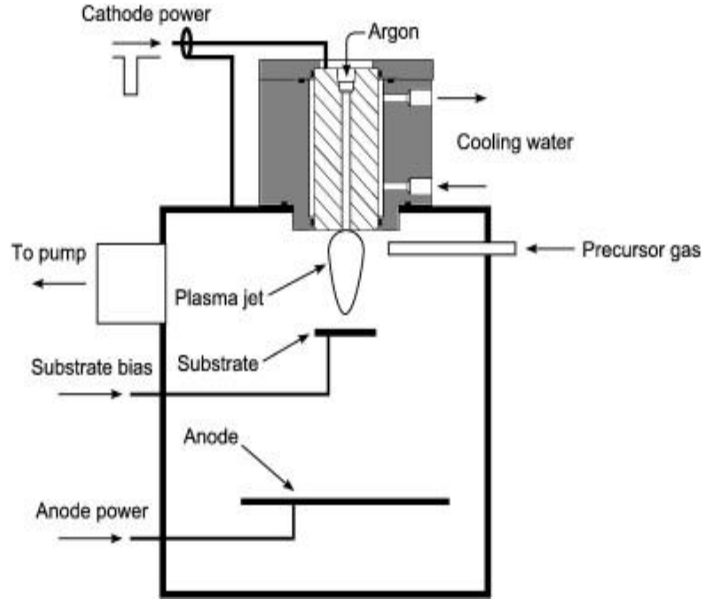

Figure 7: Schematic diagram of PECVD.

- The specific non equilibrium growth mechanism is responsible for the progressive smoothing of the surface for any substrate orientations.
- The ability to abruptly cease or initiate molecular beam that produces hyper-abrupt material interfaces and dopant profiles.
- The facility for in-situ analysis to assure the desired surface and reaction conditions that are necessary films and crystals grow.

Technology of MBE

The molecular beams reacting on the substrate crystal are generated by thermal evaporation of the constituent elements or their compounds and mixtures contained in temperature-controlled effusion cells [45]. These cells are arranged in such a way that the central part of their flux distribution intersects the substrate at an orifice, with substrate distance ranging from 60 mm to 140 mm in different MBE systems. Each source is provided with an externally operated mechanical shutter. Operation of these shutters permits rapid changing of the beam species to abruptly alter the composition and/or doping of the growing film normal to the substrate surface. With respect to the slow growth rate of about 1μm/hr, the shutter time is much less than the time for growth of monolayer. Consequently, abrupt material interfaces can be easily achieved, since any significant bulk diffusion is eliminated at the specific low growth temperatures. The stoichiometry of the layer is a function of the surface chemical composition and the sticking coefficients of the various species.

The intensities of the beams incident on the heated crystalline substrate are controlled by the temperatures of the individual effusion cells. Continuous changes in the chemical composition of the epitaxially growing film are achieved by the already programmed variation of the cell temperature, and the abrupt changes are

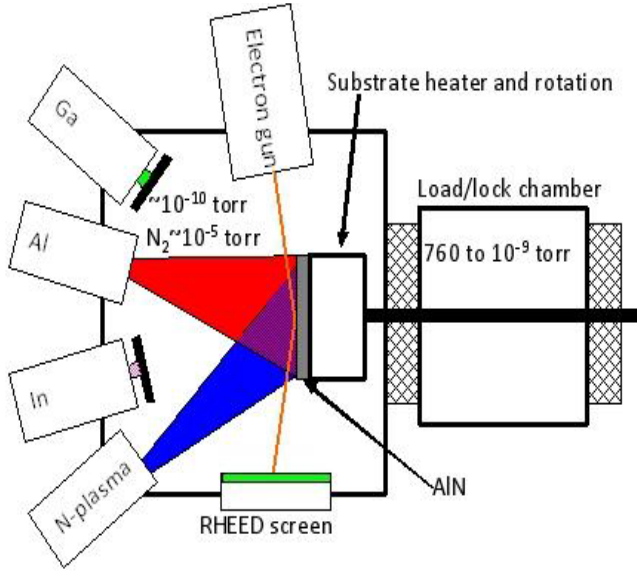

Figure 8: Schematic diagram of Molecular beam epitaxy.

obtained by operating the mechanical shutters interposed between the cell orifice and the substrate.

The slow growth rate during MBE, coupled with the obvious stringent demand for low, unintentional impurity levels incorporated in the deposited materials, require a perfect UHV environment in the growth chamber. The equipment for MBE is basically a stainless steel UHV system with a background pressure of about 10^{-10} torr pumped by standard ion pumps or by using suitably trapped diffusion or turbo-molecular pumps. Additional liquid nitrogen cyropanels assure that the partial pressures of gases with high sticking coefficient, eg.OH containing species, are kept even below 10^{-14} torr in the vicinity of the growing epitaxial crystal. In actual practice, during deposition, the total pressure in the chamber goes beyond 10^{-9} torr because of the scattered species. An inherent advantageous feature of MBE is that the UHV environment is suitable for in-situ surface analytical studies. It examines the substrate prior to epitaxial growth and provides a high degree of in-situ growth control. The incorporation of the molecular beam and surface analytical tools including Auger Electron Spectroscopy (AES) and Reflection High Energy Electron Diffraction (RHEED) in a single UHV bell jar led torapid progress in analyzing, defining and understanding the general growth.

Chemical Deposition Techniques

Chemical deposition techniques are most important methods for the growth of films owing to their versatility for depositing a very large number of elements and compounds at relatively low temperatures. The processes are very economical and have been industrially exploited to a large scale. The various chemical deposition processes are as follows:

Chemical vapour deposition (b) Spray pyrolysis (c) Electrodeposition (d) Anodization (e) Solution growth and (f) Screen printing. Of the above chemical

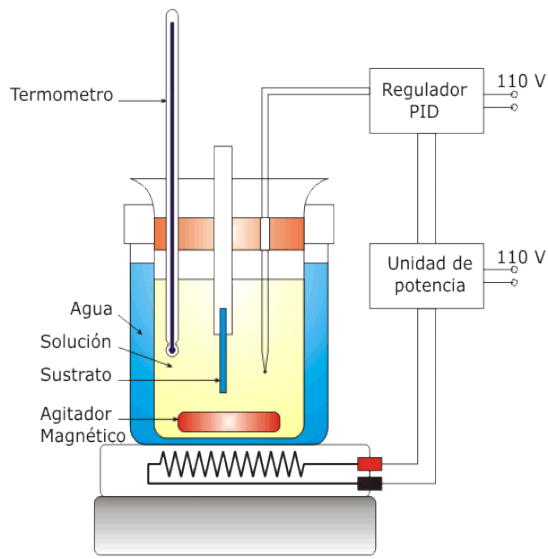

Figure 9: Chemical Bath Deposition.

techniques, due to simplicity and cost effectiveness, solution growth is discussed here.

Chemical bath deposition

Chemical Bath Deposition is becoming an important deposition technique for thin films of compound materials like chalcogenides [46], oxides and halides. It takes advantage of the use of a reaction from a solution where different precursors can be dissolved easily in the ionic or molecular form and react chemically on the substrates leading to film formation [47]. The key advantages are low cost, large area, and low temperature atmospheric processing [48]. It has the advantage with respect to other methods of the films being able to be deposited on different kinds, shapes and sizes of substrates [49]. This method has been frequently used for the deposition of metal oxide thin films. **Figure 9**.

Solution growth

Films are grown on either metallic or non-metallic substrates by dipping them in appropriate solutions containing metal salts without the application of any electric field. Deposition may occur by homogeneous chemical reactions, usually reduction of a metal ion in a solution by a reducing agent. Silvering is mostly done using this technique. One of the chief advantages of such a method is that it is possible to deposit films on non-accessible surface. ie, inside of glass tube, where they will be protected from physical damage.

Spin coating

Spin coating has been used for several decades for the application of thin films. A typical process involves a small puddle of fluid resin onto the centre of the substrate and then spinning the substrate at high speed [50, 51]. Centripetal acceleration plays a vital role in spreading the resin across the substrate.

Spin coating is a procedure used to apply uniform thin films to flat substrates shown in **Figure 10 (a-c)** in short, an excess amount of solution is placed on the substrate, which is then rotated at high speed in order to spread the fluid by centrifugal force. The machine used for spin coating is called a spin coater shown in **Figure 10**.

Spin coating can be used for several decades for the application of thin films. A typical process involves deposition a small puddle of a fluid resin onto a center of a substrate and then spinning the substrate at high speed (typically around 3000 rpm). Centripetal acceleration will cause most of the resin to spread to, and eventually off, the edge of the substrate, leaving a thin film of resin on the

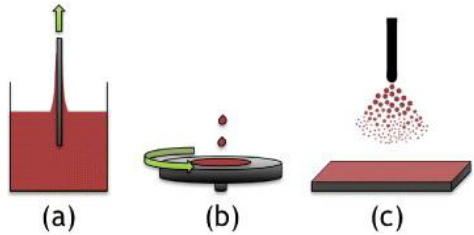

Figure 10. (a- c) Spin coating overview.

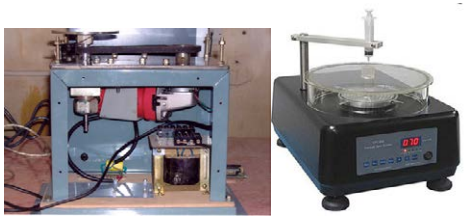

Figure 10: Front view of the spin coating unit with DC motor circuits.

surface. The final film thickness and other properties will depend on the nature of the resin, (Viscosity, drying rate, percent solids, surface tension etc,) and the parameters chosen for the spin process. Factors such as final rotational speed, acceleration, and fume exhaust contribute to how the properties of coated films are defined. One of the most important factors in spin coating is repeatability. Suitable variations in the parameters that define the spin process can result in drastic variations in the coated film. For our work we used spin coating method to prepare thin film sample. Thin transparent conducting films can be prepared by various methods, e.g., reactive sputtering, spray pyrolysis, chemical vapour deposition, high voltage anodization and vacuum deposition. Only the non-uniform thickness and the pinhole formation are the drawbacks in this technique. To overcome these drawbacks, a new cost effective spin coating unit is designed and fabricated. This chapter discusses the principles of film formation by spin coating technique followed by the design and fabrication aspects of the instrumentation.

The ideal condition of the film formation involves the deposition of the material atom by atom and layer by layer and there should be sufficient time interval so that atoms can occupy the minimum potential configuration with respect to the substrate and the subsequently on the previously deposited layers.Nucleation or small clusters formation is the basic process for all deposition method. There are several stages in the film growth process from the initial nucleation of the deposits to the final continuous film formation state and they are as follows.

Nucleation

Nucleation or small cluster formation is the basic process for all deposition modes. The ideal condition of the film formation involves the deposition of the material atom by atom (or molecule by molecule) and layer by layer there should be a sufficient time interval between two successive deposition of atoms and also layers so that these can occupy the minimum potential energy configuration with respect to the substrate and subsequently on previously deposited layers. In a thermodynamically stable film all atoms (or molecules) should be their minimum potential energy sites and the incoming atom (or molecules) will take up the positions and orientations energetically compatible with the neighboring atoms of the substrates or to the previously deposited layers. These will help for further growth of thin film.

Island structure stage

These islands consist of comparatively larger nuclei or embryos, say greater than 10 A^0 generally of 3D nature with their height however much less than their lateral dimensions. The formation of these islands and their growth take either by

direct addition of atoms from vapor phase of form other environment of by diffusion controlled process of ad-atoms or both as envisaged before. The formation of stable clusters and the subsequent capture of more ad-atoms by diffusion them to form stable islands and also sometime faceted ones.

Coalescence stage

The islands as they grow as mentioned before, develops some characteristics shapes, then with further growth coalescence with neighboring one by rounding off their edges near the joining ion where, these deposits assume a liquid like structure. The coalescence involves considerable transfer of mass between islands by diffusion. Small islands disappear rapidly. During the coalescence of two islands which occurs at there at their necks recrystallization as well as annealing takes place leading to some definite shape of larger islands.

Channel stage and holes

As the coalescence continuous with deposition there will be a resultant network of the film with channels in between. With further deposition these nuclei with increase in size along with the film thickness in addition of the formation of new islands and joining the main islands and thus bridging the gaps. Sometimes the channels may not be completely filled up even with increasing film thickness thus leaving some holes or gaps. With increasing thickness, the holes or gaps will decrease in size.

Continuous film stage

When these gaps are completely bridged by the secondary nuclei, film will be continuous. The minimum film thickness for the continuous stage depends on the nature of the deposits, modes of the deposition, deposition parameters etc. if the deposits do not have sufficient time for recrystallisation before the coalescence takes place, then the film will be in Meta stable state. The subsequent layers formed over then will also be in such a state. Thermal annealing treatment for the sufficiently long period of time will cause migration or diffusion of atoms leading to a stable phase.

Dip coating

In a dip-coating process, a substrate is dipped into a liquid coating solution and then is withdrawn from the solution at a controlled speed. Coating thickness generally increases with faster withdrawal speed. A faster withdrawal speed pulls more fluid up onto the surface of the substrate before it has time to flow back down into the solution. The thickness is primarily affected by fluid velocity, fluid density and surface tension. Dip coating, while excellent for producing high-quality, uniform coatings, requires precise control and a clean environment. The applied coating may remain wet for several minutes until the solvent evaporates. This process can be accelerated by heated drying shown in **Figure 11**.

Dip coating refers to the immersing of a substrate into a tank containing coating material, removing the piece from the tank, and allowing it to drain. The coated piece can then be dried by force drying or baking. It is popular way of crating thin film coated materials along with the spin coating procedure.

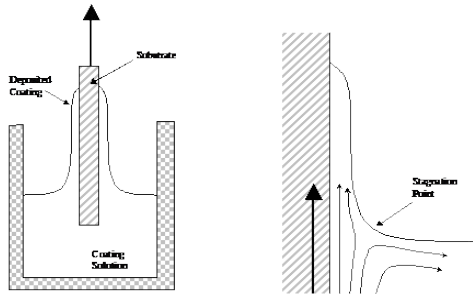

Figure 11: Shows typical dip coating process.

Sol-gel method

In this work, the thin film is deposited by Sol-gel method. The Sol-gel method is relatively cheap, simple and very attractive method for low-cost preparation of large area films. Moreover, this technique can be used in environmentally good conditions.

Spray pyrolysis method

The spray method depositing thin films is quite simple; it uses inexpensive equipment to make coatings over large areas [52, 53]. Unlike the other chemical solution deposition techniques, the film is found on a substrate kept outside the solution. The solution is sprayed onto a heated substrate, where the film is formed either by pyrolytic or hydrolytic chemical reaction of the liquid droplets, the hot substrate providing the thermal energy. Different techniques for spraying that have been employed include standard sprayers using compressed argon gas as a carrier gas and ultrasonic spraying using nozzle sprayers shown in **Figure 12**. Jet nebulizer is one of the spray pyrolysis technique which is shown in **Figure 13**.

Hydrothermal synthesis

The oxidative effect of hot water on amorphous carbon is currently used for purification of CNTs by hydrothermal treatment (immersion in water at moderate and high temperatures and pressures. It was found that the hydrothermal processing method could be developed to synthesize nano structural carbon. Recently, MWCNTs have been synthesized in the absence of metal catalyst by hrdrothermal treatment of amorphous carbon in pure water above 500 ºC. The hydrothermal nanostructures are free of amorphous carbon after treatment. The homogeneity of hydrothermal processes and availability of amorphous carbon materials, without the need for catalyst, are advantages favoring the scaling up of this new method.

Flame synthesis

Combustion is widely used in industrial processes for large scale materials synthesis, such as for carbon black and metal oxides. These flame processes are well for their many desirable features including continuous processing and energy efficiency. It was found that SWCNTs could be produced by a binary or ternary gas mixture of $CO/C_2H_2/H_2$ with a metal catalyst at 700º C in a two-stage flame. This flame system afforded the advantage that the catalyst formation step could

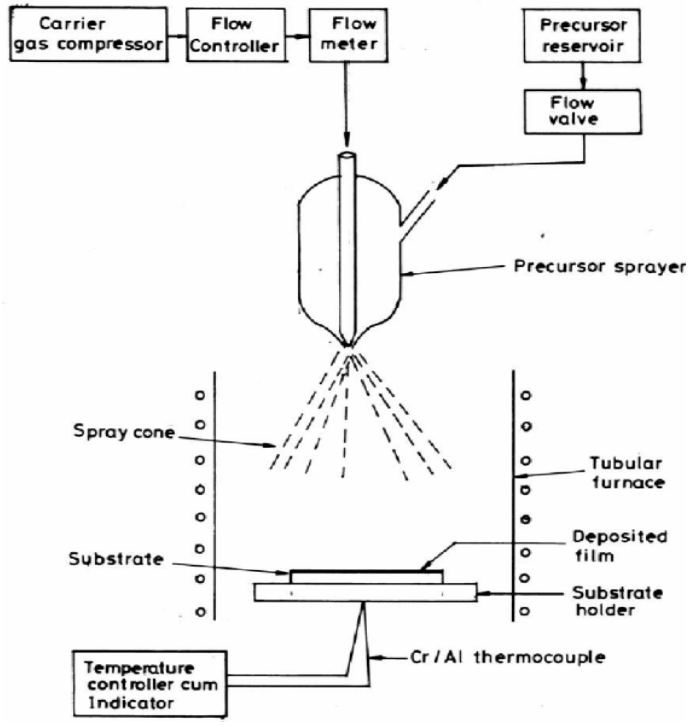

Figure 12: Experimental technique of chemical spray pyrolysis technique.

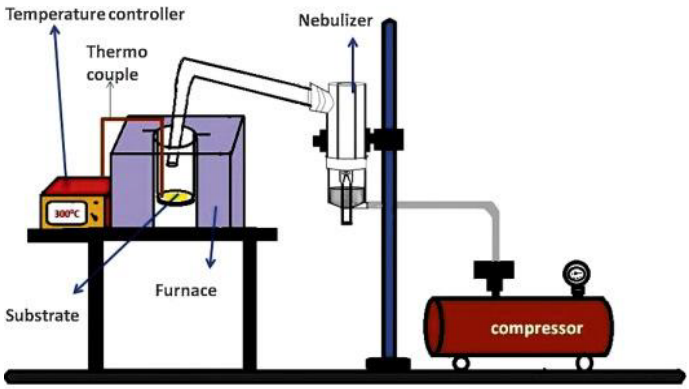

Figure 13: JET Nebuliser technique to prepare thin film.

be separated from the nanostructure growth steps, which allowed investigations of catalyst particle size dependencies upon nanostructure growth unlike methods that employ in-situ generation and concurrent growth.

Screen print/doctor bladding

Screen print is a method to adsorb/deposit a fluid substance with certain properties in a thin layer in a specific pattern with the edges shielded [54, 55]. The fluid is then dried or heat-treated to fixate the substance and remove the solvent.

Often the expression screen print is exclusively used for large-scale printing whereas the small-scale laboratory screen print method is referred to as doctor blading. In doctor blading, the shielding is not crucial and the thickness of the deposited suspension could instead be set by a device lifting the blade to a specific height.

Conclusion

In this work, authors have discussed physical vapor deposition, chemical vapor deposition, chemical deposition methods. Chemical deposition techniques are most important methods for the growth of films owing to their versatility for depositing a very large number of elements and compounds at relatively low temperatures. Meanwhile, chemical vapour deposition is the process whereby reaction precursors in vapour phase react either homogenously in the gas phase or heterogeneously at the solid-gas interface at the substrate. The objective of physical vapour deposition is to transfer atoms from a source to a substrate where film formation and growth follow automatically.

Acknowledgement

This work is supported by university.

References

1. Meglali O, Bouraiou A, Aida MS, Attaf N (2018) $CuInTe_2$ thin films synthesis using one-step electrodeposition process: structural, optical and electrical characterization. Applied Physics.
2. Ho SM, Meet M, Jaysukh M, Mariyappan S (2018) Review on dye-sensitized solar cells based on polymer electrolytes. International Journal of Engineering & Technology 7: 3001-3006.
3. Ananthan MR, Malar P, Thomas O, Kasiviswanathan S (2017) Studies on interface between In_2O_3 and $CuInTe_2$ thin films. Applied Surface Science, 418: 388-392.
4. Ho SM, Vyas CU, Pratik P, Patel KD, Somnath M, et al. (2018) A short review of CdTe and CdSe films: growth and characterization. Mediterranean Journal of Chemistry 7: 115-124.
5. Bouraiou A, Aida MS, Attaf N, Meglali O (2011) Potential effect on the properties of $CuInSe_2$ thin films deposited using two electrode system. Current Applied Physics 11: 1173-1178.
6. Ho SM, Gincy S, Sharadrao AV (2018) Studies on Cu_2SnS_3 thin films: review. ARPN Journal of Engineering and Applied Sciences 13: 4152-4159.
7. Kindyak AS, Kindyak VV, Latushko YJ (1998) Optical transitions in thin $CuIn(Te,Se)_2$ films near the fundamental absorption edge. Materials Letters 34: 237-240.
8. Ho SM, Olusola OI, Sharma DC, Mahmood W (2018) Zinc telluride thin films: a review. Asian Journal of Chemistry 30: 469-473.
9. Ho SM, Amala R (2018) A review of recent results on cyclic voltammetry studies of metal chalcogenide thin films. Journal of Engineering and Applied Sciences 13: 2773-2779.
10. Rohom AB, Chaure NB, Londhe PU (2017) The effect of citric acid and selenization onto electrochemically deposited copper indium thin films for solar cell applications. Thin Solid Films 642: 30-100.
11. Pahade VS, Chavan PS, Baisane VP (2016) A review paper on vapour deposition coating. International Journal of Engineering and Applied Sciences 3: 75-78.
12. Eman MN (2014) Surface morphology and structural properties of ZnS and ZnS: Al thin films. International Journal of Innovative Research in Science, Engineering and Technology 3: 8114-8120.

13. Maurya DK, Alameh K, Sardarinejad A (2014) Recent developments in RF Magnetron sputtered thin films for pH sensing applications. Coatings 4: 756-771.

14. Dan L, Wu L, Jiang H, Zhao Y, Zhang J, et al. (2012) Preparation and properties of SnO_2 film deposited by magnetron sputtering. International Journal of Photoenergy .

15. Ning S, Green MA, Huang J, Hu Y, Hao X, et al. (2018) Study of sputtered Cu_2ZnSnS_4 thin films on Si. Applied Surface Science 459: 700-706.

16. Chen B, Chen G, Wang W, Cai H, Yao L, et al. (2018). Magnetron sputtering deposition of GeSe thin films for solar cells. Solar Energy 176: 98-103.

17. Shongalova A, Correia MR, Teixeira JP, Leitao JP, Gonzalez JC, et al. (2018) Growth of Sb_2Se_3 thin films by selenization of RF sputtered binary precursors. Solar Energy Materials and Solar Cells 187: 219-226.

18. Li C, Wang F, Chen Y, Wu L, Zhang J, et al. (2018) Characterization of sputtered CdSe thin films as the window layer for CdTe solar cells. Materials Science in Semiconductor Processing 83: 89-95.

19. Wasa K (1993) Sputter deposition technology as a materials engineering. Bulletin of Materials Science 16: 643- 663.

20. Kassim A, Nagalingam S, Tee TE, Shariff AM, Kuang D, et al. (2009) Effects of pH value on the electrodeposition of Cu_4SnS_4 thin films. Analele Universitatii din Bucuresti 18: 59-64.

21. Gangawane SA (2017) Effect of electron irradiation on the electrodeposited cadmium telluride thin films. International Research Journal of Science and Engineering A1: 171-175.

22. Kassim A, Ho SM, Abdul HA, Noraini K, Saravanan N, et al. (2010) Influence of the deposition time on the structure and morphology of the ZnS thin films electrodeposited on indium tin oxide substrates. Digest Journal of Nanomaterials and Biostructures 5: 975- 980.

23. Magno BC, Lucia HM, Francisco W (2017) Thermal treatment effects on electrodeposited Sb_2Se_3 photovoltaic thin films. Chem Electro Chem 4: 25070-26014.

24. Mahanama GDK, Madarasinghe DA, Dharmaratna WGD, Jayasundara D (2018) Optical and structural properties of CdS thin films prepared using electro deposition technique. Ruhuna Journal of Science 9: 57-63.

25. Xu J, Wang W, Zhang X, Chang X, Shi Z, Geir MH (2015) Electro deposition of ZnSe thin film and its photocatalytic properties. Journal of Alloys and Compounds 632: 778-782.

26. Jee H, Paeng K, Myung N, Rajeshwar K (2017) Electrodeposition of cobalt selenide thin films: an electrochemical quartz crystal micro gravimetric study. Journal of the Electrochemical Society 164: D 861-866.

27. Kassim A, Abdullah AH, Ho SM, Saravanan N (2010) Influence of deposition time on the properties of chemical bath deposited manganese sulfide thin films. Avances en Quimica 5: 141-145.

28. Hankare PP, Rathod KC, Chate PA, Jadhav AV, Mulla IS, et.al, (2010) Preparation and characterization of $CuInSe_2$ thin films by chemical bath deposition technique. Journal of Alloys and Compounds 500: 78-81.

29. Anuar K, Tan WT, Ho SM, Abdul HA, Ahmad HJ, Saravanan N (2010) Effect of solution concentration on MnS_2 thin films deposited in a chemical bath. Kasetsart Journal (Natural Science) 44: 446-453.

30. Lugo S, Lopez I, Pena Y, Calixto M, Hernandez T, et al. (2014) Characterization of $CuInS_2$ thin films prepared by chemical bath deposition and their implementation in a solar cell. Thin Solid Films 569: 76-80.

31. Khor K, Anuar K, Tan WT, Saravanan N, Ho SM, et al. (2010) Effects of deposition time on the chemical bath-deposited CuS thin films. Journal of Nepal Chemical Society 25: 2-8.

32. Ayan M, Partha M (2017) Characterization of Sn doped ZnS thin films synthesized by CBD. Materials Research 20: 430- 435.

33. Atan S, Anuar K, Ho SM, Jelas H, Saravanan N, et al. (2011). Chemical bath deposition of SnS thin films: AFM, EDAX and UV-Visible characterization. Oriental Journal of Chemistry 27: 1375-1381.

34. Ezema FI, Osuji RU (2006) Preparation and characterization of chemical bath deposited $CdCoS_2$ thin films. Journal of Applied Sciences 6: 1827- 1832.

35. Loh YY, Ho SM, Anuar K, Tan WT, Saravanan N, et al. (2012) Complexing agent effect on the properties of iron sulphide thin films. Canadian Journal of Pure & Applied Sciences 6: 1863-1867.

36. Eres G, Christen HM (2008) Recent advances in pulsed laser deposition of complex oxides. Journal of Physics: Condensed Matter.

37. Yang Z, Hao J (2016) Progress in pulsed laser deposited two dimensional layered materials for device applications. Journal of Materials Chemistry C 4: 8859-8878.

38. Opoku F, Noah K, Anthony AA (2016) A comprehensive understanding of the chemical vapour deposition of cadmium chalcogenides using Cd $[(C_6H_5)_2PSSe]_2$ single source precursor: a density functional theory approach. Chemistry Central Journal.

39. John ER (2003) Chemical methods of thin film deposition: Chemical vapor deposition, atomic layer deposition and related technologies. Journal of Vacuum Science & Technology.

40. Milana CV, Kyle DA, Timothy JB, Vladimir VT, Rajesh RN, et al. (2013) Exploration of plasma enhanced chemical vapor deposition as a method for thin film fabrication with biological applications. ACS Applied Materials & Interfaces 5: 3983-3994.

41. Takuya K, Ito H, Kentaro K, Yuji H, Ozawa N, et al. (2015) The reason why thin film silicon grows layer by layer in plasma enhanced chemical vapor deposition. Scientific Reports.

42. En L, Zhang R, Li H, Liu C, Li G, et al. (2018) High quality PdTe2 thin films grown by molecular beam epitaxy. Chinese Physics B.

43. Joyce BA (1985) Molecular beam epitaxy. Reports on Progress in Physics 48: 1637-1697.

44. Yao T, Ogura M, Seiji M, Toshihide M (1983) High quality ZnSe thin films grown by molecular beam epitaxy. AUP Applied Physics Letters.

45. Lucie M, Sang MY, Sergei VK, Sylvie S, Catherine D, et al. (2015) A review of molecular beam epitaxy of ferroelectric $BaTiO_3$ films on Si, Ge and GaAs substrates and their applications. Science and Technology of Advanced Materials.

46. Gopakumar N, Anjana PS, Pillai P (2010) Chemical bath deposition and characterization of CdSe thin films for optoelectronic applications. Journal of Materials Science 45: 6653-6656.

47. Ho SM (2015) Chalcogenide thin films prepared using chemical bath deposition method: Review, Research Journal of Applied Sciences Engineering and Technology 11**:** 1058-1065.

48. Dona JM, Herrero J (1997) Chemical bath deposition of CdS thin films: an approach to the chemical mechanism through study of the film microstructure. Journal of the Electrochemical Society 144: 4081-4091.

49. Jiten PT, Sunil HC, Khimani AJ (2018) Chemical bath deposited and dip coating deposited CuS thin films- structure, Raman spectroscopy and surface study. AIP Conference Proceedings.

50. Tahir MB, Khalid N, Hafeez M, Shamsa F (2017) Review of morphological, optical and structural characteristics of TiO_2 thin film prepared by sol gel spin coating technique. Indian Journal of Pure & Applied Physics 55: 716-721.

51. Shivaraj BW, Murthy N, Sharma SC, Krishna M (2013) Investigation of influence of spin coating parameters on the morphology of ZnO thin films by Taguchi method. International Journal of Thin Films Science and Technology 2: 143-154.

52. Gunjal SD, Khollam YB, Jadkar SR, Shripathi T, Sathe VG, et al. (2014) Spray pyrolysis deposition of p-CdTe films: structural, optical and electrical properties. Solar Energy 106: 56-62.

53. Mehdi A, Mohamad MB, Hosein E (2012) Preparation and characterization of Cu_2SnS_3 ternary semiconductor nanostructures via the spray pyrolysis technique for photovoltaic applications. Physica Scripta.

54. Kumar V, Sharma DK, Bansal MK, Dwivedi DK, Sharma TP, et al. (2011) Synthesis and characterization of screen printed CdS films. Science of Sintering 43: 335-341.

55. Marc B (1998) Thin film solar cells by screen printing technology. Proceedings of the Workshop Microtechnology and Thermal Problems in Electronics; The Summer School. Technical University of Lodz.1998: 129-135.

Chapter 6

Thin Films Prepared Using Sol Gel Dip Coating Method

Bhasha[1], Shashank Shekhar[2], Purnima Jain[3]*

[1,2,3]Department of Chemistry, School of Applied Science, Advance Centre of Polymer Science, Netaji Subhas Institute of Technology, University of Delhi, India

***Corresponding author:** Purnima Jain, Department of Chemistry, School of Applied Science, Advance Centre of Polymer Science, Netaji Subhas Institute of Technology, University of Delhi, India, E-mail: prnmnsit@gmail.com

Abstract

Sol gel dip coating technique was employed to produce thin films. Sol gel chemistry is dependent on the nature and particle size of the species. This method includes transformation of liquid solution into solid gel in a phase. Also, solvent plays the important role in during the deposition process. There are several variables which can highly affect the structure of the deposited film which can be easily affected by particle size, structure, processing conditions, speed of immersion, rate of condensation and evaporation reactions, reactivity and surface tension. In this paper, basic principles of this technique were discussed.

Keywords

Sol gel dip coating; Particle size; Deposition technique; Thin films; Solvent

Introduction

A thin film fabricated by sol gel dip coating method is commercial and economically viable technology. Sol gel chemistry is dependent on the nature and particle size of the species. The sol-gel technique is a competent method for producing glass and ceramic materials. In addition, this method includes transformation of liquid sol into solid gel in a phase. On employing the sol-gel technique, it is viable to synthesize nano materials in a various forms: spherical shaped powders or ultra-fine, thin film coatings, ceramic fibers, microporous inorganic membranes, ceramics and glasses or extremely porous aerogel materials [1-5].

Also, solvent plays the important role in formation of sol and in conversion of gel. The chemistry of sol gel is governed by the sol (structure of solution) and microstructure of deposited thin films of coating process. Sol gel technique has the ability to modify micro-structure of the deposited thin film. This technique is being

Metal Chalcogenide Nanostructures: Characteristics and Synthesis, Edited by Ho Soon Min and Yarub Al-Douri

applied to a range of applications including pH sensors, membranes and protective coatings etc [6]. Coatings by sol gel method are the class of multifunctional materials which involves organic and inorganic hybrid [7] where intermolecular interactions take place within the existing structure and metallic surface which is influenced by low porosity, adhesion to substrate and low rigidity [8]. **Figure 1**.

The production of these materials can be carried out at laboratory as well as industrial scale despite of some constraints present in the resultant product. Dip coating phenomena has minimum uniform thickness, crack free thin film coated on the substrate. In this reported study, coating performance depends on three variables, first is residence time (Rt), second is cure between each deposition and third one is the presence of more than one layer of coating. This chapter reviews chemistry of recent research carried out on metal oxides through sol gel dip coating process and its application and also performance of coating, residency time, curing of each deposition and presence of more than one layers.

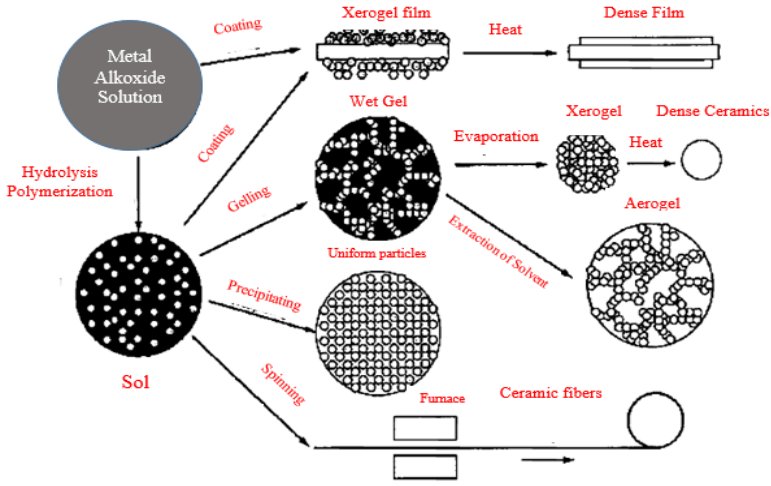

Figure 1: An Overview of Sol-Gel Technologies and their products.

Mechanism Involved in Sol-Gel Dip Coating Process

Precursor sol

Sol gel technique employs organic and inorganic based metal compounds as raw materials followed by hydrolysis and condensation reaction in organic or aqueous solvents to form polymers that are inorganic which is bridged in between the metal centers of hydroxyls and oxo groups [1]. **Figure 2**.

In inorganic compounds, hydrolysis has been carried but with the removal of proton from aqueous ion $[MO_nH_{2n}]^{Z+}$ to form oxo (M=O) or hydroxo (M-OH) ligand. Commonly used metal compounds are metal alkoxides (MOR_z) where R is an alkyl group.

As we know the solvent for alkoxide is generally alcohol and the hydrolysis reaction can be carried out by using water in acidic, neutral or basic media.

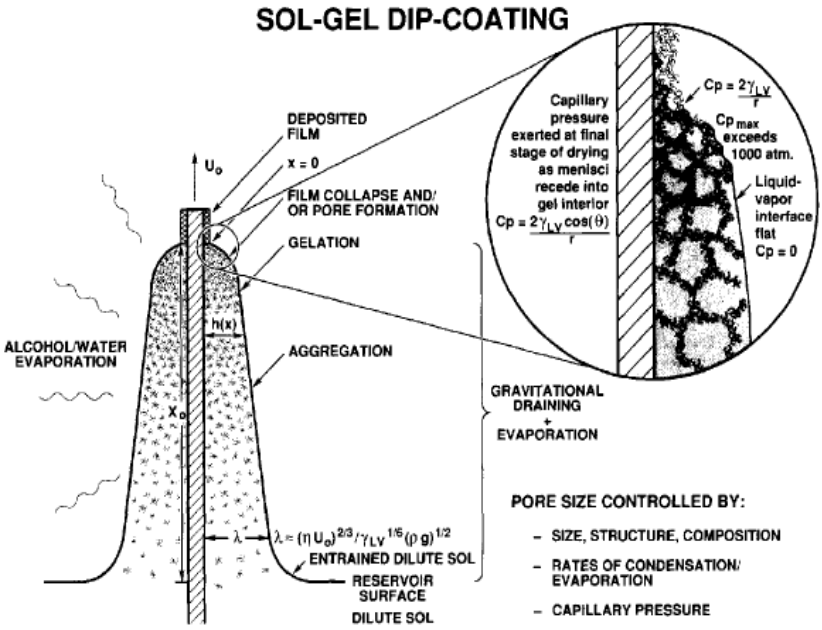

Figure 2: Illustration of Sol Gel Dip Coating Process.

Hydrolysis replaces the alkoxide with a hydroxyl ligand.

$$MOR_z + H_2O \rightarrow MOR_{z-1}OH + ROH \quad (1)$$

Condensation reaction employs hydroxyl ligands. For Eg:-Silicates

$$Si(OR_3)OH + Si(OR_4) \rightarrow (RO_3)Si\text{-}O\text{-}Si(OR_3) + ROH \quad (2)$$

$$2Si(OR_3)OH \rightarrow (RO_3)Si\text{-}O\text{-}Si(OR_3) + H_2O \quad (3)$$

Depending upon the above reaction, the structure of the resultant inorganic polymer may vary accordingly on the processing conditions, e.g. pH or the molar ratio "r" of H_2O: M in equation.

The inorganic polymers structure might differ substantially. Foregoing study on silicates have revealed that spectrum of structures are due to condensation reaction which ranges from weakly branched polymers which are characterized by a mass fractal dimension to highly condensed uniform particles. The mass fractal dimension i.e. D is related to the mass of polymer "M" to its radius "r" according to M ~z r °.

Here, D is less than the dimension "d" of space. Since in three dimensions D < 3, the density of a mass fractal object decreases radially as 1/r 3-D. As this feature permits us to modify the porosity of film by the simple aging procedure.

Phenomena of dip coating

Process of dip coating is to produce many nanomaterials and coated substrates to create thin film coatings from sol gel precursors. **Figure 3**. In general, dip coating is normal insertion and removal of the substrate at a constant speed. Here, substrate is normally vertically withdrawn from the medium or solution. The

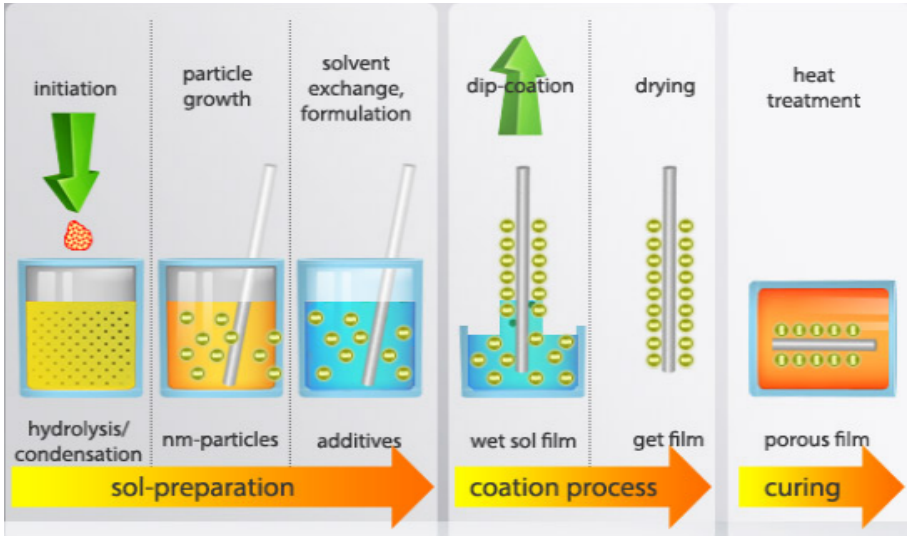

Figure 3: Sol-Gel Dip Coating Process.

thin layer of solution deposits on the substrate when the substrate is pulled off followed by evaporation of solvent forming a thin layer. In some applications this process is repeated so many times to get the desired thickness. Many factors affect the process of dip coating.

- Sequence of dipping
- Functionality of the substrate
- Time of submersion
- Withdrawal speed of substrate
- Composition of Solution
- Concentration and temperature etc.

Scriven stated that thickness of the film deposited on the substrate in which moving layers of streamline is related to the upward and downward position [9]. There are six parameters in the film deposition which regulates the thickness of film and the position of streamline. (1) force of gravity; (2) surface tension force in concavely shaped meniscus; (3) viscous drag upward by the moving substrate on liquid; (4) at the deposition point, boundary layer liquid force; (5) pressure of disjoining; (6) surface tension gradient. For depositing sols, evaporation of solvent results in thinning which induces considerable enhancement in concentration of sol, therefore it's important to study the mechanism of sol gel film deposition.

Formation of Sol-Gel Film

Inorganic film is being deposited as the inorganic precursor or polymer by the gravitational draining and evaporation by the condensation reaction. Due to concentration forces, the precursor results in formation of aggregate or gel while repellent particles appear into crystal like structure which depends on withdrawal rate. In some cases, reactive precursors compact and stiffen the structure.

Factors Which Can Control the Structure of Deposited Film

There are several variables which can highly affect the structure of the deposited film which can be easily affected by particle size, structure, processing conditions, speed of immersion, rate of condensation and evaporation reactions, reactivity and surface tension. Some of the factors has been discussed in the below section.

Influence of precursor structure

There is a range of inorganic precursors such as branched polymers and high condensed particles. Packing efficiency of some objects are dependent on dimension, size and rate of condensation. Mandelbrot stated that R radius of two structures when located severally in same region, the M_{AB} mean number of intersections is expressed as: [10].

$$M_{AB} \alpha R^{D1+D2-d} \quad (4)$$

Where D1 and D2 are the fractal dimensions and d is the dimension of space (d=3). Each object has fractal dimension of <1.5, as probability of intersection decreases, R increases indefinitely. The chemical structures formed during film formation are mutually transparent, they interpenetrate with each other in close proximity when concentration is increased. But as fractal dimension is increases from 1.5, probability of intersection increases with R. Structures become porous and opaque but they are unable to penetrate.

Every intersection result is chemically equivalent to an infinitely rate of condensation in irreversible conditions, when concept of transparency and opaque is applied. Condensation rate of silicates is very low and depends on $[H^+]$ e.g. 10^{-4} $lmol^{-1}S^{-1}$ [11-13]. Hence at any point of intersection probability of sticking is less than 1 which causes compactness in structure from equation 4.

For example, condensation rate is minimized in weakly branched silicates which produces dense films and can be explained from the adsorption-desorption isotherm curve in **Figure 4** [14-16]. It indicates the zero porosity to 0.4 nm molecules or more in diameter. However, due to low condensation rate, precursors can interpenetrate in these conditions when D is more than 1.5, as they are concentrated by evaporation on surface of substrate which leads to densely packed molecular configuration.

Effect of capillary

Hydroxyl step is carried out in processing of sol gel of alkoxides by a ratio of H_2O: M exceeding 50. Ratio of H_2O: Si is theoretically 2 which is sufficient to attain condensation and hydrolysis of $Si(OR)_4$ to form SiO_2 when water is produced by condensation in equation 3. During dip coating process, elipsometric studies of solvent mixed with alcohol and water showed that mixture is enriched in water in drying line vicinity.

At azeotropic mixture, this enrichment of water occurs by alcohol evaporation and surface tension gradient driven flows. Due to enrichment in water an increase in capillary pressure is observed during final stage of drying throughout sol deposition. In addition, increase in enrichment of water causes reduction in refractive index.

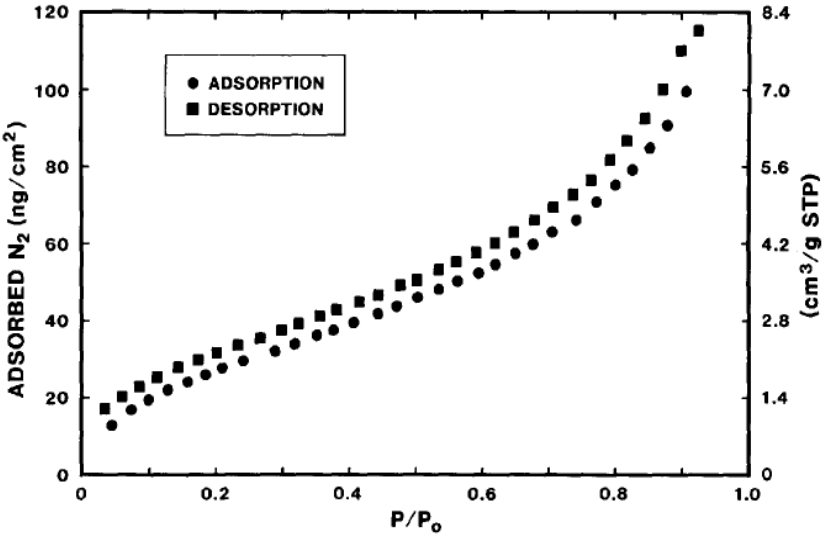

Figure 4: N_2 adsorption-desorption isotherm for a film deposited from silicate precursor (Condensation rate is minimized) obtained from SAW method.

Dip and spin coating can be differentiated on the basis of evaporation rate and also the aging time. Hence the deposited film structure is influenced by effect of capillary which also attributes the strong forces in vapour on substrate created by spinning leads to the little time of aging and increased evaporation rate [17-19].

Influence of substrate speed

As speed (Uo) of the substrate increases the thickness of the film increases. As solvent evaporation virtually occurs at exterior surface of the entrained sol. Thicker the film, longer the time taken to dry which will increase the aging time of reactive sols and ordering time of repulsive sols must be seen. The substrate speed has second effect that is induced shear field in sol deposition [20-24]. When high shear rate is gained with respect to diffusion constant by a particle than it may be anticipated that the repulsive particles may mutually align in closed packed planes which are positioned side by side to the surface of substrate.

Figure 5 shows the graph plotted between Uo and refractive index for monosized series of particulate sols [25-26] which are deposited at pH 11 where particle experiences a uniform electrostatic repulsion caused by deprotonation of surface silanols. A graph showing Uo and refractive index illustrated correlation of a polymeric sol which is deposited nearby about pH 3, weakly charged and the rate of condensation is elevated. There is monotonic increment in refractive index with increase in Uo for all sizes of repulsive particles. But the relationship was opposite for reactive or polymeric sol.

By SAW techniques Nitrogen adsorption desorption isotherm is acquired by 55 nm particulate sols which explicit the porosity volume fraction decreased from 36~Uo to 26~Uo as the rate of coating increased from 12.7 to 45.7 cm rain. For monosized spherical sols packing correlated to the change to fcc closed packing from random dense packing [27]. So we can infer that particles are ordered with increase coating rate.

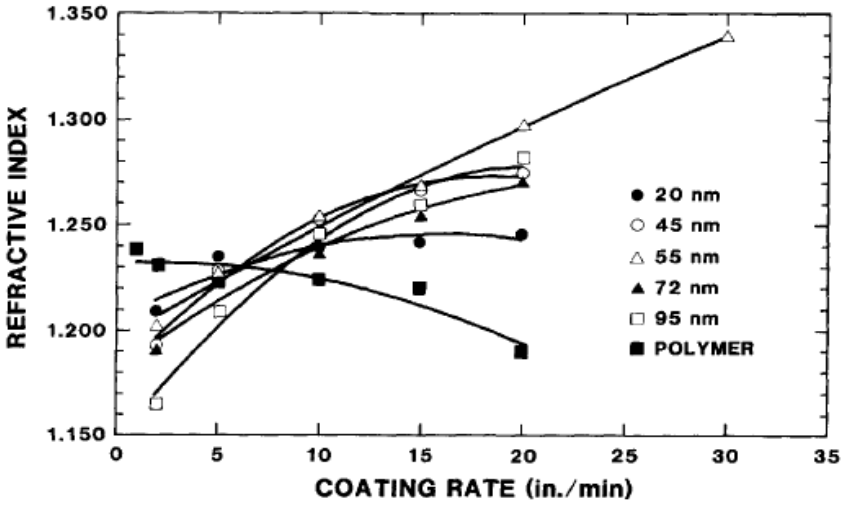

Figure 5: This curve depicts the refractive index vs withdrawal speed (Uo) for deposited silicate films at approximately 11 pH.

Sol gel Synthesis of Some Metal Oxides

Sol gel technique has been employed to fabricate various metal oxide nanoparticles due to its chemical stability, control of oxidation and good resistance for corrosion for metal substrates. Some of the examples has been discussed in brief to understand the process involved in fabrication of metal oxides.

Zinc oxide

By using sol-gel method zinc oxide nanostructure were synthesized. In this process. Zinc acetate di-hydrate has been utilized as precursor agent, distilled water as solvent system and ethanol as reagent. Sodium Hydroxide (NaOH) was dissolved in 10 ml of deionized water and 2 g Zinc acetate di-hydrate was added in 15 ml of deionized water. The two obtained solutions were constantly stirred for five minutes. After that Sodium Hydroxide solution was poured in Zinc acetate solution with constant mixing on magnetic stirrer for five minutes. Then, the mixture of two solutions was titrated against ethanol. After the completion of reaction, the white precipitate of ZnO was obtained. **Figure 6**.

According to experimental work there are number of chemical reactions involved. When hydrolysis of zinc acetate with sodium hydroxide solution in ethanol is carried out, the result should be the formation of Zinc oxide colloid. The final product result with the establishment of condensation and hydrolysis reaction. Zinc Acetate undergoes the hydrolysis due to heating as zinc ion and acetate ion. Due to high reactivity of lone pair present in oxygen of hydroxyl (-OH) group forms a bond with zinc ion [28-29].

Overall reaction is given below:

$$(Zn\ (CH_3COO)_2.2H_2O) + 2NaOH \qquad ZnO + 2NaCH_3COO + H_2O \qquad (1)$$

An intermediate product which is Zinc Hydroxide Acetate produced in the existence of H_2O and OH^- ions as hydrolysis reaction. This intermediate can easily

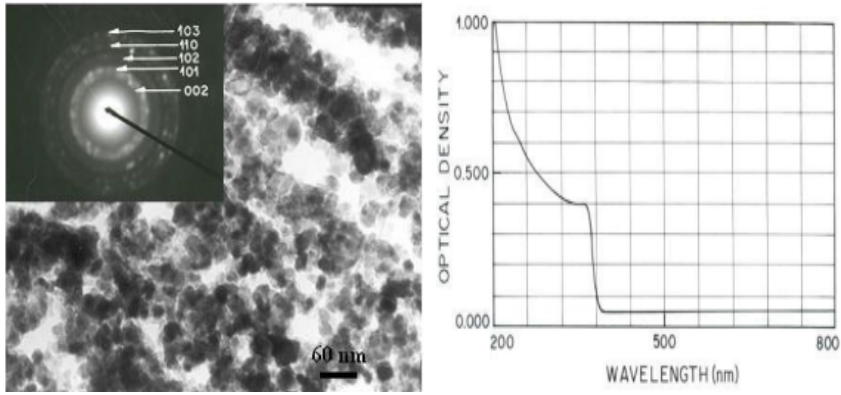

Figure 6: TEM image, electron diffraction pattern and UV visible spectra of ZnO nanoparticles.

be transformed into Zinc Oxide at high temperature and prolonged refluxing. Zinc Oxide with high purity can be obtained through sol gel method as the byproduct i.e. Sodium acetate thus obtained can be removed by dissolving it in water as it is water soluble [30-32]. Purnima et al. reported the fabrication of zinc oxide nanoparticles via sol gel route for ethanol vapour sensor application and measured its selectivity, sensitivity and found quick response recovery systems [33-34]. A change in electrical resistance was detected at different temperatures under a range of ethanol concentrations which is a potential candidate for semiconducting material applications for detection of ethanol vapour.

UV-Visible absorption spectra showed strong absorption band at 335 nm and excitonic peak found at around 258 nm which is due to the formation of ZnO nanoparticles which is below the band gap of wavelength 358 nm.

Applications of Zinc Oxide Nano Particles

Zinc Oxide is an inorganic compound which finds a large application in our day to day life. Some applications are given below.

- Zinc oxide is known as a safe and nontoxic material reported by Food and Drug Administration, so it can be used as additive in food applications. With the help of nanotechnology the material ZnO has got new properties like antimicrobial activity and finds application as food preservative. Polymeric materials incorporative with ZnO nanoparticles provide antimicrobial activity in packaging and improvement in packaging properties [35-36].
- ZnO nanomaterial finds application in bioimaging and drug delivery due to its versatile surface chemistry and large surface area. Some studies also shown that ZnO nanoparticles are highly toxic for cancer cells. So that is why it is not only used in drug delivery but also used for cancer therapy.
- As ZnO has semiconducting properties but it also exhibits bio sensing properties such as strong adsorption capability, high catalytic efficiency and high isoelectric point which is suitable for the absorption of proteins by isoelectric interactions.

- When ZnO nanoparticle is synthesized with reduced graphene oxide by sol-gel method, then photocatalyst activity revealed that high MB removal efficient than ZnO. It can be used for removal of pollutant from waste water in large scale.

Titanium dioxide

Thin films of titanium dioxide nanomaterials were fabricated by sol-gel approach using hydrolysis of titanium peroxide precursor. This method can also be applied for the synthesis of powders and membranes. Oxides with difference in physical and chemical properties may be produced which depends on synthesis approach used. Advantage of this technique is its purity, flexibility, ease of processing and its eco-friendly nature and also the capability to coat intricate and complex areas [37-42]. Titanium dioxide pigment is a fine white powder. The two forms of this metal oxide that is metastable anatase and brookite phases convert irreversibly to the other equilibrium rutile phase upon heating above temperatures in the range 600- 800 °C [43-47].

Titanium Dioxide Nanoparticles were synthesized by using Neem leaves and Titanium isopropoxide. The healthy Neem leaves were collected from local places of Delhi, India [48-51]. The leaves were carefully washed with distilled water to eradicate dust particles and contaminates. After that drying of Neem leaves is done at room temperature for 7 days (summer season) under condition free of dust particles [52-55]. Dried Neem leaves were grinded and sieved to get the powder of Neem [56-57].

The extract of Neem leaves was mixed with 50 ml of ethanol under reflux condition at 50 °C. After 5 hours the prepared ethanolic solution can be used in the fabrication of Tio_2 nanoparticles. 0.4M titanium iso-propoxide added in ethanolic leaf extract and mixing done at 50 °C for 5 hours to form titanium dioxide nanoparticles [58-59]. Centrifugation of prepared solution is done at 1000 rpm for 15 minutes then washing with ethanol has been carried out & again centrifugation has been done at 5000 rpm for 5 minutes, then drying at 500 °C temperature for 2 hours take place to get the dried powder.

Particle size of TiO_2 nanoparticles were obtained by SEM image is in range of 10- 50 nm. IR transmission spectrum of TiO_2 nanoparticles prepared by green chemistry route shown in **Figure 7** is dominated by the titanium iso-propoxide peaks [60]. The characteristic stretching modes of TiO_2 are submerged in the broad transmission in the region 1000- 500 cm^{-1}, these peaks at ~ 560 cm^{-1} and 472 cm^{-1} are resolved by deconvulting the spectrum in 600- 400 cm^{-1} region.

Applications of Titanium Dioxide

- It is a widely studied metal oxide used in paints and varnishes area. Also it is being used as photocatalyst for removal of waste water and in solar cell devices.
- It is also used as pigments such as cosmetic products, inks, rubbers and foodstuffs.
- It is also used in the large scale production of the pure titanium, glass and glass ceramics, electrical ceramic.

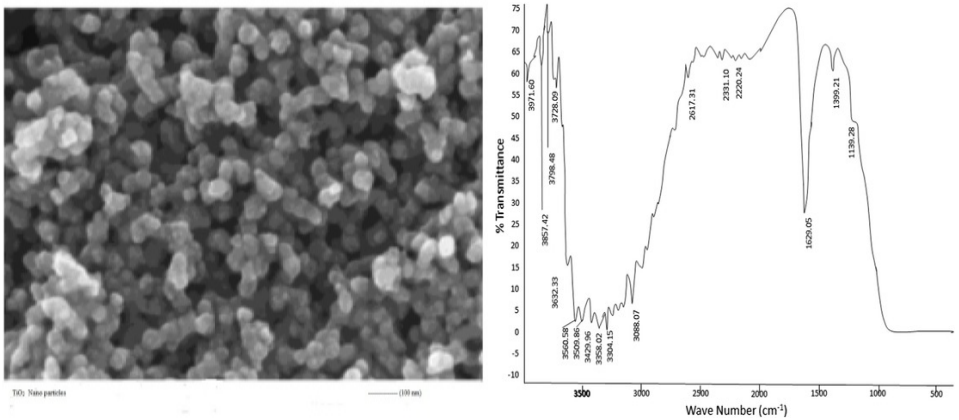

Figure 7: SEM micrograph and IR transmission spectrum of TiO_2 nanoparticles prepared from Green chemistry.

Conclusion

During sol gel dip coating process, precursors are rapidly concentrated on the surface of substrate followed by hydrolysis and condensation reactions. Some factors which can affect the structure of deposited film has been also discussed; (1) size and opacity, (2) withdrawal speed of substrate, (3) pressure of capillary. These factors can be controlled by modification of pore size, pore volume, surface area and refractive index of the film. This process has advantage over other conventional techniques used that is its eco-friendly nature, cost effective and can be carried out on small scale also.

Acknowledgement

This work is supported by Netaji Subhas Institute of Technology, University of Delhi, India.

References

1. Thomas I M (1986) Optical coatings by the sol-gel process. Optics News 12: 18-22.
2. Malik P, Jain P, Bhasha B (2018) Influence of surface modified graphene oxide on mechanical and thermal properties of epoxy resin. Oriental Journal of Chemistry 34: 1597-1603.
3. Hench LL, Ulrich DR (1984) Ultrastructural Processing of Ceramics, Glasses and Composites. Department of Materials Science and College of Engineering, University of Florida, Wiley-Interscience publication. ISBN: 0471896691.
4. Baiju KV, Warrier K (2007) Aqueous sol-gel process for nanocrystalline photocatalytic titania, transparent functional coatings and ceramic membrane (Doctoral dissertation, National Institute for Interdisciplinary Science and Technology, CSIR).
5. Lewis J A (2000) Colloidal processing of ceramics. Journal of the American Ceramic Society 83: 2341-2359.
6. Brinker C, Scherer G (2013) Sol-gel Science. The Physics and Chemistry of Sol Gel Processing. ISBN: 9780080571034.
7. Balgude D, Sabnis A (2012) Sol–gel derived hybrid coatings as an environment friendly surface treatment for corrosion protection of metals and their alloys. Journal of Sol-gel Science and Technology 64: 124-134.

8. Guglielmi M (1997) Sol-gel coatings on metals. Journal of Sol-gel Science and Technology 8: 443-449.

9. Bergna HE, Roberts WO (2005) Colloidal silica: fundamentals and Applications. CRC Press, ISBN: 9780824709679.

10. Mandelbrot B (1982) The fractal geometry of nature New York: WH freeman.

11. Brinker CJ, Frye GC, Hurd AJ, Ashley CS (1991) Fundamentals of sol-gel dip coating. Thin Solid Films 201: 97-108.

12. Gregg SJ, Sing KSW (1982) Adsorption, Surface Area and Porosity, Academic Press, London.

13. Stawski TM, Veldhuis SA, Besselink R, Castricum HL, Portale G, et al. (2011) Nanoscale Structure Evolution in Alkoxide–Carboxylate Sol-Gel Precursor Solutions of Barium Titanate. The Journal of Physical Chemistry C 115: 20449-20459.

14. Livage J, Henry M, Sanchez C (1988) Sol-gel chemistry of transition metal oxides. Progress in Solid State Chemistry 18: 259-341.

15. Sanchez C, Ribot F, Rozes L, Alonso B (2006) Design of hybrid organic-inorganic nanocomposites synthesized via sol gel chemistry. Molecular crystals and Liquid Crystals Science and Technology. Section A. Molecular crystals and Liquid Crystals 354: 143-158.

16. Bari AR, Shinde MD, Deo V, Patil LA (2009) Effect of solvents on the particle morphology of nanostructured ZnO. Indian Journal of Pure & Applied physics 47: 24-27.

17. Bhasha S, Malik P, Santosh S, Purnima J (2015) Synthesis and characterization of nanocrystalline zinc oxide thin films for ethanol vapor sensor. Journal of Nanomedicine & Nanotechnology.

18. Espitia PJP, Soares N, Jane S, Nekio J, Renato S, et al. (2012) Zinc oxide nanoparticles: synthesis, antimicrobial activity and food packaging applications. Food and Bioprocess Technology 5: 1447-1464.

19. Hanley C, Layne J, Punnoose A, Reddy KM, Coombs I, et al. (2008) Preferential killing of cancer cells and activated human T cells using ZnO nanoparticles. Nanotechnology.

20. Wei A, Sun XW, Wang JX, Lei Y, Cai XP, et al. (2006) Enzymatic glucose biosensor based on ZnO nanorod array grown by hydrothermal decomposition.

21. Azarang M, Shuhaimi A, Yousefi R, Moradi GA, Sookhakian M, et al. (2014) Synthesis and characterization of ZnO NPs/reduced graphene oxide nanocomposite prepared in gelatin medium as highly efficient photo-degradation of MB. Ceramics International 40: 10217-10221.

22. Belot V, Corriu R, Guerin C, Henner B, Leclercq D, et al. (1990) Sol gel chemistry of hydrogenosiliconates: the role of hypervalent silicon species. In Better ceramics through chemistry IV: Symposium held April 16- 20, 1990 San Francisco, California, USA. Editors: Brian JJZ, Brinker CJ, Clark DE, Donald RU: 3 -14. Materials Research Society, Pittsburgh, Pennsylvania.

23. Roger AA, Kay BD (1990) Current issues in sol gel reaction kinetics. In Better ceramics through chemistry IV: Symposium held April 16-20, 1990 San Francisco, California, USA. Editors: Brian JJZ, Brinker CJ, Clark DE, Donald RU. 21-28. Materials Research Society, Pittsburgh, Pennsylvania.

24. Gregg SJ, Sing KSW (1982) Adsorption, Surface Area & Porosity, 2nd edition, Academic Press, ISBN-10: 0123009561.

25. Yang A, Cui Z (2007) Controlling the orientation of ZnO nanorods arrays using TiO_2 thin film templates dip-coated by sol gel. Journal of Nanoparticle Research 9: 245-250.

26. Sharma B, Malik P, Jain P (2018) Biopolymer reinforced nanocomposites: A comprehensive review. Materials Today Communications 16: 353- 363.

27. Sharma B, Shekhar S, Gautam S, Sarkar A, Jain P, et al. (2018) Nanomechanical analysis of chemically reduced graphene oxide reinforced poly (vinyl alcohol) nanocomposite thin films. Polymer Testing 70: 458-466.

28. Thapa S (2016) Defects and Ferromagnetism in Transition Metal Doped Zinc Oxide (Doctoral dissertation, Bowling Green State University).

29. Gao F, Zhao J, Wu K (2010) Structure and magnetic properties of Ni-doped ZnO powder. Journal of Wuhan University of Technology-Materials Science 25: 770-773.

30. Lee YC, Chang YS, Teoh LG, Huang YL, Shen YC, et al. (2010) The effects of the nanostructure of mesoporous TiO_2 on optical band gap energy. Journal of Sol-gel Science and Technology 56: 33-38.

31. Ying L, Shuo C, Xie Q, Yu H (2011). Fabrication of a TiO_2/Au nanorod array for enhanced photocatalysis. Chinese Journal of Catalysis, 32(11-12), 1838-1843.

32. Eshaghi A, Mozaffarinia R, Pakshir M, Eshaghi A (2011) Photocatalytic properties of TiO_2 sol-gel modified nanocomposite films. Ceramics International 37: 327-331.

33. Laidani N, Cheyssac P, Perriere J, Bartali R, Gottardi G,et al. (2010). Intrinsic defects and their influence on the chemical and optical properties of TiO_{2-x} films. Journal of Physics D: Applied Physics 43.

34. Sharma B, Shekhar S, Gautam S, Jain P (2018) Dynamic shear rheology behavior and long term stability kinetics of reduced graphene oxide filled poly (vinyl alcohol) biofilm. Polymer Testing 69: 583- 592.

35. Sergey EL (2014) Dekker Encyclopedia of Nanoscience and Nanotechnology. 3rd edition, CRC Press.

36. Rajammal R, Rajaram K, Savarimuthu E, Arumugam S (2012) Influence of number of coatings on properties of sol–gel spin coated CdO thin films. Surface Engineering 28: 205-208.

37. Nam SH, Cho SJ, Jung CK, Boo JH, Šícha J, et al. (2011) Comparison of hydrophilic properties of TiO2 thin films prepared by sol–gel method and reactive magnetron sputtering system. Thin Solid Films 519: 6944-6950.

38. Xagas AP, Androulaki E, Hiskia A, Falaras P (1999) Preparation, fractal surface morphology and photocatalytic properties of TiO_2 films. Thin Solid Films 357: 173-178.

39. Cheng H, Huang B, Dai Y (2014) Engineering BiOX (X= Cl, Br, I) nanostructures for highly efficient photocatalytic applications. Nanoscale 6: 2009-2026.

40. Shankar AR, Raju VR, Rao MN, Mudali UK, Khatak HS, et al. (2007) Corrosion of Zircaloy-4 and its welds in nitric acid medium. Corrosion Science: 49: 3527-3538.

41. Eshaghi A, Pakshir M, Mozaffarinia R (2010) Preparation and characterization of TiO_2 sol-gel modified nanocomposite films. Journal of Sol-gel Science and Technology 55: 278-284.

42. Lewkowicz A, Synak A, Grobelna B, Bojarski P, Bogdanowicz R, et al. (2014). Thickness and structure change of titanium (IV) oxide thin films synthesized by the sol–gel spin coating method. Optical Materials 36: 1739-1744.

43. Aziz SB, Ahmed HM, Hussein M, Fathulla AB, Wsw RM, et al. (2015) Tuning the absorption of ultraviolet spectra and optical parameters of aluminum doped PVA based solid polymer composites. Journal of Materials Science: Materials in Electronics 26: 8022-8028.

44. Augugliaro V, Loddo V, Pagliaro M, Palmisano G, Palmisano L, et al. (2011) Clean by light irradiation: Practical applications of supported TiO_2. Royal Society of Chemistry.

45. Xu S, Wang ZL (2011) One-dimensional ZnO nanostructures: solution growth and functional properties. Nano Research 4: 1013-1098.

46. Luo L, Rossell MD, Xie D, Erni R, Niederberger M, et al. (2012) Microwave-assisted nonaqueous sol–gel synthesis: from Al: ZnO nanoparticles to transparent conducting films. ACS Sustainable Chemistry & Engineering 1: 152-160.

47. Rojviroon T, Sirivithayapakorn S (2013) Properties of TiO_2 thin films prepared using sol-gel process. Journal of Surface Engineering 29: 77-80.

48. Tiwari V, Jiang J, Sethi V, Biswas P (2008) One-step synthesis of noble metal–titanium dioxide nanocomposites in a flame aerosol reactor. Applied Catalysis A: General 345: 241-246.

49. Yu J, Yu H, Ao CH, Lee SC, Jimmy CY, et al. (2006) Preparation, characterization and photocatalytic activity of in situ Fe-doped TiO_2 thin films. Thin Solid Films 496: 273-280.

50. Syarif DG, Miyashita A, Yamaki T, Sumita T, Choi Y, et al. (2002) Preparation of anatase and rutile thin films by controlling oxygen partial pressure. Applied Surface Science 193: 287-292.

51. Bhasha S, Singh S, Malik P (2015) Synthesis and Characterization of Nanocrystalline Zinc Oxide Thin Films via Green Chemistry. Journal of Nanoanalysis 2: 10-16.

52. Sayılkan H (2007) Improved photocatalytic activity of Sn^{4+}-doped and undoped TiO_2 thin film coated stainless steel under UV-and VIS-irradiation. Applied Catalysis A: General 319: 230-236.

53. Pelaez M, Nolan NT, Pillai SC, Seery MK, Falaras P, et al. (2012) A review on the visible light active titanium dioxide photocatalysts for environmental applications. Applied Catalysis B: Environmental 125: 331-349.

54. Rojviroon T, Sirivithayapakorn S (2013) Properties of TiO_2 thin films prepared using sol–gel process. Journal of Surface Engineering 29: 77-80.

55. Lin S, Zhou T, Lu J, Sun Q (2016) Fabrication of Nitrogen-modified Tio2 Immobilized on Glass-fiber and Its Photocatalytic Activity under Simulated Solar Irradiation. Feb-fresenius Environmental Bulletin, 4837.

56. Mardare D, Luca D, Teodorescu CM, Macovei D (2007) On the hydrophilicity of nitrogen-doped TiO_2 thin films. Surface Science 601: 4515-20.

57. Sharma B, Shekhar S, Malik P, Jain P (2018) Study of mechanism involved in synthesis of graphene oxide and reduced graphene oxide from graphene nanoplatelets. Materials Research Express.

58. Im JS, Yun SM, Lee YS (2009) Investigation of multielemental catalysts based on decreasing the band gap of titania for enhanced visible light photocatalysis. Journal of Colloid and Interface Science 336: 183-188.

59. Sridhar S, Arunnellaiappan T, Rameshbabu N, Mika S, Viswanathan A, et al. (2017) Solar photocatalytic activity of nitrogen doped TiO_2 coating by micro-arc oxidation. Journal of Surface Engineering, 33: 779-786.

60. Gao F, Zhao J, Wu K (2010) Structure and magnetic properties of Ni-doped ZnO powder. Journal of Wuhan University of Technology-Materials Science 25: 770-773.

Chapter 7

Physical and Optical Properties of Cu_4sns_4 Nanostructured Thin Films

Ho Soon Min*

Centre for Green Chemistry and Applied Chemistry, INTI International University, Putra Nilai, 71800, Negeri Sembilan, Malaysia

***Corresponding author:** Ho Soon Min, Faculty of Information Technology Mathematic & Science, INTI International University, Malaysia , E-mail: soonmin.ho@newinti.edu.my

Abstract

Solar energy is an example of renewable energy. It is free, clean and inexhaustible. Currently, there are two types of semiconductors, namely n-type and p-type. These semiconductors consist of n-type and p-type absorb sunlight, then produce electricity. Thin films based solar cells have many advantages if compared to silicon based solar cells, such as light in weight, low cost, simple design and eco-friendly. In this work, chemical bath deposition method has been used to synthesis ternary nanostructured Cu_4SnS_4 films. Na_2EDTA solution was served as complexing agent during the deposition process. The influence of Na_2EDTA on the properties of thin films was studied using X-ray diffraction (structural properties), atomic force microscope (topography property) and UV-Visible Spectrophotometer (optical property).

Keywords

Solar energy; Electricity; Semiconductor; Thin films; XRD analysis

Introduction

Solar energy is considered as clean energy and inexhaustible. It is definitely free, and is a renewable energy. Currently, there are two types of semiconductors, namely n-type and p-type. These semiconductors absorb sunlight, then generate electricity (electrons loose from atom and flow via these semiconductors). Silicon based solar cells [1-5] have dominated photovoltaic market (about 90 %) because of no toxicity, availability, long life time and sustainability. On the other hand, thin film technology has attracted many researchers [6-10] because of less expensive and abundant material. For example, cadmium telluride films [11-14] and copper indium gallium diselenide thin films [15-18] have been successfully prepared by many scientists. However, less efficiency if compared to silicon technology. Another type of solar cells was organic solar cells. They are synthesized from polymer and

Metal Chalcogenide Nanostructures: Characteristics and Synthesis, Edited by Ho Soon Min and Yarub Al-Douri

earth abundant materials. They have a lot of advantages such as light in weight, low cost, simple design and eco-friendly [19-21]. Application of organic solar cells including glass, rods, cabinet, window, flexible electronics and walls. Dye sensitized solar cell was developed by Gratzel and co-workers. It is considered as low-cost solar cells also. Researchers [22-29] have explained that electricity will be produced according to semiconductor and electrolyte.

Metal chalcogenide thin films could be grouped into binary [30-38], ternary [39-48], quaternary [49-57] and pen ternary thin films [58-62]. There are many methods that have been used to prepare thin films such as spray pyrolysis [63, 64], pulsed electro deposition [65-67], chemical bath deposition [68-71], electro deposition [72, 73], chemical vapor deposition [74,75], brush plating [76, 77], successive ionic layer adsorption and reaction [78, 79], magnetron sputtering [80, 81], dip sol method [82, 83], vacuum evaporation [84, 85], and thermal evaporation [86, 87]. It seems that chemical bath deposition method becomes more and more attractive if compared to the deposition techniques. Because of simple [88], low-cost [89] and convenient for large area deposition [90] at low temperature. During the deposition process [91-93], substrate was immersed in chemical bath containing chalcogenide source, metal ion and complexing agent. Complexing agent was used to control reaction rate, to avoid the homogeneous precipitation (as the ionic product slowly exceeds the solubility product) and improve the quality of films. Complexing agents are extensively applied in many research works **(Table 1)**. Nucleation and growth process could be observed during the deposition. Researcher describes that film thickness increases up to the terminal phase, and longer times cause film to peel off.

In this paper, Cu_4SnS_4 thin films were prepared using simple chemical bath deposition technique in the presence of Na_2EDTA (complexing agent). The influence of Na_2EDTA on the properties of thin films was studied using X-ray diffraction (structural properties), atomic force microscope (topography property) and UV-Visible Spectrophotometer (optical property).

Materials and Methods

All the chemicals used for the deposition were analytical grade and all the solutions were prepared in deionised water (Alpha-Q Millipore). The chemical bath contains copper sulfate ($CuSO_4$), tin chloride ($SnCl_2$) and sodium thiosulfate ($Na_2S_2O_3$). The effect of disodium ethylenediaminetetraacetic acid (0.01 to 0.10 M of Na_2EDTA) on the properties of films was studied. During the deposition process, 10 ml of Na_2EDTA solution was added into 10 ml of 0.05 M of $SnCl_2$ and 0.05 M of $CuSO_4$, respectively. Then, 10 ml of 0.05 M of $Na_2S_2O_3$ solution was added into mixture slowly. The resultant solution was stirred for few minutes. The pH of was adjusted (pH 1.5) by adding hydrochloric acid. The ultrasonically cleaned indium doped tin oxide glass substrate was immersed vertically into acidic bath. The deposition process was carried out for 2 hours, at temperature of 50 °C.

X-ray diffraction (Philips PM 11730 diffractometer equipped with a CuK_α (λ=1.5418 Å) and atomic force microscopy (Q-Scope 250, Quesant Instrument Corporation, contact mode) studies have been conducted to investigate the structure of morphology of samples. UV-Visible spectrophotometer was applied in order to study optical properties and band gap of sample.

Complexing agent	Highlighted results	References
disodium ethylenediaminetetraacetate (Na_2EDTA)	• NiSe films were prepared using chemical bath deposition in the presence of Na_2EDTA. • Higher absorbance value could be observed for the films deposited at longer time.	[94]
Tri-sodium citrate	• Nanocrystals with diameter (less than 5 nm) were obtained for the films deposited on glass substrate and flexible polymeric based on TEM results.	[95]
Tri-sodium citrate	• SEM analysis indicated that large amount of pinholes, cracks and vacancies. • The obtained films prepared at pH 10.5, show uniform and free of agglomerates .	[96]
Nitrilotriacetic acid	• CdS films were deposited onto transparent conducting oxide coated soda lime glass substrates. • Faster growth rate could be seen for the films prepared using complexing agent.	[97]
EDTA	• XRD patterns show that amorphous (without complexing agent) and crystalline (with complexing agent) structure for the Bi_2S_3 films.	[98]
Tartaric acid	• High transmittance (visible region), high band gap value (3.7 eV), well-crystallized films with pure-wurtzite structure, could be obtained for the ZnS films.	[99]
Ammonia	• Significant differences (deposition mechanism, optical properties, surface morphologies) were found in ZnS films.	[100]
Ammonium sulphate	• Studies reveal that complexing agent can improve quality of CdS films.	[101]
EDTA & Na_3-citrate	• XRD studies reveal that ZnS films are polycrystalline hexagonal structure (using complexing agent).	[102]
Hydrazine, ammonia	• The deposition PbS films were smooth, homogeneous and have cubic structure. • The presence of complexing agent reduces the deposition rate (because of to slow generation of Pb^{2+} ions). The deposition PbS films were smooth, homogeneous and have cubic structure.	[103]
Tri sodium citrate	• Morphology studies indicate some overgrown particles on the surface of Cu_2ZnSnS_4 films (with complexing agent), while exhibited well-covered surface morphology (without complexing agent).	[104]
Triethanolamine, Diethanolamine, Hexamine	• Chemical bath deposited PbS thin film using hexamine was proved to be the best in structural, optical and electrical properties.	[105]
Ethylenediaminetetraacetic (EDTA) acid, Triethanolamine (TEA)	• Different band gap values could be obtained for the cadmium zinc selenide films prepared using EDTA (2.03 eV) and TEA (1.75 eV).	[106]
Triethanolamine	• Preparation of uniform and smooth Cu_2ZnSnS_4 thin films by using 1 mL of 7 M of TEA was described.	[107]
Triethanolamine	• Researchers highlight that obtained films were highly crystalline (cubic zinc blende), and have band gap values ranging from 4.1 to 3.9 eV.	[108]
Triethanolamine	• TEA added into chemical bath to slow down the precipitation process and enable the formation of $CdCoS_2$. • Fast precipitation implies that a thin film cannot form on the substrate immersed in the solution.	[109]

Hydrazine	• Band gap was found 3.7 eV for the films prepared at pH 11.5, using complexing agent.	[110]
Acetylacetone	• Acetylacetone is grouped as bidentate ligand. • CdS films have hexagonal structure, band gap of 2.4 eV.	[111]
Trisodium citrate	• Complexing agent can be used to improve film quality, and reduce growth rate. • PbS films indicate quantum confinement effects with blue shifted optical properties.	[112]
Ethylenediamine tetra-acetate acid (EDTA), Hexamethylene tetramine (HMTA)	• The addition of HMTA proved that increases the amount of Zn^{2+} ions in order to produce ZnS films. • The addition of EDTA showed poor uniformity and greater cracking phenomenon.	[113]
Ethylenediamine tetra-acetate acid (EDTA)	• Compositions of nanocrystals were highly depending on the concentration of complexing agent. They are varied from Cu_2S to CuS as concentration of EDTA was increased. • Better crystalline and sheet-like morphology could be observed for the films prepared using higher concentration.	[114]
Ammonia	• Copper sulphide films (grey in colour) strongly adhere to the glass slide substrate.	[115]
Disodium Ethylenediamine tetraacetate (Na_2EDTA)	• AFM and XRD studies reveal that the films prepared in the presence of complexing are uniform, homogeneous and have better crystalline phase.	[116]
Ethylenediamine tetra-acetate acid (EDTA), citrate and nitrilotriacetate (NTA)	• NTA reduces deposition rate slowly while EDTA reduces suddenly over time	[117]

Table 1: Preparation of thin films by using various complexing agents.

Results and Discussions

Figure 1 indicates that XRD patterns of the films prepared under various concentrations of complexing agent. XRD data supported that these films were polycrystalline (orthorhombic phase) and matched standard JCPDS data (Reference code: 010710129). The number of peaks increased from three to nine when the concentration of complexing agent was increased from 0.01 M **(Figure 1a)** to 0.05 M **(Figure 1b)**. However, reduced to five peaks, as the concentration was increased to 0.1 M **(Figure1c)**. The most prominent peak corresponding to (221) plane, occurred at 2θ =30.2° (*d*-spacing=2.96 Å). Based on the XRD pattern, the highest intensity peak could be seen for the film deposited using 0.05 M Na_2EDTA.

Morphology studies (20 µm x 20 µm) have been performed by using atomic force microscopy (AFM) as indicated in **Figure 2**. The Cu_4SnS_4 films obtained using 0.05 M of complexing agent show smooth, homogeneous and film thickness of 981 nm. Also, the AFM images show that formation of grain (0.9 to 1.2 µm) completely covers the surface, and uniformly distributed on the substrate **(Figure 2b)**.

Other concentrations of complexing agent such as 0.01 M and 0.10 M are considered not favorable for the growth of films. Because of thin films obtained are very thin (125 and 640 nm), not compact and incomplete coverage over the substrate surface **(Figure 2a, c)**.

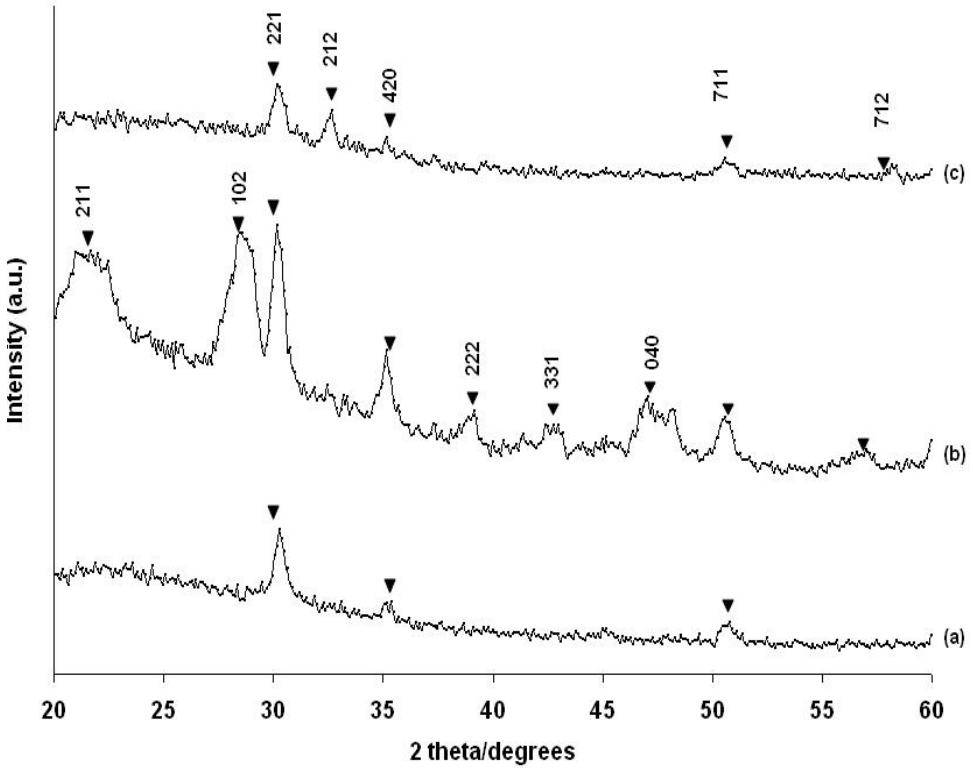

Figure 1: X-ray diffraction patterns of Cu_4SnS_4 thin films prepared under various concentrations of Na_2EDTA. **(a)** 0.01 M, **(b)** 0.05 M, **(c)** 0.10 M.

Optical properties were studied by using UV-Visible spectrophotometer (300-800 nm) as shown in **Figure 3**. UV-Visible spectra showed that absorbance value increases as the concentration of complexing agent was increased up to 0.05 M **(Figure 3a)**. However, lower absorbance value could be obtained for the Cu_4SnS_4 films prepared using 0.10 M **(Figure 3b)**, indicating the presence of complexing agent will hinder deposition process.

Band gap energy value could be calculated by using data from UV-Visible spectra (Stern relationship of near-edge absorption as indicated in Equation 1).

$$A=\frac{[k\,h\upsilon-E_g]^{n/2}}{h\upsilon} \quad (1)$$

where υ=frequency, h=Planck's constant, k=constant, n=value of either 1 or 4. Direction transition was identified if n is 1, and while 4 for the indirect transition. The plots of $(A h\upsilon)^2$ versus $h\upsilon$ for the obtained samples as indicated in **Figure 4**.

The band gap values were determined from The intercept of the straight-line portion (represent direct transition of films) of the $(A h\upsilon)^2$ against the $h\upsilon$ on the $h\upsilon$-axis using computer fitting program will be used to calculate band gap. Different band gap values such as 1.56 (0.01 M), 1.60 (0.05 M) and 1.59 (0.10 M) were estimated for the films prepared using various concentrations of complexing agent.

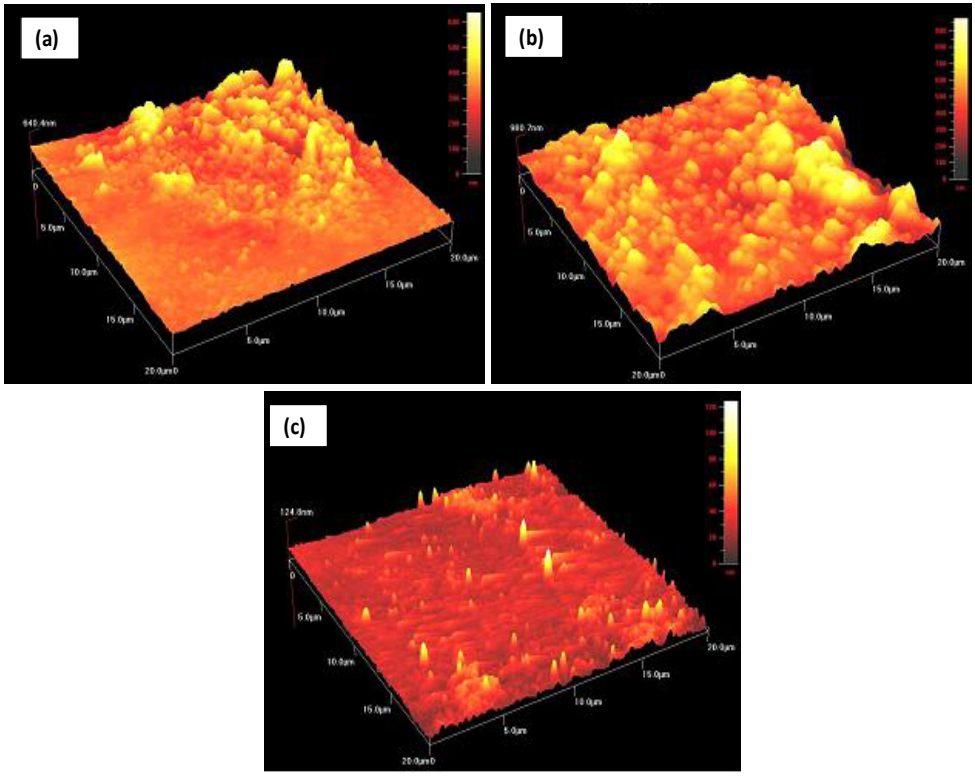

Figure 2: Atomic force microscopy images of Cu_4SnS_4 thin films prepared under various concentrations of Na_2EDTA. **(a)** 0.01 M, **(b)** 0.05 M, **(c)** 0.10 M.

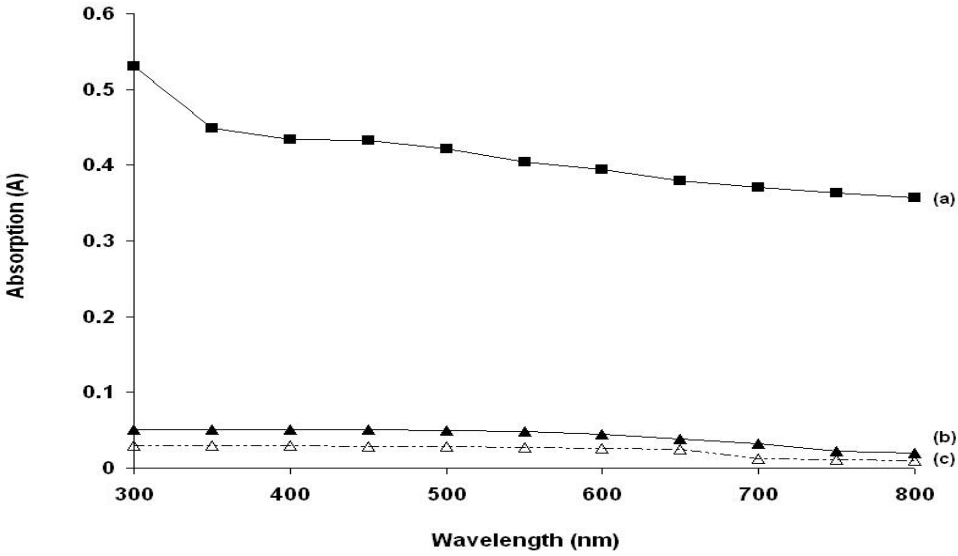

Figure 3: The optical absorption versus wavelength of Cu_4SnS_4 thin films prepared under various concentrations of Na_2EDTA. **(a)** 0.05 M, **(b)** 0.10 M, **(c)** 0.01 M.

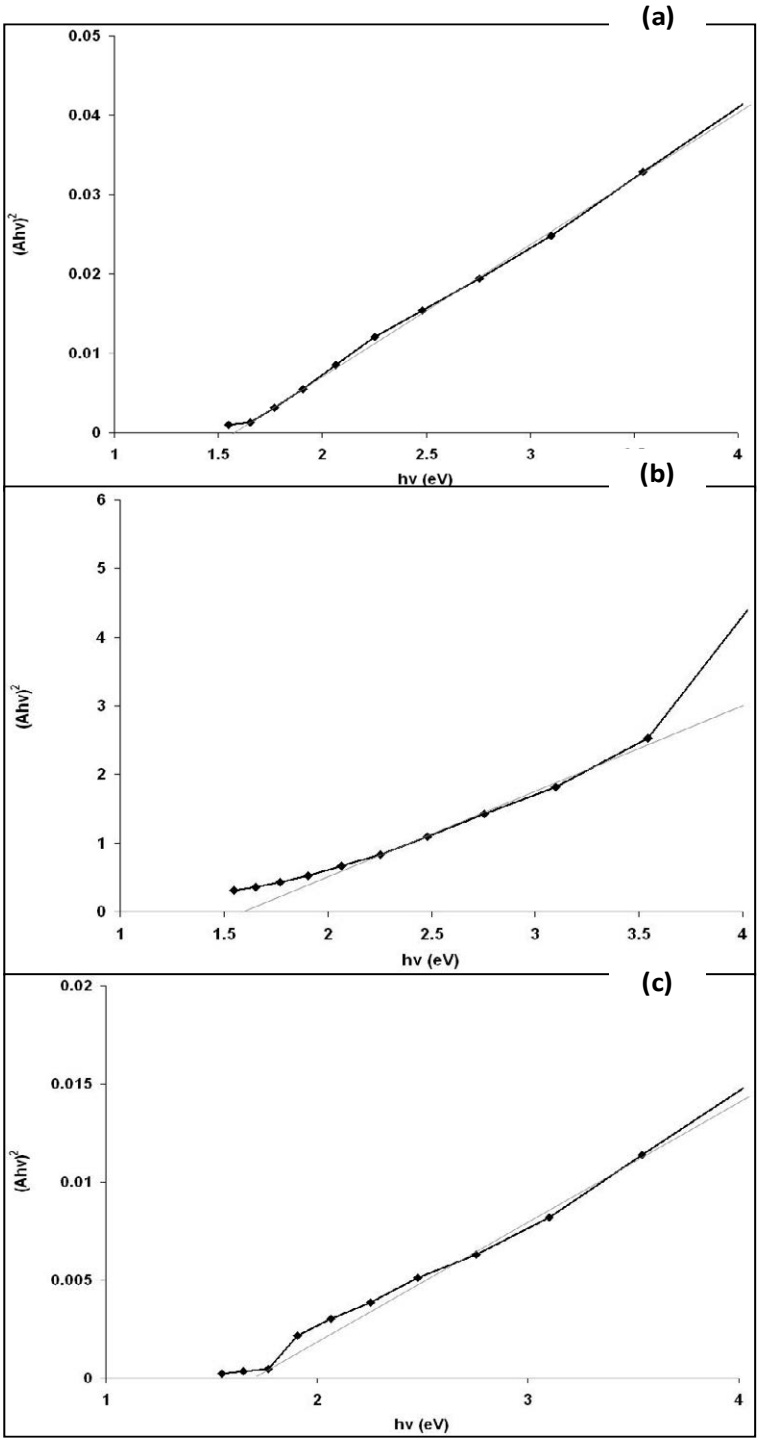

Figure 4: Plots of $(Ahv)^{2/n}$ versus hv when n=1 of Cu_4SnS_4 thin films prepared under various concentrations of Na_2EDTA. **(a)** 0.01 M, **(b)** 0.05 M, **(c)** 0.10 M.

Conclusion

Simple and inexpensive chemical bath deposition method has been used to synthesis Cu_4SnS_4 thin films. The substrate was indium tin oxide glass substrates and precursors were copper sulphate, tin chloride & sodium thiosulfate. In this work, the influence of complexing agent (Na_2EDTA) on the properties of thin films was investigated. The XRD data confirmed that the obtained films are polycrystalline, orthorhombic structure with preferential orientation along (221) plane. Experimental results show that 0.05 M of Na_2EDTA favors the formation of thin films. These films showed good uniformity, good surface coverage with bigger grains, higher absorbance value and better polycrystalline.

Acknowledgement

The author would like to thank INTI International University for financial support.

References

1. Kluth O, Reach B, Houben L, Wieder S, Schope G, et al. (1999) Texture etched ZnO: Al coated glass substrates for silicon based thin film solar cells. Thin Solid Films 351: 247-253.
2. Stelzner T, Pietsch M, Andra G, Falk F, Ose E, et al. (2008) Silicon nanowire based solar cells. Nanotechnology.
3. Peter B, Luo C, Zeng L, Lionel CK, John DJ, et al. (2007) Improving thin film crystalline silicon solar cell efficiencies with photonic crystals. Optics Express 15: 16986-17000.
4. Hideki M (1998) Formation of silicon based thin films prepared by catalytic chemical vapor deposition (Cat-CVD) method. Japanese Journal of Applied Physics.
5. Pillai S, Catchpole KR, Trupke T, Green MA (2007) Surface plasmon enhanced silicon solar cells. Journal of Applied Physics.
6. Alireza A, Hosein K (2018) Physical and electrochemical properties of electrodeposited undoped and Se-doped ZnS thin films. Ceramics International 44: 17124-17137.
7. Zhang Y, Zhang K, Huang W, Xiong S (2018) Determination of infrared refractive index of ZnS and YbF_3 thin films by spectroscopy. Optik 170: 321-327.
8. Jeyakumar R, Udai PS (2017) Copper indium gallium selenide based solar cells-a review. Energy & Environmental Science 10: 1306-1319.
9. Manjeet S, Jiu J, Tohru S, Katsuaki S (2014) Thin film copper indium gallium selenide solar cell based on low temperature all printing process. ACS Applied Materials & Interfaces 6: 16297-16303.
10. Keshav R, Mahesha MG (2018) Photoluminescence and Raman spectroscopic analysis of PV deposited ZnS thin films. Materials Research Bulletin 105: 360-367.
11. Brian EM, Wayne AB, Christopher PT, Gowri S, Robert JL, et al. (2018) Overcoming carrier concentration limits in polycrystalline CdTe thin films with In situ doping. Scientific Reports.
12. Ho SM, Vyas CU, Pratik P, Patel KD, Somnath M, et al. (2018) A short review of CdTe and CdSe films: growth and characterization. Mediterranean Journal of Chemistry 7: 115-124.
13. Chen Y, Mei X, Liu X, Wu B, Yang J, et al. (2018) Solution processed CdTe thin film solar cells using ZnSe nanocrystal as a buffer layer. Applied Sciences.
14. Md A, Ali NB, Mohammad MRB, Md AH (2017) Impacts of temperature on the performance of CdTe based thin film solar cell. IOP Conference Series: Materials Science and Engineering.
15. Craig S, Dennis N, Dimosthenis S, Miguel C, Weng T, et al. (2017) Soft x-ray absorption spectroscopy

investigation of the surface chemistry and treatments of copper indium gallium diselenide (CIGS). Solar Energy Materials and Solar Cells 160: 390-397.

16. Liu CP, Chuang CL (2012) Fabrication of copper indium gallium diselenide absorber layer by quaternary alloy nanoparticles for solar cell applications. Solar Energy 86: 2795-2801.

17. Tobias B, Marika E (2009) Copper indium gallium diselenide thin films for sun angle detectors in space applications. Thin Solid Films 517: 2063-2068.

18. Puvaneswaran C, Mohammad IH, Amin N (2010) Performance analysis of copper indium gallium diselenide (CIGS) solar cells with various buffer layers by SCAPS. Current Applied Physics 10: S387-391.

19. Yeh N, Yeh P (2013) Organic solar cells: Their developments and potentials. Renewable and Sustainable Energy Reviews 21: 421-431.

20. Scharber MC, Sariciftci NS (2013) Efficiency of bulk heterojunction organic solar cells. Progress in Polymer Science 38: 1929-1940.

21. Eva B, Krebs F (2007) Low band gap polymers for organic photovoltaics. Solar Energy Materials and Solar Cells 91: 954-985.

22. Kung C, Chen H, Lin C, Lai Y, Vittal R, et al. (2014) Electrochemical synthesis of a double layer film of ZnO nanosheets/nanoparticles and its application for dye sensitized solar cells. Progress in Photovoltaics: Research and applications 22: 440-451.

23. Chen Z, Tang Y, Zhang L, Luo L (2006) Electrodeposited nanoporous ZnO films exhibiting enhanced performance in dye sensitized solar cells. Electrochemica Acta 51: 5870-5875.

24. Thomas WH, Rebecca AJ, Alex BFM, Hal VR, Joseph TH, et al. (2008) Advancing beyond current generation dye sensitized solar cells. Energy and Environmental Science 1: 66-78.

25. Hamadanian M, Ghomi JS, Hosseinpour M, Masoomi R, Jabbari V, et al. (2014) Uses of new natural dye photosensitizers in fabrication of high potential dye sensitized solar cells (DSSCs). Materials Science in Semiconductor Processing 27: 733-739.

26. Lin Y, Yang J, Meng Y (2013) Nanostructured ZnO thin films by SDS-assisted electrodeposition for dye-sensitized solar cell applications. Ceramics International 39: 5049-5052.

27. Rahman MYA, Roza I, Umar AA, Salleh MM (2015) Effect of boric acid composition on the properties of ZnO thin film nanotubes and the performance of dye-sensitized solar cell (DSSC). Journal of Alloys and Compounds 648: 86-91.

28. Prashant B, Ahmed E, Babasaheb S (2014) Influence of processing parameters on chemically grown ZnO films with low cost Eosin-Y dye towards efficient dye sensitized solar cell. Solar Energy 105: 445-454.

29. Vijayalakshmy S, Subramanian B (2014) Effect of ZnO block layers fabricated by pulsed laser deposition and mesoporous layers by chemical method on the performance of dye sensitized solar cells. Electrochimica Acta 137: 131-137.

30. Ho SM, Anuar K, Tan WT, (2013) Thickness dependent characteristics of chemically deposited tin sulfide films. Universal Journal of Chemistry 1: 170-174.

31. Anuar K, Ho SM, Nagalingam S, Tan WT, Darren T, (2010) Chemical bath deposition of nickel sulphide (Ni_4S_3) thin films. Leonardo Journal of Sciences 16: 1-12.

32. Ezema FI, Ekwealor ABC, Asogwa PU, Ugwuoke PE, Chigbo C, et al. (2007) Optical properties and structural characterizations of Sb_2S_3 thin films deposited by chemical bath deposition technique. Turkish Journal of Physics 31: 205-210.

33. Ezema FI, Ekwealor ABC, Osuji RU (2006) Effect of thermal annealing on the band GAP and optical properties of chemical bath deposited ZnSe thin films. Turkish Journal of Physics 30: 157-163.

34. Ho SM, Anuar K, Atan S, Saravanan N (2010) X-ray diffraction and atomic force microscopy studies of chemical bath deposited FeS thin films. Studia Universitatis Babes-Bolyai Chemia 55: 5-11.

35. Kassim A, Ho SM, Tan WT, Ngai CF (2011) Influence of triethanolamine on the chemical bath deposited NiS thin films. American Journal of Applied Sciences 8: 359-361.

36. Oztas M, Bedir M, Bakkaloglu OF, Ormanci R (2005) Effect of Zn:Se ratio on the properties of sprayed ZnSe thin films. Acta Physica Polonica A 107: 525-534.

37. Raniero L, Ferreira CL, Cruz LR, Pinto AL, Alves RM, et.al, (2010) Photoconductivity activation in PbS thin films grown at room temperature by chemical bath deposition. Physica B: Condensed Matter 405: 1283-1286.

38. Wei AX, Zhao XH, Liu J, Zhao Y (2013) Investigation on the structure and optical properties of chemically deposited ZnSe nanocrystalline thin films. Physica B: Condensed Matter 410: 120-125.

39. Alaa AA (2013) The structural and optical properties of nonstoichiometric $AgAlS_2$ thin films prepared by chemical spray pyrolysis method. Tikrit Journal of Pure Science 18: 145-149.

40. Alias MFA, Naji S, Taher BY (2014) Influence of substrate temperatures on the optical properties of thin Cu_3SnS_4 films prepared by CBD. IPASJ International Journal of Electrical Engineering 2: 1-7.

41. Chaudhari JB, Deshpande NG, Gudage YG, Ghosh A, Huse VB, et.al, (2008) Studies on growth and characterization of ternary $CdS_{1-x}Se_x$ alloy thin films deposited by chemical bath deposition technique. Applied Surface Science 254: 6810-6816.

42. Haron MJ, Ho SM, Anuar K, Tan WT, Atan S, et.al, (2009) Effect of deposition period and bath temperature on the properties of electrodeposited Cu_4SnS_4 films. Solid State Science and Technology 17: 226-237.

43. Deshmukh LP, Mane ST, Lendave SA, Pingale PC, Suryawanshi RV, et.al, (2012) Photovoltaic studies of $Cd_{1-x}Co_xS$ based electrochemical cells. Journal of Nepal Chemical Society 30: 151-158.

44. Ho SM (2014) Influence of complexing agent on the growth of chemically deposited $Ni_3Pb_2S_2$ thin films. Oriental Journal of chemistry 30: 1009-1012.

45. Kassim A, Ho SM, Tan WT, Saravanan N (2010) Composition, structure and photoelectrochemical characterization of electrodeposited Cu_4SnS_4 thin films. Oriental Journal of Chemistry 26: 389-394.

46. Manauti MS, Patil SM, Mane RM, Patil SV, Bhosale PN (2012) Photoelectrochemical cell performance of chemically deposited $MoBi_2Te_5$ thin films. Advanced Materials Letters 3: 71-76.

47. Mehrez NB, Khemiri N, Kanzari M (2016) Study of structural and morphological properties of thermally evaporated $Sn_2Sb_6S_{11}$ thin films. Materials Chemistry and Physics 182: 133-138.

48. More PD, Shahane GS, Deshmukh LP, Bhosale PN (2003) Spectro-structural characterization of $CdSe_{1-x}Te_x$ alloyed thin films. Materials Chemistry and Physics 80: 48-54.

49. Chet S, Matthew GP, Vahid A, Brian G, Bonil K, et.al, (2009) Synthesis of Cu_2ZnSnS_4 nanocrystals for use in low cost photovoltaics. Journal of the American Chemical Society 131: 12554-12555.

50. Ennaoui A, Steiner ML, Weber A, Abou-Ras D, Kotschau I (2009) Cu_2ZnSnS_4 thin film solar cells from electroplated precursors: Novel low cost perspective. Thin Solid Films 517: 2511-2514.

51. Bushra AH, Muthafar FA, Duaa AU (2011) The optical properties of (CuInSTe) thin films. Al-Mustansiriyah Journal of Science 22: 211-221.

52. Colantoni A, Longo L, Boubaker K (2014) Structural investigation of photocatalyst solid $Ag_{1-x}Cu_xInS_2$ quaternary alloys sprayed thin films optimized within the lattice compatibility theory scope. Journal of Materials.

53. Patil SP, Mane RM, Kharade RR, Mali SS, Bhosale PN, et al. (2012) Novel synthetic route for quaternary $MoBiGaSe_5$ mixed metal chalcogenide (MMC) thin films. Digest Journal of Nanomaterials and Biostructures 7: 237-245.

54. Schubert B, Marsen B, Cinque S, Unold T, Klenk R, et al. (2011) Cu_2ZnSnS_4 thin film solar cells by fast co-evaporation. Progress in Photovoltaics: Research and Applications 19: 93-96.

55. Shinde NM, Dubal DP, Dhawale DS, Lokhande CD, Kim JH, et al. (2012) Room temperature novel chemical synthesis of Cu_2ZnSnS_4 (CZTS) absorbing layer for photovoltaic application. Materials Research Bulletin 47: 302- 307.

56. Tsukasa W, Tomokazu S, Shin T, Tatsuo F, Tomoyoshi M, et al. (2012) 6 % efficiency Cu_2ZnSnS_4 based thin film solar cells using oxide precursors by open atmosphere type CVD. Journal of Materials Chemistry 22: 4021-4024.

57. Wang K, Gunawan O, Todorov T, Shin B, Chey SJ, et al. (2010) Thermally evaporated Cu_2ZnSnS_4 solar cells. Applied Physics Letters.

58. Ingo R, Jan K, Jurgen P, Thomas D, Alejandro A, et al. (2014) One dimensional simulation of sequentially processed $Cu(In_{1-x}Ga_x)(Se_{1-y}S_y)$ heterojunction solar cells with vertically graded absorber composition. Physica B: Condensed Matter 439: 9-13.

59. Keller J, Schlesiger R, Riedel I, Parisi J, Schmitz G, et al. (2013) Grain boundary investigations on sulfurized $Cu(In,Ga)(S,Se)_2$ solar cells using atom probe tomography. Solar Energy Materials and Solar Cells 117: 592-598.

60. Mario G, William NS (2005) Five source PVD for the deposition of $Cu(In_{1-x}Ga_x)(Se_{1-y}S_y)_2$ absorber layers. Thin Solid Films 480-481: 33-36.

61. Richter M, Schubbert C, Eraerds P, Riedel I, Keller J, et al. (2013) Optical characterization and modeling of $Cu(In,Ga)(Se,S)_2$ solar cells with spectroscopic ellipsometry and coherent numerical simulation. Thin Solid Films 535: 331-335.

62. Taunier S, Sicx J, Grand PP, Chomont A, Ramdani O, et.al, (2005) $Cu(In,Ga)(S,Se)_2$ solar cells and modules by electrodeposition. Thin Solid Films 480-481: 526-531.

63. Radaf IM, Fouad SS, Ismail AM, Sakr GB (2018) Influence of spray time on the optical and electrical properties of $CoNi_2S_4$ thin films. Materials Research Express.

64. Radaf IM, Talaat AH, Yahia IS (2018) Synthesis and characterization of F-doped CdS thin films by spray pyrolysis for photovoltaic applications. Materials Research Express.

65. Christiana N, Anna Z, Grigorios I, John G (2018) Influence of process parameters on the properties of pulsed laser deposited $CuIn_{0.7}Ga_{0.3}Se_2$ thin films. Solar Energy 174: 793-802.

66. Ho SM (2016) A brief review of the growth of pulsed laser deposited thin films. British Journal of Applied Science & Technology 14: 1-6.

67. Beres M, Yu KM, Syzdek J, Mao SS (2018) Stoichiometry control in Cu_2ZnSnS_4 thin films grown by pulsed laser deposition. Materials Chemistry and Physics 205: 90-96.

68. Beggas A, Benhaoua B, Attaf A, Aida MS (2016) Growth study of CdS thin films deposited by chemical bath. Optik 127: 8423-8430.

69. Madhuri P, Deepika S, Avinash D, Sandip M, Ramphal S, et al. (2018) Synthesis and characterization of Cu_2S thin film deposited by chemical bath deposition method. Procedia Manufacturing 20: 505-508.

70. Ho SM (2017) Influence of deposition time on optical properties of chemically deposited nickel lead sulphide thin films. International Journal of Applied Chemistry 13: 111-120.

71. Ho SM (2015) Role of complexing agent in chemical bath deposition of thin films: a review. Australian Journal of Basic and Applied Sciences 9: 625-629.

72. Atef YS, El SM (2015) Electrodeposition, characterization and photo electrochemical properties of CdSe and CdTe. Ain Shams Engineering Journal 6: 341-346.

73. Henriquez R, Badan A, Grez P, Munoz E, Vera J, et al. (2011) Electrodeposition of nanocrystalline CdSE thin films from dimethyl sulfoxide solution: Nucleation and growth mechanism, structural and optical studies. Electrochimica Acta 56: 4895-4901.

74. Devika M, Koteeswara RN, Sreekantha DS, Jang WK, Sung HP, et al. (2017) Growth of single

crystalline cubic structured tin (II) sulfide (SnS) nanowires by chemical vapor deposition. RSC Advances 7: 41452-41459.

75. Firsov KN, Gavrishchuk EM, Ikonnikov VB, Kazantsev SY, Kononov IG, et al. (2017) CVD grown Fe^{2+}:ZnSe polycrystals for laser applications. Laser Physics Letters.

76. Clara D, Rita J, Murali KR (2017) Synthesis and characterization of ZnS_xSe_{1-x} films using brush plating technique. Materials Today Proceedings 4: 5185-5189.

77. Murali KR, Clara A, Rita J (2008) Structural, optical and electrical properties of brush plated ZnSe films. Chalcogenide Letters 5: 277-280.

78. Henry J, Prema P, Duraipandi PP, Kannusamy M, Ganesan S, et.al, (2016) Shape dependent optoelectrical investigation of $Cu_{2+x}Cd_{1-x}SnS_4$ thin films for solar cell applications. New Journal of Chemistry 40: 2609-2618.

79. Sartale D, Lokhande CD (2000) Deposition of cobalt sulphide thin films by successive ionic layer adsorption and reaction (SILAR) method and their characterization. Indian Journal of Pure & Applied Physics 38: 48 52.

80. Galina IK, Ruslan PM, Gennadily SK, Andrey ID (2017) Structure and optical properties of CdS nanoscale thin films obtained by direct current magnetron sputtering. 2017 IEEE 7th International Conference Nanomaterials: Application & Properties.

81. Sun YH, Ge YJ, Li WW, Huang DJ, Chen F, et al. (2011) Structural and optical analysis of CdS thin films grown by magnetron sputtering technique. Journal of physics: Conference Series.

82. Yogesh VM, Shrivastava VS (2011) Synthesis and application of CdS nanocrystalline thin films. Advances in Applied Science Research 2: 295-301.

83. Samir GP (2016) Study of zinc sulphide thin films obtained by dip coating method. International Journal of Recent Scientific Research 7: 14895-14898.

84. Ramya M, Ganesan S (2010) Annealing effects on resistivity properties of vacuum evaporated Cu_2S thin films. International Journal of Pure and Applied Physics 6: 243-249.

85. Ariswan HS, Prasetyawati R (2017) Crystal structure, optical and electrical properties of SnSe and SnS semiconductor thin films prepared by vacuum evaporation techniques for solar cell applications. IOP Conference Series: Materials Science and Engineering.

86. Sarita B, Subodh S, Vijay YK (2018) Preparation of InSe thin films by thermal evaporation method and their characterization: structural, optical and thermoelectrical properties. Journal of Nanotechnology.

87. Maykel C, Tenoch G, Nini RM, Xavier M (2018) Cu_2ZnGeS_4 thin films deposited by thermal evaporation: the impact of Ge concentration on physical properties. Journal of physics D: Applied Physics.

88. Hong J, Lim D, Eo Y, Choi C (2018) Chemical bath deposited ZnS buffer layer for $Cu(In,Ga)Se_2$ thin film solar cell. Applied Surface Science 432: 250-254.

89. Hariech S, Aida MS, Bougdira J, Belmahi M, Medjahdi G, et al. (2018) Cadmium sulfide thin films growth by chemical bath deposition. Journal of Semiconductors.

90. Zhang L, Erik S, Ivan M, Anthony L, William C, et al. (2018) Deposition of cadmium sulfide and cadmium selenide thin films using chemical bath deposition technique. Proceedings Volume 10543, Quantum dots and nanostructures: Growth, Characterization and Modeling XV.

91. Deshmukh SG, Vipul K, Panchal AK (2018) Effect of annealing on the properties of Cu_3BiS_3 thin films deposited via chemical bath deposition. Materials Today Proceedings 5: 10712-10716.

92. Demir R, Gode F (2018) Preparation and characterization of polycrystalline CdS thin films deposited by chemical bath deposition. Materials Focus 7: 351-355.

93. Tzvi T, Sucheta S, Nitzan M, Eyal B, Michael S, Vladimir E, Eyal Y, Gabby S, Iris V, Yuval G (2018) Oriented attachment: a path to columnar morphology in chemical bath deposited PbSe thin films. Crystal Growth & Design 18: 1227-1235.

94. Anuar K, Mohd YR, Ho SM (2011) UV-Visible studies of chemical bath deposited NiSe thin films. International Journal of Chemical Research 3: 21- 26.

95. Karimi A, Sohrabi B, Vaezi M (2018) Highly transparent, flexible and hydrophilic ZnS thin films prepared by a facile and environmentally friendly chemical bath deposition method. Thin Solid Films 651: 97-110.

96. Luque PA, Olivas A, Lopez MA, Nestor AR (2015) Influence of pH on properties of ZnS thin films deposited on SiO_2 substrate by chemical bath deposition. Materials Letters 140: 148-150.

97. Hani K, Isaiah OO, Lee C (2008) Optimization of chemical bath deposited CdS thin films using nitrilotriacetic acid as a complexing agent. Thin Solid Films 516: 5967-5973.

98. Ubale AU (2010) Effect of complexing agent on growth process and properties of nanostructured Bi_2S_3 thin films deposited by chemical bath deposition method. Materials Chemistry and Physics 121: 555-560.

99. Roy P, Ota JR, Suneel KS (2006) Crystalline ZnS thin films by chemical bath deposition method and its characterization. Thin Solid Films 515: 1912-1917.

100. Wei A, Liu J, Zhuang M, Zhao Y (2013) Preparation and characterization of ZnS thin films prepared by chemical bath deposition. Materials Science in Semiconductor Processing 16: 1478-1484.

101. Soundeswaran S, Kumar OS, Dhanasekaran R (2004) Effect of ammonium sulphate on chemical bath deposition of CdS thin films. Materials Letters 58: 2381-2385.

102. Seung WS, Agawane GL, Myeng GG, Moholkar AV, Moon JM, et al. (2012) Preparation and characteristics of chemical bath deposited ZnS thin films: Effects of different complexing agents. Journal of Alloys and Compounds 526: 25-30.

103. Castillo A, Lazaro R, Perez A, Perez C, Terrazas E, et al. (2014) Role of complexing agents in chemical bath deposition of lead sulfide thin films. Materials Letters 121: 19-21.

104. Pawar BS, Pawar SM, Shin SW, Choi DS, Park CJ, et al. (2010) Effect of complexing agent on the properties of electrochemically deposited Cu_2ZnSnS_4 (CZTS) thin films. Applied Surface Science 257: 1786-1791.

105. Preetha KC, Deepa K, Dhanya AC, Remadevi TL (2015) Role of complexing agents on chemical bath deposited PbS thin film characterization. IOP Conference Series: Materials Science and Engineering.

106. Bagade CS, Ghanwat VB, Kharade SD, Khot KV, Kharade RR, et al. (2016) Rapid formation of ternary $CdZnSe_2$ chalcogenide thin film by microwave assisted chemical bath deposition. Macromolecular Symposia.

107. Arepalli VK, Challa KK, Kim E (2015) Effects of complexing agents on the chemical bath deposition of uniform Cu_2ZnSnS_4 thin films. Nanoscience and Nanotechnology Letters 7: 729-733.

108. Alireza G, Azimeh DN, Ha C (2014) Fabrication and characterization of nano-structured ZnS thin films as the buffer layers in solar cells. RSC Advances 4: 59764-59771.

109. Ezema FI, Osuji RU (2006) Preparation and optical characterization of chemical bath deposited $CdCoS_2$ thin films. Journal of Applied Sciences 6: 1827-1832.

110. Nasr TB, Kamoun N, Kanzari M, Bennaceur R (2006) Effect of pH on the properties of ZnS thin films grown by chemical bath deposition. Thin Solid Films 500: 4-8.

111. Iribe AA, Enriquez MC, Lopez MA, Bon RR, Castillo SJ, et al. (2011) Acetylacetone as complexing agent for CdS thin films grow chemical bath deposition. Chalcogenide Letters 8: 77-82.

112. Sucheta S, Maayan P, Alexander R, Golan Y (2016) In situ monitoring the role of citrate in chemical bath deposition of PbS thin films. Cryst Eng Comm 18: 149-156.

113. Park SY, Park JE, Eom T, Park JH, Bweupe J, et al. (2018) characterization of ZnS thin films grown using chemical bath deposition with three different complexing agents. Journal of Nanoscience and Nanotechnology 18: 6294- 99.

114. Lu Y, Jia J (2014) The effect of complexing agent on crystal growth, structure and properties of nanostructured $Cu_{2-x}S$ thin films. Chinese Chemical Letters 25: 1473-1478.

115. Chidozie OM (2015) The growth and characterization of copper sulphide thin film using CBD (Chemical bath deposition) technique. Journal of Materials Science and Engineering B 5: 181-186.

116. Kassim A, Ho SM, Atan S, Kuang Z, Tan WT, et al. (2010) Preparation and studies of chemically deposited Cu_4SnS_4 thin films in the presence of complexing agent Na_2EDTA. Indian Journal of Engineering & Materials Sciences 17: 295-298.

117. Opasanont B, Jason B (2015) Dynamic speciation modeling to guide selection of complexing agents for chemical bath deposition. Case study for ZnS thin films. Crystal Growth & Design 15: 4893-4900.

Metal Chalcogenide Nanostructures: Characteristics and Synthesis

In the current scenario, there has been lots of attention in metal chalcogenides because of their essential physical, electronics and optical characteristics. They have been found to be potential candidates for electronic, photonics, optoelectronic devices among others. Solar cells, solar selective coatings, resistive switches, filament memories, infrared detectors are examples of applications for these materials. The physio-chemical characteristics of these substances are mostly relying upon method applied for the synthesis of the metal chalcogenide samples. Its miles vital to choose the appropriate methods for the preparation of metal chalcogenide. In this book, there are several deposition techniques will be discussed which include spin-coating method, sol gel method, chemical bath deposition, solid vapor reaction, physical and chemical vapor deposition method. During the deposition process, nanocrystalline films were grown on various clean substrates such as soda lime glass, fluorine-doped tin oxide coated glass, indium tin oxide coated glass and stainless steel. These substrates are used for several different industrial and scientific applications. The choice of an appropriate substrate depends on cost production, the properties of desired thin films and the deposition conditions. The obtained films were characterized using X-ray diffraction, scanning electron microscopy, atomic force microscopy, energy dispersive X-ray analysis, photoluminescence technique, and UV-Visible spectrophotometer.

Ho Soon Min

Dr Ho Soon Min is presently working as Associate Professor at Centre for Green Chemistry and Applied Chemistry, INTI International University, Putra Nilai, 71800, Negeri Sembilan, Malaysia. He received his Ph.D. in Materials Chemistry at University Putra Malaysia. He taught academic courses in physical chemistry, general chemistry, chemistry & society since last seven years. His research areas include green chemistry, semiconductor, Nano materials, applied chemistry, activated carbon and thin film solar cell. He has authored or co-authored for more than 130 articles in international referred journals and book chapter as well. He was appointed as journal reviewer, editorial board member, thesis evaluator and head of center of applied chemistry and green chemistry.

Yarub Al-Douri

Dr Yarub Al-Douri has gained Doctorat D'etat, MSc and BSc in Materials Science and Physics, respectively. He has been appointed as Professor, Adjunct Professor, Consultant Expert, Visiting Professor, Associate Professor, Assistant Professor, Research Fellow (A), Scientific Collaborator and Post-doc in Malaysia, Turkey, Algeria, Yemen, Singapore, Germany and France, respectively. He has more than quarter century experience of scientific research, university teaching and administrative duties, more than 519 publications currently including patents, books, chapters review, papers, articles and conferences and US$ 4.2M research grants. His citations = 3735, h-index = 27 and i10-index = 103 for the moment. He has graduated under his supervision many of PhD and MSc students. He is Founding Editor-in-Chief of Journal of Experimental and Theoretical Nanotechnology Specialized Researches, Editor-in-Chief of World Journal of Nano Science and Engineering, Associate Editor of Nano-Micro Letters (Q1), Editor and Peer-reviewer of different international journals, member of different international scientific associations and has been honored 60 awards internationally. He has initiated Nanotechnology Engineering MSc Program and Nano Computing Laboratory, the first ones in Malaysia. His research interests are Modeling and Simulation, Semiconductors, Optical Studies, Nanoelectronics, Nanomaterials and Renewable Energy.

978-1-63278-029-4

ISBN: 978-1-63278-029-4